Intrinsic Fiber Optic Chemical Sensors for Subsurface Detection of CO_2

FINAL TECHNICAL REPORT

Reporting Period/Period of Performance:
10/01/12 to 10/31/15

Principal Investigator/Author:
Jesús Delgado Alonso, Ph.D.
424-263-6321

Report Issued on:
January 2016

DOE Award No.:
DE-FE0010318

Submitting Organization:
Intelligent Optical Systems
2520 West 237th Street
Torrance, California 90505

Significant Contributors:
GeoMechanics Technologies
103 East Lemon Avenue
Monrovia, California 91016

DISCLAIMER

ABSTRACT

Intelligent Optical Systems, Inc. has developed distributed intrinsic fiber optic sensors to **directly quantify the concentration of dissolved or gas-phase CO_2** for leak detection or plume migration in carbon capture and sequestration (CCS). The capability of the sensor for highly sensitive detection of CO_2 in the pressure and temperature range of 15 to 2,000 psi and 25°C to 175°C was demonstrated, as was the capability of operating in highly corrosive and contaminated environments such as those often found in CO_2 injection sites. The novel sensor system was for the first time demonstrated deployed in a deep well, detecting multiple CO_2 releases, in real time, at varying depths. Early CO_2 release detection, by means of a sensor cable integrating multiple sensor segments, was demonstrated, as was the capability of quantifying the leak. The novel fiber optic sensor system exhibits capabilities not achieved by any other monitoring technology. This project represents a breakthrough in monitoring capabilities for CCS applications.

TABLE OF CONTENTS

EXECUTIVE SUMMARY

This report describes the work performed by Intelligent Optical Systems, Inc. (IOS) under the contract entitled "Intrinsic Fiber Optic Chemical Sensors for Subsurface Detection of CO_2" (Contract No. DE-FE0010318). Collaborating with IOS on this project was GeoMechanics Technologies (subcontractor). The overall goal of this project was to design, build, and deploy in the field an intrinsic fiber optic sensor system for subsurface CO_2 monitoring and above-zone leak detection.

Virtually all current CO_2 sequestration-monitoring systems rely on physical measurements (temperature, pressure, water level, geophysical characteristics) or indirect/delayed dissolved CO_2 measurements (near-surface soil-gas, gas-phase measurements using accumulation/flux chambers, or "grabbed-sample" analysis of deep subsurface water).

The stand-alone system developed in this project can continuously and directly quantify the concentration of dissolved or gas-phase CO_2 caused by leaks or plume migration in the subsurface. In our monitoring system, **the entire length of an optical fiber is a sensor**. Fiber optic sensors distributed throughout the length of a sensor cable are capable of operating in the unsaturated zone and capable of operating immersed in complex aqueous media. These unique characteristics are the main differences between the sensor system developed in this project and any other sensor for direct detection of subsurface CO_2, overcoming the limitations of CO_2 point sensors for carbon sequestration applications and sensors based on direct spectroscopy.

To accomplish our goals, we developed novel indicator-based polymeric sensor materials for monitoring dissolved carbon dioxide in an aqueous matrix, and for monitoring carbon dioxide in gas phase. The light absorption of polymers doped with a selected indicator dye changes, at the wavelength of absorption of the indicator dye, when it is exposed to CO_2. That change is proportional to the CO_2 concentration, and is reversible.

Studies were conducted to make the sensor materials resistant to adverse environmental conditions, and effective ways to do so were identified and implemented. They are resistant to corrosive environments, including high salinity, low pH, elevated water flow rate, high pressure, and the presence of hydrocarbons. The effectiveness of strategies to protect the sensor material from biofouling contamination has also been studied, and selected approaches have been implemented.

The capability of the sensor materials to survive and operate at the elevated temperatures found in deep wells was optimized, and operation at up to 175°C was demonstrated. The sensor materials showed the capability of operating continuously at up to 140°C. Accelerated degradation studies were conducted in the laboratory to enhance and evaluate the life of the sensor materials, and the data collected projects sensor operation for over five years without sensor recalibration or replacement. Capability for leak detection even after five years is also projected.

Optimized sensor materials were used to fabricate intrinsic fiber optic sensors, in which the entire length of the optical fiber is sensitive to CO_2. Glass and plastic core fiber are coated with the sensitive polymers. When light is launched through the fiber, the evanescent field of the light interacts with the cladding, so chemical exposure anywhere along the fiber dramatically affects the spectrum and intensity of the light it transmits, proportionally to the CO_2 concentration. The instrumentation and fabrication protocols for manufacturing fiber optic sensor cable at a rate of hundreds of meters per day using either UV-curing or heat-curing polymers were established at IOS.

The analytical characteristics of the sensor system were determined in the laboratory, at a range of temperature and pressure conditions. A limit of detection of 0.8 mg/L CO_2 (which corresponds to 0.05% v/v CO_2 or 0.35 mmHg pCO_2) under standard conditions was determined. Direct determination of dissolved CO_2 at elevated pressures of up to 2,050 psi was demonstrated for the first time using fiber optic sensors, and the capability of detecting a leak of 0.1% CO_2 v/v under realistic conditions of pressure and temperature in the range of 15 to 2,000 psi and 25°C to 175°C was demonstrated.

A multi-sensor optoelectronic unit has been developed for use with sensor cables integrating multiple sensor segments. The system has dual wavelength optical modules, integrating high power LEDs. The emission of one LED is centered at the absorption wavelength of the indicator dye, and the second LED is used as reference, launching light far from the sensitive wavelength. The transmission of light through the sensor cable at both wavelengths is measured by means of a highly sensitive photodetector. The reference signal is used to compensate the sensor for environmental effects on the light transmitted through the fiber. The capability of the system to operate over sensor cables as long as 3,000 m with excellent signal to noise readings (noise 0.03% of signal) was demonstrated.

The system has been demonstrated in the field, deployed in a deep well. Field tests demonstrated the capability of the sensor cables to survive and operate properly immersed in highly contaminated aqueous matrixes. Multiple CO_2 releases were conducted simulating gas leaks reaching an observation well, locating sensor segments at various depths and pressure. Early leak detection with high sensitivity was demonstrated in the field tests. The capability of multiple sensor segments distributed at various depths along a sensor cable to profile the CO_2 concentration vs. depth was demonstrated. Field data demonstrate that using multiple sensor segments enables us not only to detect the leak but to quantify it, based on the dissolution and distribution rate of CO_2 from sensor segment to sensor segment.

A new generation of fiber optic sensors for direct subsurface detection and monitoring of carbon dioxide was developed under this project and demonstrated in the field, exhibiting capabilities not achieved yet by any other monitoring technology. For the first time, low levels of dissolved carbon dioxide have been monitored, in-situ and in real time, at varying depths, in a deep monitoring well, at elevated pressure and temperature. This project represents a breakthrough in our monitoring capabilities for CCS applications.

RESEARCH AND RESULTS

The overall objective of this project is to design, build, and deploy in the field an intrinsic fiber optic sensor system for subsurface CO_2 plume migration monitoring and above-zone leak detection that will be mature enough at the end of the project to be incorporated into monitoring wells in the injection projects planned for Phase III of the DOE Carbon Sequestration Program. The originally-planned 36-month project was divided into three phases. The tasks performed for this project are described below in relation to the project objectives for each phase.

1.0 *TASK 1.0* PROJECT MANAGEMENT AND PLANNING

The Principal Investigator, Dr. Jesús Delgado Alonso, led the team to accomplish the overall goal and objectives, including the maintenance and revisions of the Project Management Plan, coordination of project work with DOE/NETL and the subcontracted organizations, and submitting required NEPA documentation. Concrete, quantitative milestones enabled us to benchmark the progress of each phase of the project. Each series of milestones culminates in the achievement of the Success Criteria, which was evaluated at key decision points at the end of each phase.

PHASE I. Development of field-deployable intrinsic fiber optic sensors.

Objective 1. Demonstrate fiber optic sensor prototypes (20 to 100 m long) for gas-phase and/or dissolved CO_2 monitoring capable of withstanding corrosive liquids (with traces of nitrous oxides or sulfur oxides, with pH near 4 and salinity up to 250,000 ppm), and elevated temperatures.

Objective 2. Manufacture fiber optic sensors with lengths ranging from 2,500 to 12,000 ft.

Objective 3. Develop a stand-alone multichannel read-out unit for distributed intrinsic fiber optic sensors, with wireless communication capability.

Milestone 1. CO_2 and/or dissolved CO_2 fiber optic sensor prototypes at least 20 meters long withstand corrosive liquids (pH near 4, salinity up to 250,000 ppm and with traces of nitrous oxides or sulfur oxides).

Milestone 2. Fiber optic sensor cable created with length of at least 2,500 ft.

Milestone 3. Compact, stand-alone DICAST readout electronics provide signal-to-noise readings as good as, or better than, bench-top readings on the same fibers.

Success Criterion I: System reaches TRL 4.

The chemically sensitive fibers and optoelectronic readout created during Tasks 2-6 were integrated and tested at the end of Phase I. The integrated system met all of the criteria embodied in Milestone 3, and that established that basic technological components of the subsurface DICAST CO_2 monitoring system work together – the definition of TRL 4 according to DOE G413.3-4.

PHASE II. Sensor evaluation and demonstration in simulated subsurface conditions.

Objective 4. Demonstrate that the sensors exhibit sensitivity (better than 0.1% CO_2), measurement range (0 to 100%), and response time (in the minutes range) adequate for monitoring plume migration, and above zone leak detection of CO_2.

Objective 5. Determine the matrix of signal-dose response at variable temperatures and pressure in simulated reservoir conditions.

Objective 6. Demonstrate the capability of the sensors to support long-term monitoring.

Milestone 4. Sensors exhibit sensitivity to 0.1% (W:W) CO_2 for a 10-meter section, measurement range of 0 to 100%, in less than 10 minutes adequate for monitoring plume migration, and above zone leak detection of CO_2.

Milestone 5. Sensors meet the performance criteria of Milestone 4 at temperatures of at least 175°C.

Milestone 6. Sensors meet the performance criteria of Milestone 4 at pressures of at least 300 psi.

Milestone 7. ADT support fiber lifetime projections of at least 5 years.

Success Criterion II: System Reaches TRL 5.

Testing cabled fibers in a test rig capable of operating at elevated pressure (up to 3,000 psi) enabled the team to perform a high fidelity simulation of the field deployment that was to be carried out in Phase III. A key measure of the success of Phase II was whether the team could gain an analytical understanding of what the experimental results mean for the eventual operating system. This understanding then guided the fabrication and deployment of the engineering-scale model in Phase III.

PHASE III. Demonstrate sensor deployment and operation in the subsurface.

Objective 7. Design and manufacture a sensor cable integrating multiple fiber optic sensors.

Objective 8. Design and implement a technique for the deployment of the fiber optic sensor in monitoring wells.

Objective 9. Deploy and demonstrate the sensor system in a 5,200 ft. deep well in a field study, and demonstrate the feasibility of using the system to detect actual injection of carbon dioxide at hydrostatic pressures up to 2,000 psi.

Milestone 8. IOS takes delivery of commercially-fabricated fiber sensor cables with length ranging from 2,500 to 12,000 ft.

Milestone 9. Complete engineering drawings and site plans for downhole sensor cable pass IOS-Geomechanics design review.

Milestone 10. Sensor cable deployed at hydrostatic pressures up to 2,000 psi in a 5,000 ft. deep monitoring well.

Milestone 11. DICAST sensor cable, connected to the DICAST optoelectronic controller, detects actual injection of carbon dioxide at variable depths in a 5,000 ft. deep monitoring well.

Success Criterion III: System Reaches TRL 6.

Testing a complete DICAST carbon dioxide sequestration system in the 5,200-ft. San Pedro monitoring well, actually releasing CO_2, analyzing the data, and comparing the results with the laboratory simulation data from Phase II enabled us to identify the scaling factors necessary for us to design the final operational system. At the end of this phase of the project, the team conducted a Critical Design Review that has identified what is required for full-scale deployment of an actual prototype system at a working carbon sequestration site.

All objectives and milestones of the project were achieved through the performance of the tasks described below.

Milestone Title/Description	Planned Completion Date	Actual Completion Date	Verification Method	Comments
Milestone 1	Jun. 2013	June 2013	Experimental results	Achieved
Milestone 2	Aug. 2013	Aug. 2013	Experimental results	Achieved
Milestone 3	Sep. 2013	Sep. 2013	Validation/verification matrix performed	Achieved
Milestone 4	Mar. 2014	Mar. 2014	Experimental results	Achieved
Milestone 5	Jun. 2014	Jun. 2014	Experimental results	Achieved
Milestone 6	Aug. 2014	Jun. 2014	Experimental results	Achieved
Milestone 7	Sep. 2014	Jun. 2014	Experimental results	Achieved
Milestone 8	Dec. 2014	Mar. 2015	Action completed	Achieved
Milestone 9	Apr. 2015	Aug. 2015	Action completed	Achieved
Milestone 10	May 2015	Sep. 2015	Action completed	Partially Met*
Milestone 11	Jul. 2015	Sep. 2015	Experimental results	Achieved

*The sensor cable was deployed at 2,350 ft.

2.0 *TASK 2.0* ESTABLISH A FUNCTIONAL REQUIREMENTS DOCUMENT (FRD)

IOS generated the Functional Requirement Document, which includes all the fundamental functions and capabilities that the prototypes must exhibit. Our plan included developing a system demonstrator that exhibits all the main functionalities of the final product and, after conducting laboratory and field tests, reviewing the design and correcting errors and system limitations, in order to design and fabricate a second generation system. The FRD included the requirements that both the initial demonstration unit and the final instrument would have to meet.

3.0 *TASK 3.0* DEVELOP THE OPTOELECTRONIC UNIT FOR REMOTE OPERATION

The optoelectronic unit is based on the distributed intrinsic chemical agent sensing and transmission (DICAST®) systems developed by IOS for absorbance-based distributed fiber optic chemical sensors, and on the Multi-element Optical Sensor Array (MOSA) system developed by IOS for colorimetric-based chemical sensors.

3.1 Subtask 3.1 – Prepare Preliminary Design

In this step we developed general design concepts that meet the requirements in the Functional Requirements Document (FRD) for the SUS-CO2-DICAST system. After evaluating the preliminary designs, we selected the following approaches to developing the instrumentation:

- We selected the zone-by-zone design for the SUS-CO2-DICAST system.
- The initial system was to include four optical channels, to measure CO_2 at four depths at a time.
- The instrument was to have the capability of interrogating sensor cables with total cable lengths ranging from 1,000 to 3,000 m. The sensor would cover depths ranging from 200 m to 1,000 m. Depth resolution would be from 50 m to 250 m (see Table 1, and 3227 (JDA) DOE RPPR Jan13 for further detail).

Table 1 Calculation of Sensor Cable Attenuation for Combinations of Cable Range and Cable Coverage (total attenuation of less than 80 dB is considered feasible)

Distribution Fiber Length (m) (each segment)	Distribution Fiber Attenuation (dB)	Sensing Segment Length (m)	Sensing Segment Attenuation (dB)	Total Attenuation (dB)	Cable range (m)	Cable Coverage for 4 segments (m)
1,000	20	25	2	21	1,000	200
1,000	19	50	4	23	1,000	400
1,000	18	100	7	25	1,000	800
2,000	40	25	2	41	2,000	200
2,000	39	50	4	43	2,000	400
2,000	38	100	7	45	2,000	800
3,000	60	25	2	61	3,000	200
3,000	59	50	4	63	3,000	400
3,000	58	100	7	65	3,000	800
3,000	55	250	18	73	3,000	1,000

The selected system structure is shown in Figure 1.

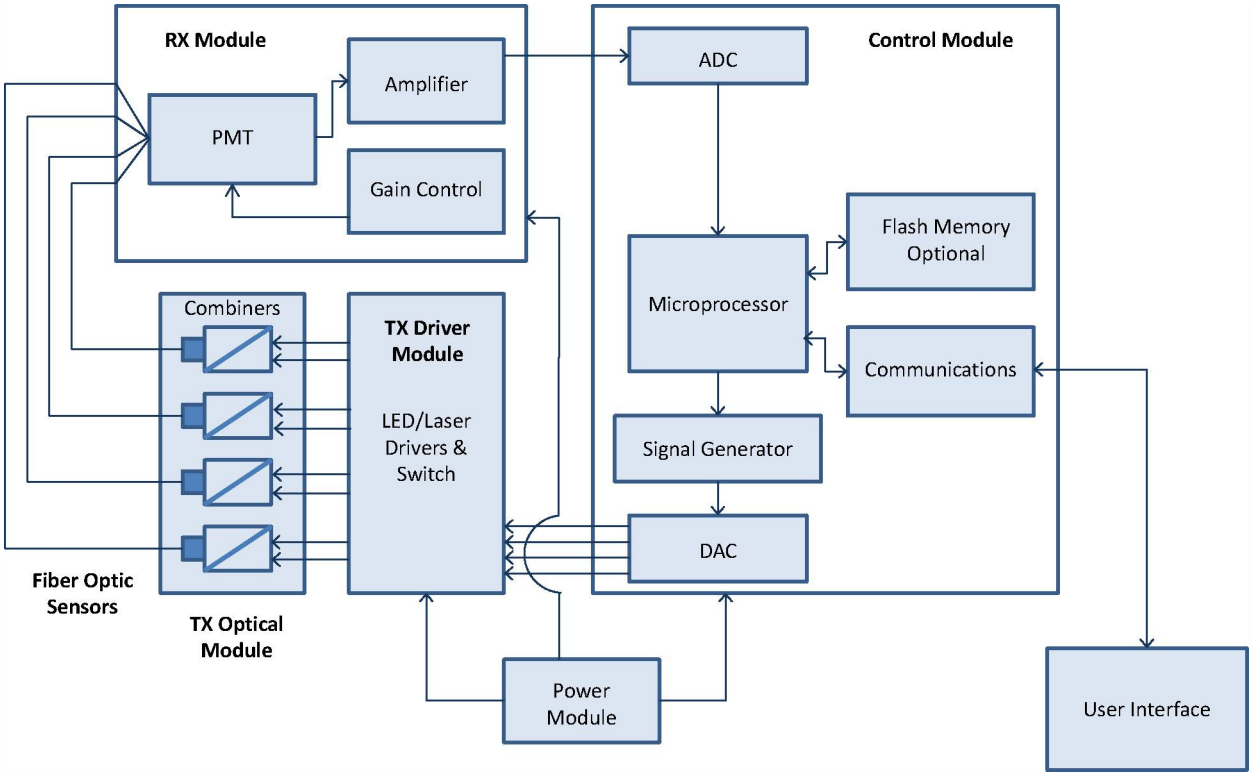

Figure 1 SUS-CO2-DICAST system.

3.2 Subtask 3.2 – Prepare Electronics Detailed Design

Tx-Rx Board. Based on the architecture defined in Figure 1, we performed the detailed design of the Tx-Rx board, which includes the Tx driver module and the Rx module, generating schematics, simulating system performance, and selecting components. Then we designed the PCB, completing the engineering documentation needed for fabrication (Subtask 3.3).

Control Board. The control board development is based on electronics previously developed by IOS, and several units of this board had already been fabricated and were available for the project. The modifications to be performed on the existing control board to adapt the hardware for the SUS-CO2-DICAST system were identified and implemented before system integration. A complete new firmware version was coded for the SUS-CO2-DICAST system. Software Problem Reports (SPR) were generated and solutions suggested and reviewed. Engineering Change Requests (ECR) were also generated, with proposed enhancements for the software. Approved ECRs were implemented.

Tx Optical Module. The Tx optical block consists of four combiners, each of them including an LED (for a sensor signal at 580 nm), initially a laser diode (for a reference signal at 850 nm), which was later replaced by a red LED, and optical components. The optical signal from the sensor LED and the optical signal from the reference LED are monitored by separate photodiodes, and the photodiode output is fed back to stabilize the intensity of the light sources. The Tx optical module was designed and the initial design reviewed several times until approval of the final version to be used for fabrication. The latest revision of the optical module design incorporates an XY fiber optic adjustment, which enabled us to optimize light coupled into the fiber.

Graphical User Interface. A document including the functional requirements for the graphical user interface (GUI) was generated, and a high level design was performed, defining the visual composition (windows, buttons...) and the temporal operation. The LabView-based graphical user interface was coded and reviewed several times until we completed the version used for the final tests.

3.3 Subtask 3.3 – Manufacture Optoelectronics and Integrate System

Produce Tx-Rx Board. We fabricated a PCB series. Two Tx-Rx PCBs were assembled. We verified the design and the assembly with these first two units. Hardware Problem Reports (HPR) were generated, and solutions were suggested, reviewed, and implemented. ECRs were also generated, with proposed enhancements for the hardware. The main ECR was related to the control loop of the LED output. The photodiode-control loop maintained a stable sensor signal and reference signal when the system was operated at varying temperature. However, the system did not operate properly when all eight optical channels (four sensor LEDS and four reference LEDs) were configured to operate with the photodiode-control loop simultaneously. To overcome this problem, new circuitry was designed and the corresponding PCB as well. The PCBs were fabricated and assembled (Figure 2).

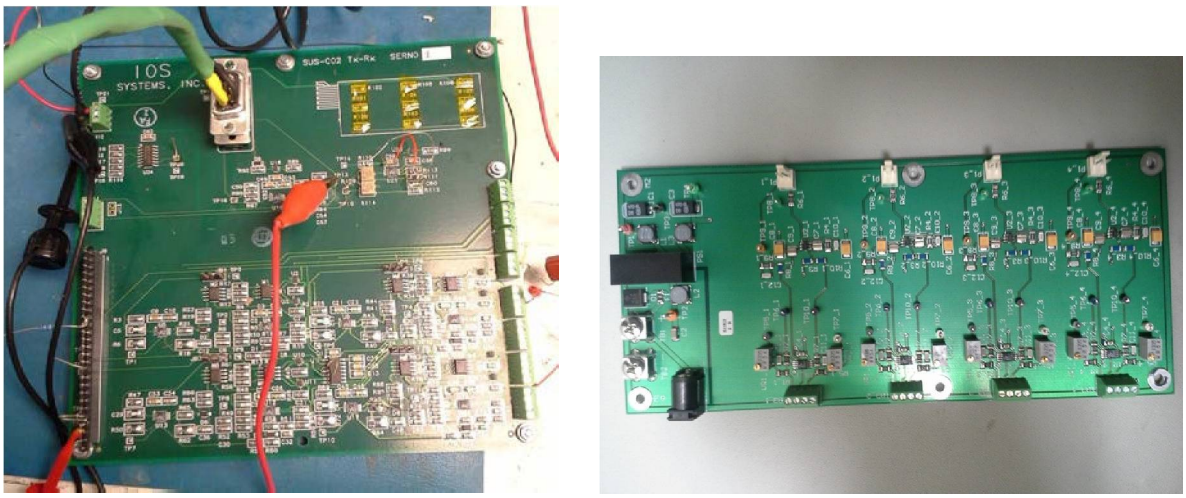

Figure 2 (left) Tx - Rx board. (right) PCB designed to improve photodiode-control loop.

Produce Control Board. The control board development is based on electronics previously developed by IOS, and several units of this board had already been fabricated and were available for the project. Hardware and firmware modification to interface with the new Tx-Rx board were performed during system integration (Figure 3).

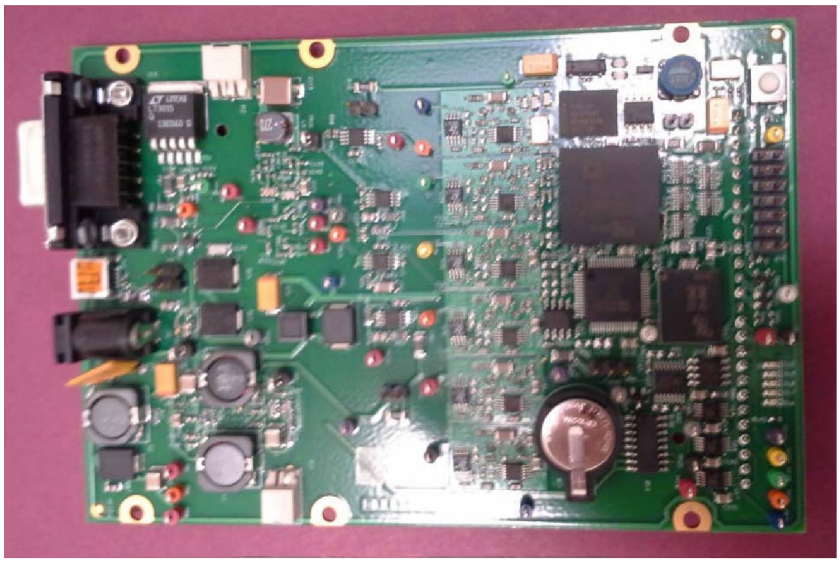

Figure 3 Control board.

Produce Tx Optical Module. The optical modules were fabricated.

- The high current that drives the LED requires the device to be attached to a cooling block; 60 of the selected LEDs were assembled on a high performance cooling substrate were produced. The cooling efficiency was tested driving the LED at the maximum current of 750 mA, and no overheating was measured.
- Sixty of the optical prisms included in the Tx optical block were fabricated. Forty of them were coated to reflect the 850 nm reference light and transmit the 580 nm sensor light. Twenty units were coated for use as mirrors for the reference signal.
- Mechanical parts for eight complete optical blocks were fabricated.

Eight complete optical modules were assembled and tested (Figure 4). The light power levels before and after the optical prisms were determined and validated for our application. As for the Tx-Rx board, hardware problem reports and engineering change requests have been generated and solutions suggested.

Studies confirmed the stability of the output light in all eight channels of the system using LEDs for the sensor signal and lasers for the reference signal. However, we observed that variations in the laser reference signal differ from the variations in the LED sensor signals under varying environmental conditions and depending on the optical fiber connected to the system. In particular, the laser light transmitted through the fiber was more sensitive to these varying conditions than the LED light. Such a difference in effect between reference and sensor signal could compromise system performance.

We modified the optical blocks, replacing the laser reference with LEDS at a similar wavelength (850 nm), since those had demonstrated better stability.

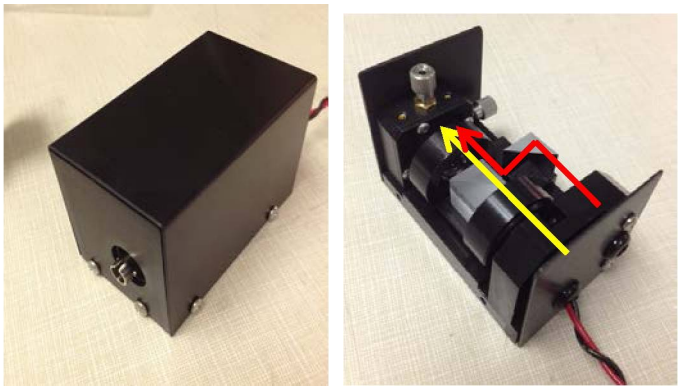

Figure 4 Tx optical module.

Integrate System. Once the design of each circuit or optical element was tested, and modified when required, the system was integrated in the following steps:

1. Integration of Tx-Rx board and Tx optical modules
2. Integration of Tx-Rx board and photodetector module
3. Integration of Tx-Rx board and power supply module
4. Integration of control board and graphical user interface
5. Integration of Tx-Rx and control boards
6. System integration, including the Tx-Rx board, control board, optical modules, and power supply units
7. Assembly of first SUS-CO2-DICAST unit (Figure 5).

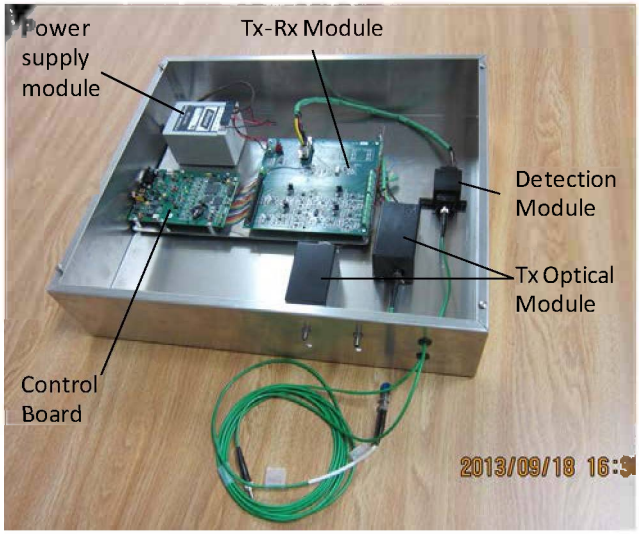

Figure 5 First unit of the SUS-CO2-DICAST system.

3.4 Subtask 3.4 – Conduct System Verification/Validation and Design Review

At the conclusion of system integration, the entire system was tested and the main functionalities have been characterized. That includes system stability, signal stability, and signal-to-noise ratio.

System stability. The system was demonstrated to be stable in regular operation, and no problem was found in the course of the four tests conducted, operating the system continuously.

Signal stability. After around five minutes of system stabilization, the signal level was stable in the tests under ambient conditions (signal variation <1%). However, the signal level was affected by varying temperature, with variation >1% in the temperature range of 20°C to 40°C. Compensation of the sensor signal with the reference signal, using the revised optical block, was an effective way to correct for temperature variations.

Signal-to-noise ratio. The initial tests to determine the signal-to-noise ratio were performed with fiber optic sensor segments 5 and 25 m long. Figure 6 shows the sensor signal profile when a 25 m segment was exposed to varying levels of CO_2. The noise was determined as the standard deviation of 50 consecutive measurements at 5% CO_2, at ambient temperature and pressure, and at 50% RH. Data was collected at intervals of 10 s, integrating and averaging the signal over the 10 s. Lower acquisition frequencies, compatible with the final application, will result in longer integration times and lower noise. The noise level was 0.0003 V for a median signal of 0.8979 V, which results in a signal-to-noise ratio of 30:1.

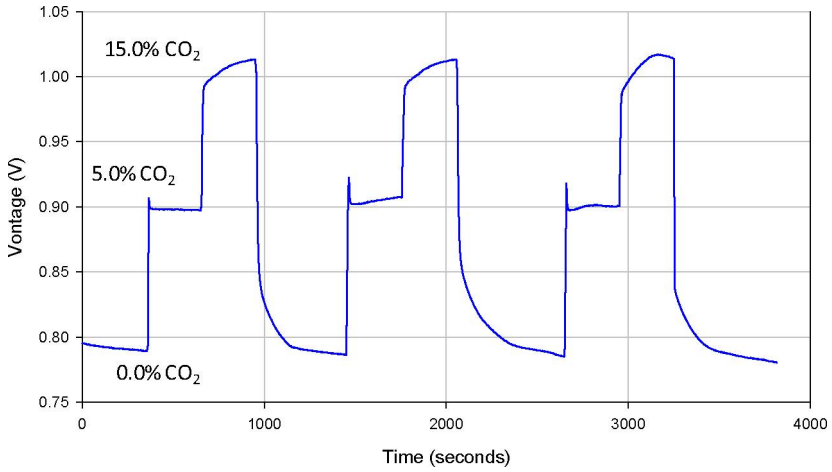

Figure 6 Response profiles of a SUS-CO2-DICAST system CO_2 fiber optic sensor segment to varying levels of CO_2.

Additional tests were performed in which the signal from the fiber optic sensors was recorded in parallel through an Ocean Optics USB4000 spectrometer with optics upgraded to Jazz configuration. Figure 7 shows that the noise-to-signal ratio of the SUS-CO2-DICAST system compares well to the bench-top instrument readings.

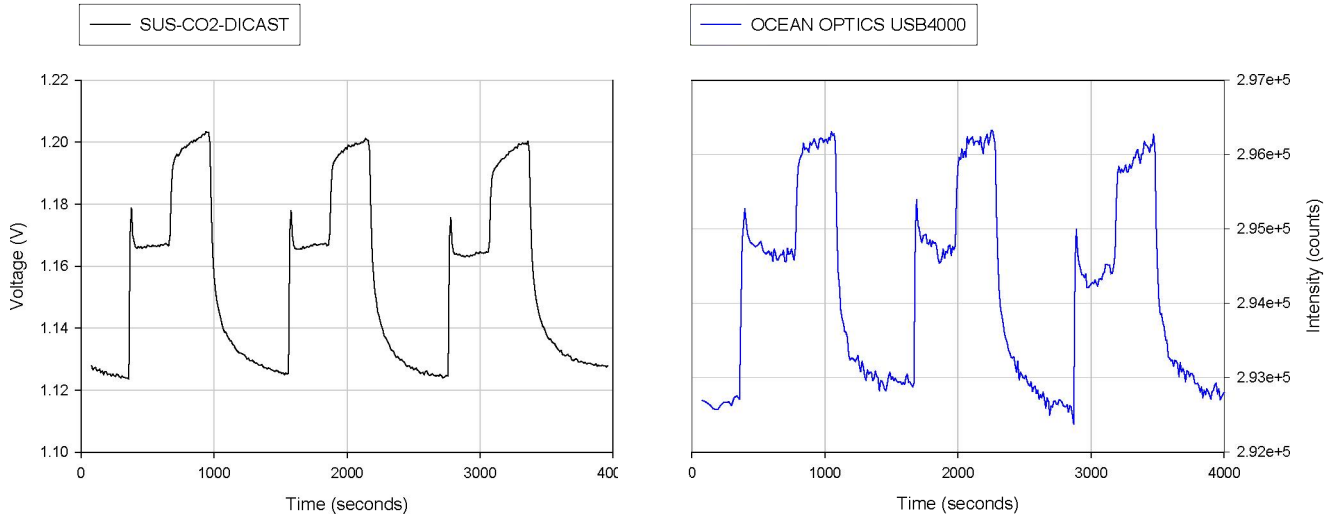

Figure 7 Response profiles of a CO_2 fiber optic sensor segment to varying levels of CO_2, comparing the SUS-CO2-DICAST system and USB4000 spectrometer.

4.0 *TASK 4.0* DEVELOP ENHANCED SENSITIVE MATERIALS

The purpose of this task was to formulate and fabricate sensor cladding materials exhibiting improved stability at elevated temperature, and enhanced light transmission for long fiber optic sensors. We prepared candidate sensor structures by coating layers of doped polymers onto optical glass slides, as initial substitutes for the optical fibers. This first approximation enabled us to rapidly fabricate and test a wide battery of sensitive materials. The selected materials were then used in Task 5 to fabricate fiber optic prototypes. Based on the result obtained with the fiber optic sensors, the sensor formulations were reviewed and new cladding materials were evaluated coated

on glass slides, repeating the process until we achieved the desired sensor performance. The work flow is shown in Figure 8.

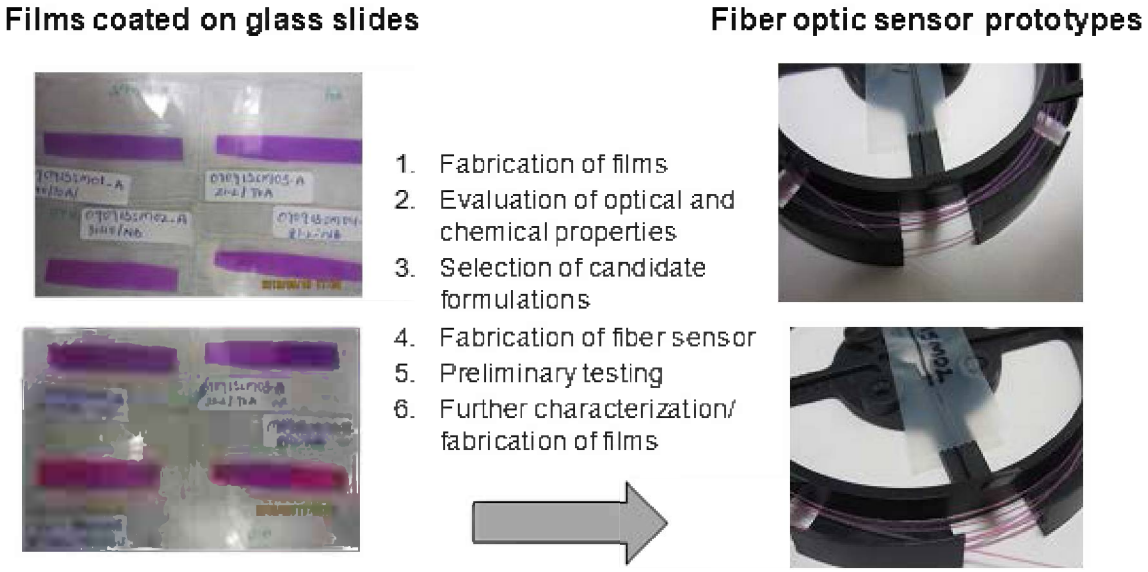

Figure 8 Sensor materials coated on glass slides for preliminary evaluation and fiber optic sensor prototypes fabricated with the selected formulations.

4.1 Subtask 4.1 – Prepare and Test Sensor Materials with Enhanced Light Transmission

In our effort to enhance the light transmission properties of the fiber optic sensors, we evaluated UV curing polymers designed for high gas permeability, and good transmission in the visible region of the spectrum.

The four base polymers tested were:

- IOS-690-4 UV (IOS proprietary formulation) UV curing urethane-acrylic hybrid polymer
- IOS-137 UV (IOS proprietary formulation) UV curing urethane-acrylic hybrid polymer
- OFF 208 (from Shin-Etsu) UV curing silicone-based polymer (formulation not provided by the supplier)
- IOS-21-2 UV (IOS proprietary formulation).

A set of films coated onto glass slides (at least six samples) without the indicator chemistry and a corresponding set incorporating the indicator chemistry were prepared for each of the polymers we wanted to evaluate. The preparation protocols were optimized for fast curing. Once optimized, all four UV curing polymers, prepared according to similar formulation protocols, were evaluated for their optical properties. Based on previous results using the heat curing polymers DC-1944 and DC-3140, these four UV curing polymers were examined in the presence and absence of POSS-OH. Transmittance—at a range of wavelengths, and refractive index *n* at 580 nm, and sensitivity to CO_2 under ambient and higher temperature conditions—was evaluated for each type of film. The results are summarized in Table 2, and the transmission spectra are shown in Figure 9.

Table 2 Optical Characteristic Features and CO_2 Sensitivity of Four Candidate Polymers

Polymer	Without Indicator Chemistry			POSS-OH	With Indicator Chemistry			n	Sensitivity** to 1% CO_2 at Ambient
	T# 532* nm	T# 580* nm	T#800* nm		T# 532* nm	T# 580* nm	T#800* nm		
IOS-137	96%	96%	97%	Y	69%	62%	88%	1.456	1.41±0.03
				N	NA	NA	NA	NA	NA
IOS-6904	98%	98%	98%	Y	85%	73%	98%	1.442	1.31±0.01
				N	82%	67%	98%	1.442	1.70±0.01
OFF 208	99%	99%	99%	Y	74%	57%	91%	1.437	1.14±0.01
				N	70%	59%	93%	1.437	1.48±0.04
IOS-21-2	99%	99%	99%	Y	84%	65%	98%	1.425	1.18±0.01
				N	87%	71%	98%	1.425	1.31±0.01

*T# Optical transmittance determined for 10 μ thick films.

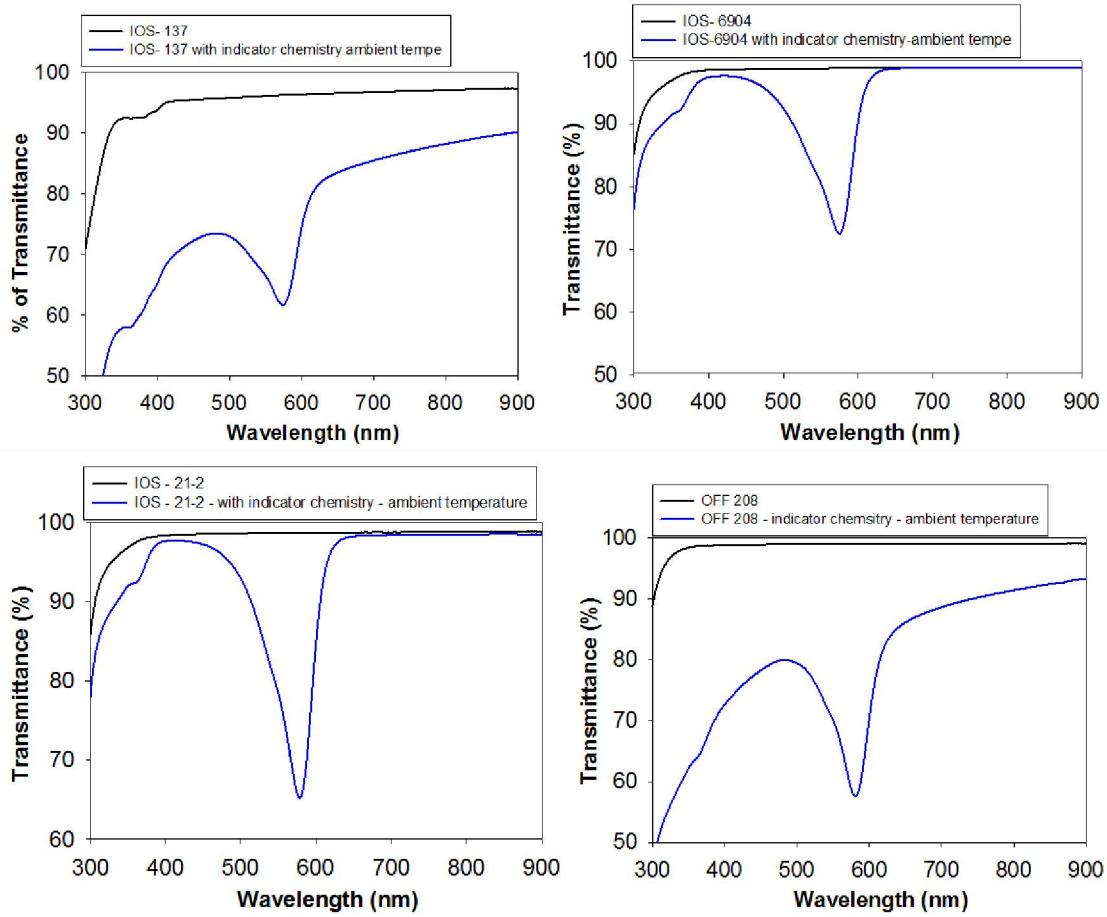

Figure 9 Transmittance spectra of sensitive materials fabricated with four UV curing polymers.

All four polymers exhibited notable advantages in optical properties over the matrixes previously used, DC-1944 and DC-3140, all showing sensitivity to CO_2. Incorporating the indicator chemistry reduced the transmittance of the films prepared with IOS-137, IOS-6904, and OFF 208, but did not affect the excellent transmittance of films prepared with IOS-21-2. Therefore, IOS-21-2 polymer emerged as the most promising candidate for the preparation of fiber optic sensors. Further studies on these sensing polymers with respect to their stability at elevated temperature and in water, and their response to CO_2, were conducted in Subtask 4.2.

4.2 Subtask 4.2 – Prepare and Test Sensor Materials with Enhanced Stability at Extreme Conditions

To improve stability at elevated temperature, we prepared sensors with three polymeric layers as shown in Figure 10.

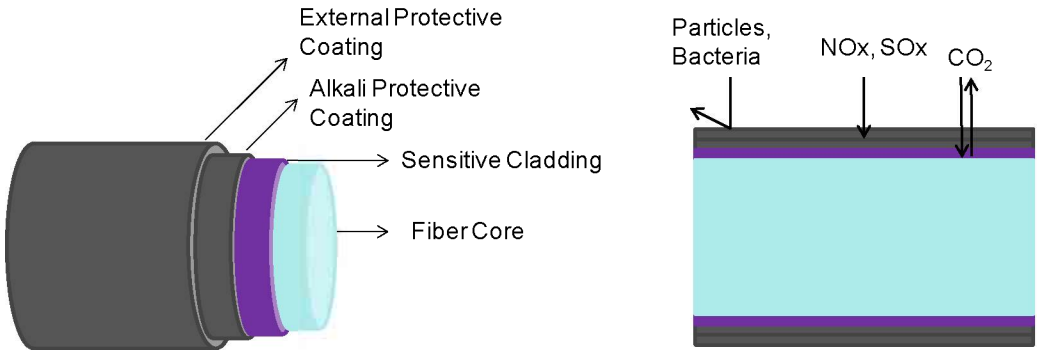

Figure 10 Sensor designed for improved resistance to temperature and corrosive media.

Sensitive Cladding Material. The sensitive fiber cladding is a gas-permeable, water-impermeable polymer embedded with a chemical mixture optically sensitive to CO_2 level variations.

Alkali Protective Coating. The alkali protective coating is a gas permeable polymer loaded with a hydrophobic base (tetraoctylamonium hydroxide).

External Protective Coating. The external protective coating is a gas permeable polymer made of commercial silicone rubber, which can be loaded with biocides.

The protective layer improves sensor stability, and at the same time gives us more flexibility in selecting cladding material with good optical properties, since some polymers that exhibit high light transmission have limited chemical stability, and thus would not be suitable alone for the sensor use, but can be stabilized and used as sensitive cladding.

Activate Glass Surface. During the test we conducted at elevated temperature, and in fabricating fiber optic prototypes, we observed that the interface between the sensitive cladding and the glass could be critical to the optical transmission of the fiber and to sensor stability at elevated temperature. Fiber optic sensor prototypes we prepared with the same cladding formulation but different fiber cores resulted in fiber optic sensors exhibiting very different light transmission features, which can be explained by their core-cladding interfaces. Films prepared with the selected polymers were observed to delaminate from the glass when tested at elevated temperature in water, while maintaining the integrity of the film, suggesting that the cladding-glass interface is the weakest zone of the sensors.

We incorporated into the sensor fabrication process a treatment of the supporting glass surface to improve adhesion between the cladding material and the fiber optic core. The glass surface was

activated by a short exposure to fluoride anions, in the form of either ammonium fluoride or a combination of ammonium fluoride and hydrogen fluoride.

Based on this three-layer design, we prepared candidate sensor structures by coating layers of doped polymers onto optical glass slides, as initial substitutes for the optical fibers. This first approximation enabled us to rapidly fabricate and test a wide battery of sensitive materials. Over 100 different formulations were prepared and tested, and for many of those several replicates were fabricated to evaluate repeatability.

Test Sensor Materials at Elevated Temperature. Among the extreme conditions under evaluation (elevated temperature and pressure, low pH, high salinity, presence of nitrous oxides or sulfur oxides…), elevated temperature is the most challenging, and for that reason our first screening evaluation addressed the performance of the candidate cladding materials at elevated temperature.

All the formulations we prepared were evaluated for stability at elevated temperature, starting at 80°C. Those materials showing good stability in the screening tests were further evaluated for thermal stability and sensitivity at 80°C, for monitoring dissolved CO_2. Formulations selected based on their thermal stability at 80°C were selected for fiber fabrication and the sensors were evaluated at temperatures up to 175°C (Task 5).

From the initial sensor materials evaluated to the final sensor materials selected and further studied, we saw a significant increase in thermal stability and sensitivity. The improved protective coating, the selection of the hydrophobic base, and the activation of the glass surface have all contributed substantially to meeting our stability objective. Figure 11 shows the typical response of the films to the thermal stability and sensitivity tests, and the evolution in sensor material performance through the project. A significant drift in the sensor signal of sensor materials initially tested is observed, and sensitivity to CO_2 is not detected. In the plots showing the response profile of the sensor materials developed in the first and second reporting periods, sensitivity to CO_2 is observed, and the signal does not drift down during the tests. In the plot showing the results obtained with the formulation developed in the third reporting period, a stable sensor signal, good sensitivity, and excellent reversibility are observed. In our revised testing protocol, the sensor materials are exposed to 3% and 16% CO_2 during the test at 80°C, which results in dissolved CO_2 concentrations equal to those reached with 1% and 6% CO_2 at 25°C and at atmospheric pressure (CO_2 solubility decreases with temperature). Nevertheless, the enhanced stability of the sensor materials prepared in the third reporting period, taking advantage of the preparation strategies discussed above, is clear in Figure 11. The stability of those sensitive cladding was further enhanced later in the project in Task 5.

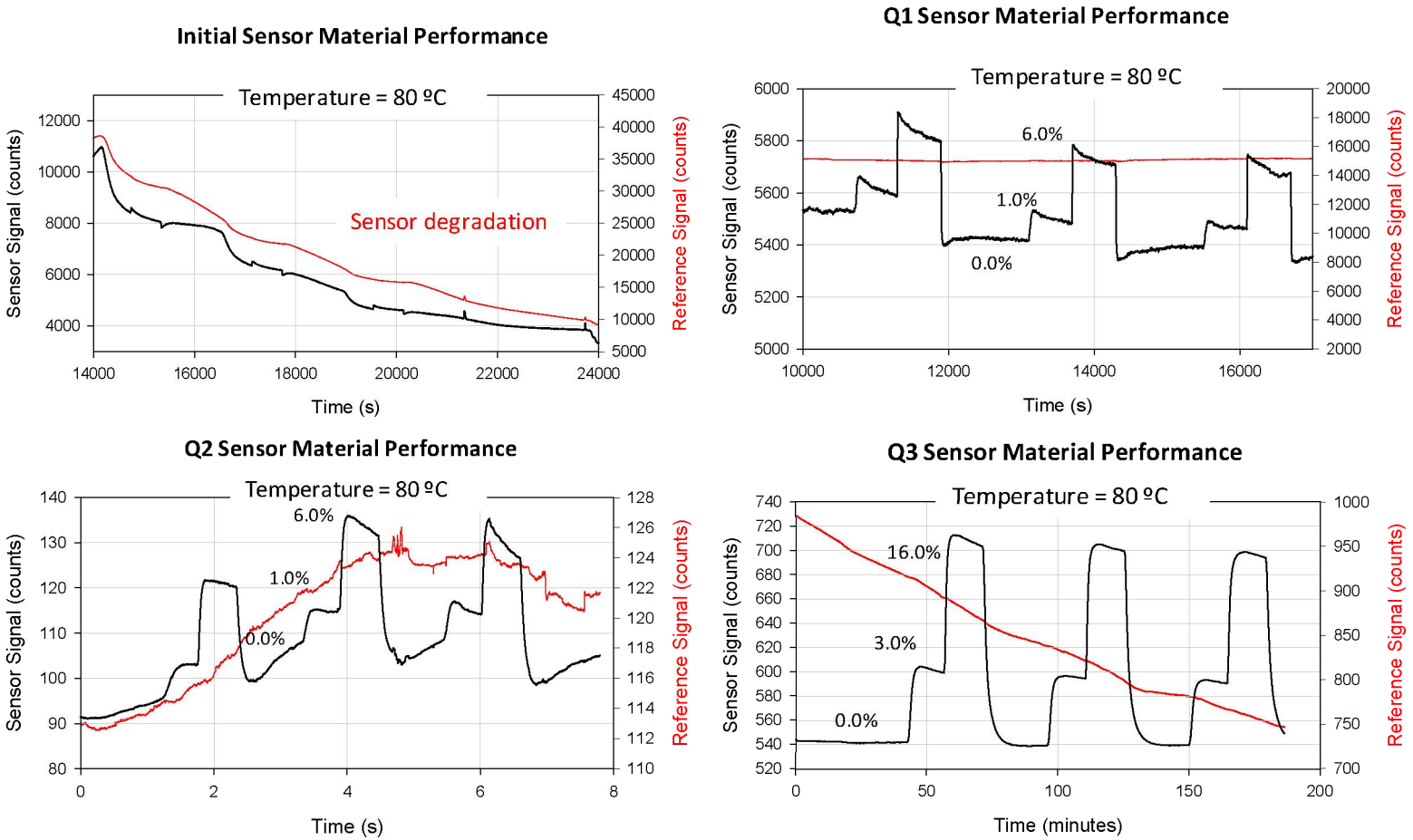

Figure 11 Response profiles of CO_2 sensitive sensor materials prepared in the first nine months of the project, when exposed to water equilibrated at variable levels of CO_2 at 80°C.

Test Sensor Materials at Corrosive Conditions. Based on thermal stability results, we tested a selection of sensor materials for resistance to pH 4 and salinity up to 250,000 ppm of NaCl. Only sensor materials prepared with polymer 21-2 showed limited resistance to the testing conditions, and that was overcome by activating the glass surface.

As we were progressing in Task 4, candidate formulations, using both heat curing and UV curing polymers, were being selected for fiber optic sensor fabrication in Task 5. Further studies were conducted with the optical fiber sensors as describe below until the selection of the final sensor formulation and fabrication protocol.

5.0 *TASK 5.0* SELECT AND COAT OPTICAL FIBER PROTOTYPES

5.1 Subtask 5.1 – Fiber Sensor Design

Designing the fiber sensor involved selecting the optical fibers for the distribution segment and selecting the core and cladding for the sensor segment. We initially selected the optical fibers for the distribution segment based on their numerical aperture, transmission properties, and cost. The main characteristics were:

- Supplier: Polymicro Technologies
- Core 110 ± 4 μm, Low-OH, NA = 0.48 ± 0.03 or NA = 0.37 ± 0.03
- Hard polymer cladding 130 ± 10 μm
- Cost for 40,000 m $16,000.

5.2 Subtask 5.2 – Fiber Sensor Prototype Fabrication and Testing

We initially implemented fabrication protocols to fabricate sensor fiber tens of meters long at IOS, using an optical fiber spooling machine built specially for fiber coating. With this system we can cost-effectively prepare and test a number of fiber optic sensor prototypes in the course of sensor development. Our initial plan was to retain the services of a fiber optic manufacturer for the industrial production of the sensors, once the core material, cladding material, and general conditions for coating were established. However, in the course of the project we expanded the fabrication capabilities at IOS, with both UV curing and heat curing systems, and we were able to produce sensors fast enough to manufacture thousands-of-meter-long sensors at IOS, without the need of external services.

Based on the stability and optical property characterization performed in Task 4, we selected sensor materials fabricated with the UV-curing polymer IOS 21-1 as the first candidates for fiber optic sensor fabrication. In addition, we selected formulations with the heat curing polymers DC 3-1944 and D3140. Those materials, protected with the proper alkali coating and external coating, have also shown great potential in the stability tests, and the industrial fabrication of fiber optic sensors using these RTV silicone rubbers had already been demonstrated in previous work.

UV-Curing Polymer. The conditions for coating the fiber depend on the polymer selected for the cladding. With this system and commercial low-cost fiber ("test fiber"), we optimized the manufacturing parameters for 21-1-based coatings. The operating parameters are first defined for a particular polymer and test fiber, and then the actual fiber (glass core treated with NH_4F) was used to prepare the fiber optic sensor.

The critical parameters we optimized were the tension applied to the fibers, the coating thickness, the spooling speed, and the total light power. The most challenging parameter is the light power for curing the polymer, because there is a very narrow margin between the minimum light power

that can cure the polymer and the maximum light power the indicator chemistry can receive before being photo-degraded. In order to control the light power applied to the coating, three variables were studied:

- *Light source*: Three light source setups were evaluated, listed here in order of increasing light power.
    - EFOS Ultracure 100SS PLUS unit
    - Fusion model Reflectance lamp system (from Fusion UV Systems Inc.), which includes an I300MB UV irradiator bulb, a P300M power supply, and a Reflectance module
    - Fusion model F300 lamp system (from Fusion UV Systems Inc.), which includes an I300MB UV irradiator bulb, a P300M power supply, and an R500 reflector.
- *Length of the light source window*: A metallic opaque tube with a window in the center is placed in the light source setup. The cladding material is only exposed directly to the light passing through the window. The length of the window can be varied from 6.7 to 0.25 in., which enables us to control the curing time for a particular spooling speed.
- *Spooling speed*: The faster the fiber is spooled, the shorter the exposure to the light source. The optimal spooling speed also depends on the viscosity of the polymer, and there is a minimum speed required to produce a homogenous cladding.

Over 60 setting were evaluated to establish the initial conditions for producing fiber optic sensor prototypes with cladding materials based on the 21-2 polymer. In each test, the cladding homogeneity, the indicator chemistry integrity, and the polymer curing were evaluated. The best parameters for producing the fiber optic prototypes were finally established as: Fusion model F300A lamp system, spooling speed between 4.0 and 4.7 feet/minute, and a 0.5 in. optical window. Figure 12 shows segments of test fiber coated with the selected cladding formulation. Figure 13 shows the fiber spooling machine as used to produce fiber optic sensor prototypes.

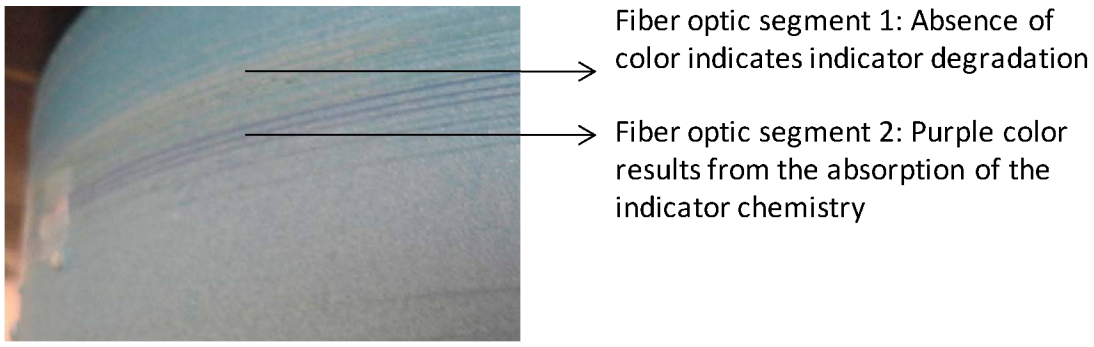

Figure 12 Collecting spool with several segments of the test fiber coated with the selected cladding material at various conditions. The purple color in Segment 2 in the picture reveals the integrity of the indicator chemistry after fiber fabrication.

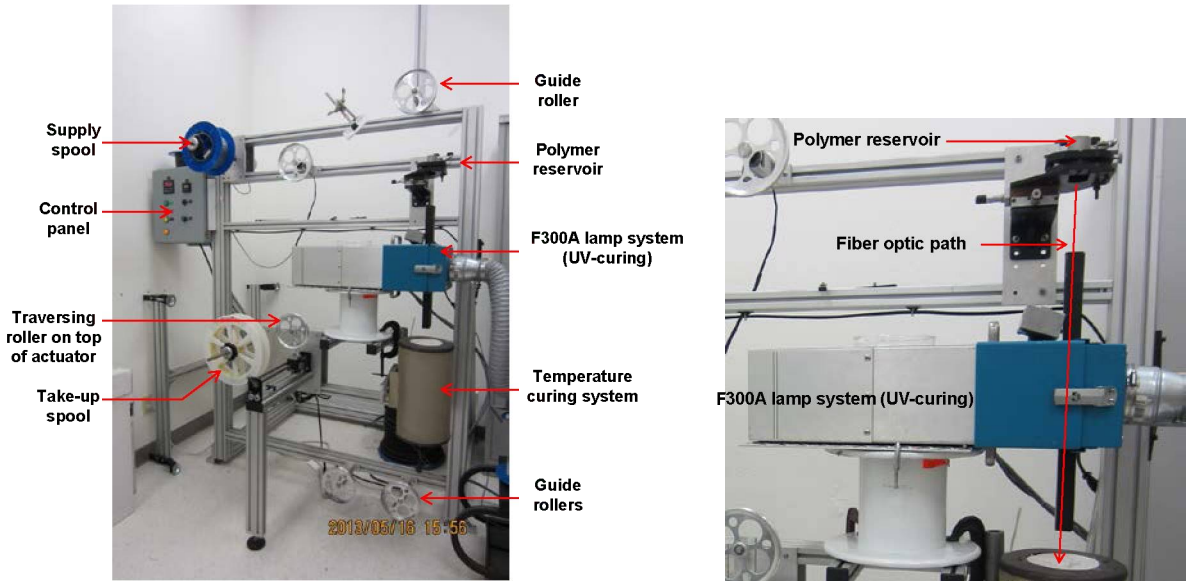

Figure 13 Fiber optic spooling machine equipped with a Fusion model F300A lamp system.

Once the fabrication parameters were set using the test fiber, the first prototypes of coating-treated glass-core fiber with polymer 21-2-based cladding were produced and tested to validate the fabrication protocols, showing excellent sensitivity and reversibility (Figure 14). Several batteries of fiber optic sensors were then produced for further characterization.

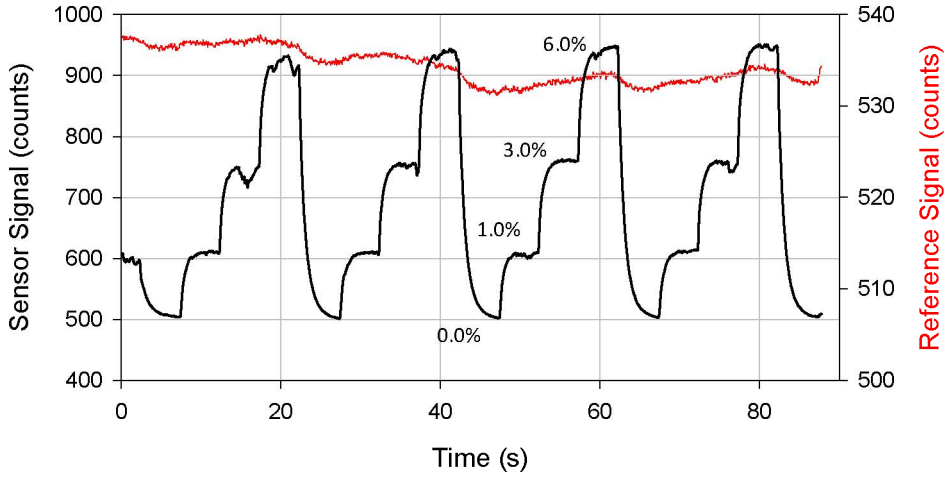

Figure 14 Response profile of a CO_2 fiber optic prototype produced with polymer 21-2-based sensor material as the cladding, after exposure to four levels of CO_2.

Heat-Curing Polymer. Prior to sensor fabrication, a glass core bare fiber was treated with NH_4F. The treatment was performed on the spooling machine, which enabled us to produce hundreds of meters of treated fiber in a reasonable time, and to accurately control the treatment conditions for repeatability. Furthermore, this enabled us to implement the fiber treatment in-line with the fiber coating process.

In prior work, IOS had established the optimal conditions for fabricating fiber optic sensors with the heat-curing polymers DC 1944 and DC 3140. Those conditions were refined for the new

formulations prepared for enhanced stability, and a first batch of fiber optic sensor prototypes was produced (Figure 15).

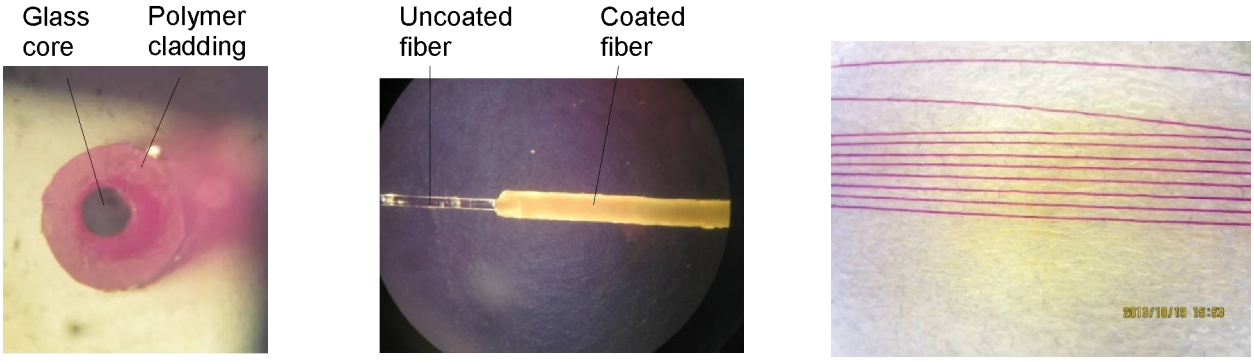

Figure 15 Fiber optic sensor prototypes fabricated at IOS.

Ten-meter segments were cut for testing purposes and placed in flow-through cells specially designed for sensor testing. IOS has demonstrated that the analytical characteristics can then be extrapolated to longer sensor segments, with sensitivity proportional to the sensor length, while the measurement range, response time, and stability do not depend on the length of the sensor segment. The objective of those tests was to validate the fabrication protocols. To test the sensor fibers for monitoring dissolved CO_2, we pumped water equilibrated with known levels of CO_2 through the flow cell by means of a peristaltic pump. For further details of the experimental setup, see the progress report from January 30, 2013. The fiber optic sensors were initially tested for measurement range and sensitivity for monitoring dissolved CO_2 at ambient conditions. The sensors showed excellent reversibility, measurement range from 0 to 75% CO_2, or 0 to 1,200 mg/L (ppm) of dissolved CO_2, and a limit of detection below 2 mg/L (for the 10 m segments). The limit of detection for 50 m segments would be below 0.5 mg/L. Figure 16 shows the typical response profile of the fiber optic sensors.

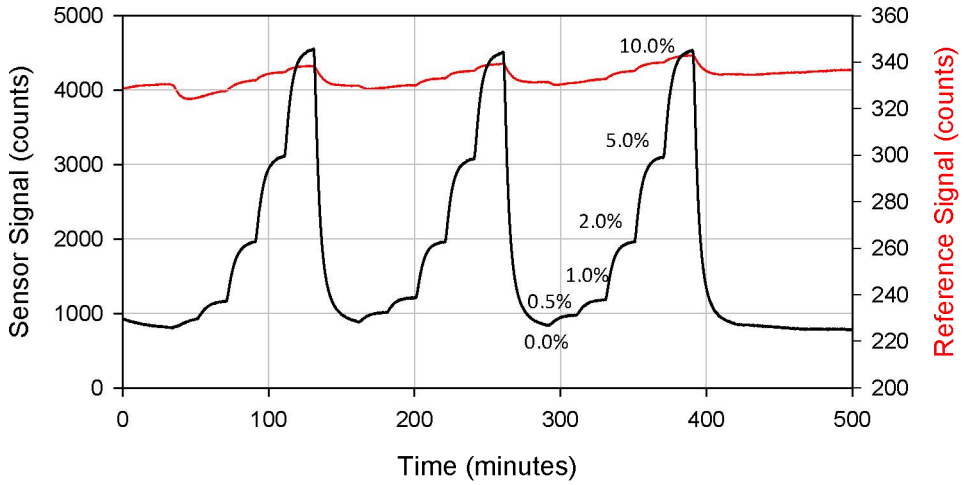

Figure 16 Response profiles of a CO_2 fiber optic prototype immersed in water equilibrated with six levels of CO_2.

The fiber optic sensor prototypes were tested for resistance to corrosive liquids. The tests included sensor behavior at pH 4, at salinity of 250,000 ppm, and exposure to traces of NO_2. The response

profile of the fiber sensor at pH=4 is shown in Figure 17. The sensor exhibits reversibility and stability at low pH equal to those when it was tested in pure water. The protective coating proved to be very effective, and the external pH of the matrix did not affect the sensor behavior. The slow variation of the sensor signal observed in Figure 16 when the CO_2 level changed is mostly due to the equilibration time of the solution to the CO_2 conditions.

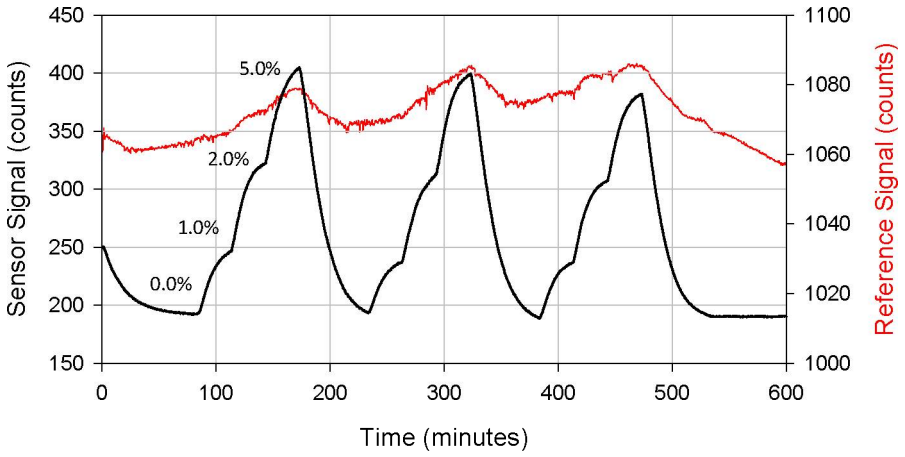

Figure 17 Response profile of a CO_2 fiber optic prototype immersed in a pH 4 solution equilibrated with four levels of CO_2.

The fiber optic sensors were tested at varying salinity up to 250,000 ppm of NaCl, similar to the salinity in subsurface brine. The response profile of the sensor is shown in Figure 18. Excellent reversibly and good sensitivity were observed. As mentioned above, the selected protective coating and cladding materials were resistant to the corrosive conditions, and sensor operation was not affected by the salty matrix.

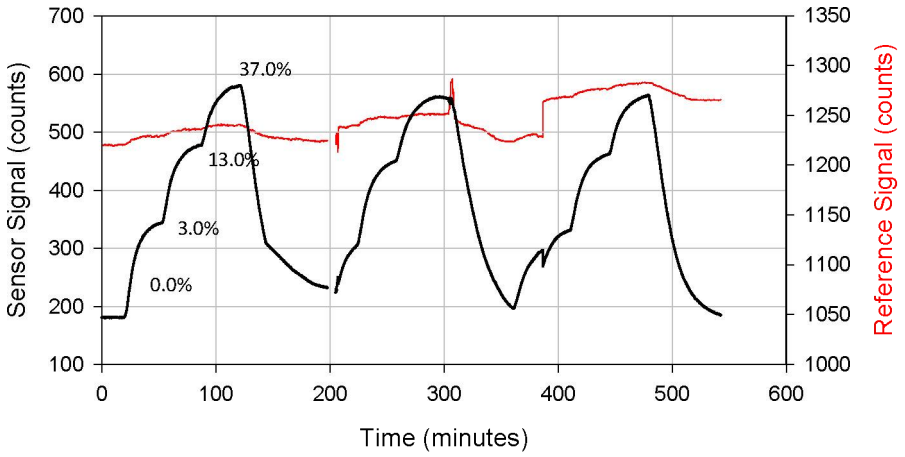

Figure 18 Response profile of CO_2 fiber optic prototype immersed in a 250,000 ppm NaCl solution equilibrated with four levels of CO_2.

Finally, the sensor was tested with an aqueous solution exposed to a constant flow of nitrous oxides. The response of the sensor to CO_2 before and after the release of NO_2 into the water was very similar (Figure 19).

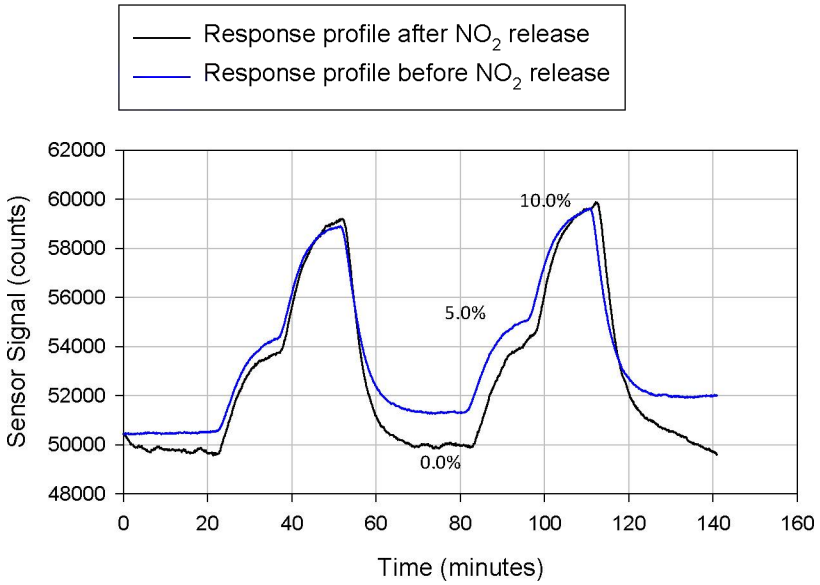

Figure 19 Response profile of CO_2 fiber optic prototype immersed in solution before and after equilibration with traces of NO_2 (40 ppm) and equilibrated with three levels of CO_2.

6.0 *TASK 6.0* PERFORM INDUSTRIAL FABRICATION OF FIBER OPTIC SENSORS

We first upgraded our fiber optic recoating system and expanded our capabilities for producing long fiber optic sensors with the UV-curing system. Fiber optic sensors were prepared in-house at a rate of 4.5 m/min., so we can fabricate a 100 m long sensor in 22 min. (2,000 m/day), a production rate similar to that of the sensor fabrication previously performed for us by Polymicro Technologies, an optical fiber manufacturer. Our capability for industrial fabrication of long sensors in-house was established, which resulted in cost-effective production.

In addition, based on the data collected with that first sensor batch produced using heat curing polymers, we further reviewed the heat curing system and decided to implement a long curing oven that enables us to increase the fabrication speed with those polymers. This gave IOS the capability of producing sensors in the length range requested for the project (lengths up to hundreds of meters with temperature curing polymer) and for future products. That completed our capability for manufacturing sensors at a reasonable scale.

Fiber optic sensors fabricated at IOS were connected with distribution segments to create sensor cables up to 3,000 m in length, and CO_2 monitoring was performed in the laboratory.

7.0 *TASK 7.0* PERFORM ACCELERATED DEGRADATION TEST DESIGN

We designed tests based on the philosophy of Highly Accelerated Life Test (HALT), which we refer to as Accelerated Degradation Tests (ADT). As in HALT, the first step in the ADT testing was to collect information that enabled us to improve sensor lifetime. The ADT design included high power sensor illumination (one day of illumination can simulate up to two years of real sensor operation), exposure to elevated temperature, exposure to corrosive water, and exposure to highly biologically contaminated media.

ADT Study for CO_2 Monitoring in Gas Phase – Elevated Temperature. We initiated the ADT studies exposing the fiber optic sensor cyclically to elevated temperature and ambient temperature,

which was shown to be a factor in sensor lifetime; this is a standard protocol in Highly Accelerated Life Testing of sensors for other devices. Based on the results of the first study, the sensor was modified to improve robustness. The sensors that best withstood the elevated temperature tests were selected for evaluation under other stress conditions. Similar protocols for cyclically exposing the fiber optic sensor to varying temperature were designed and optimized for sensor operation in gas and water. The ADT protocol is represented in Figure 20. Fiber optic sensors were tested before and after each temperature cycle, which lasted 8 hours.

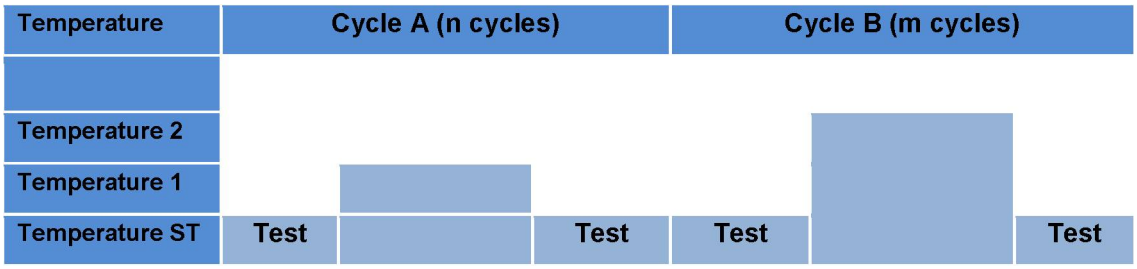

Figure 20 ADT protocol for exposing the sensor cyclically to varied temperatures.

Sensors prepared with low molecular weight hydroxide (LOH) in the sensitive cladding showed stability superior to those prepared with high molecular weight hydroxide (HOH). The best two formulation were 012014SM01 B and 012014SM01 C. Both fibers showed greater stability than any other fiber sensors, and withstood exposure to 120°C. When exposed to 150°C, the fibers seemed to hit a breaking point; the sensor signal exhibited significant changes.

After a number of ADT studies and based on the data collected, the procedure for fabricating the EOH fibers was further improved, enhancing stability. The final fiber optic sensor prototypes showed good sensitivity and stability operating at up to 150°C.

Also based on the observations during the ADT studies, a different fiber formulation from all those previously used throughout the project was fabricated and subjected to ADT in gas phase, with neither LOH, HOH, nor MOH as base; rather, the internal alkalinity is due to the incorporation of nanoblocks. **This fiber proved extremely stable in the ADT studies conducted in water. We demonstrated that this new fiber is also stable in gas phase, and its operation in the temperature range from 80°C to 175°C** is reported in Section. 2.1.3, Task 8 – Sensor System Analytical Characterization.

ADT Study for CO_2 Monitoring in Aqueous Matrices. ADT studies for CO_2 monitoring in aqueous matrices included subjecting the sensor to temperature cycles, high water flow, corrosive solutions (elevated salinity and low pH), and biologically contaminated media.

ADT Aqueous Matrices - Elevated Temperature

The protocol was similar to the one for the ADT studies for monitoring CO_2 in gas phase, but the sensors were only exposed to temperature A, which was set at 70°C. Because these tests were conducted at ambient pressure, operation for hours at high temperature quickly evaporated the water, degrading the repeatability of testing conditions and producing unrepresentative results. The selected sensors were later subjected to higher temperature in Task 9 – Evaluation of the Sensor System in Simulated Field Conditions.

The fiber sensors prepared with no hydroxide base but nanoblocks exhibited superior stability. Further analysis extending the fiber exposure time at elevated temperature confirmed the great stability of these sensors. The transmission at the absorption band of the indicator chemistry did

not vary, although the attenuation of the fiber at longer wavelengths is affected, as seen in Figure 21, which shows the spectra recorded in the ADT study.

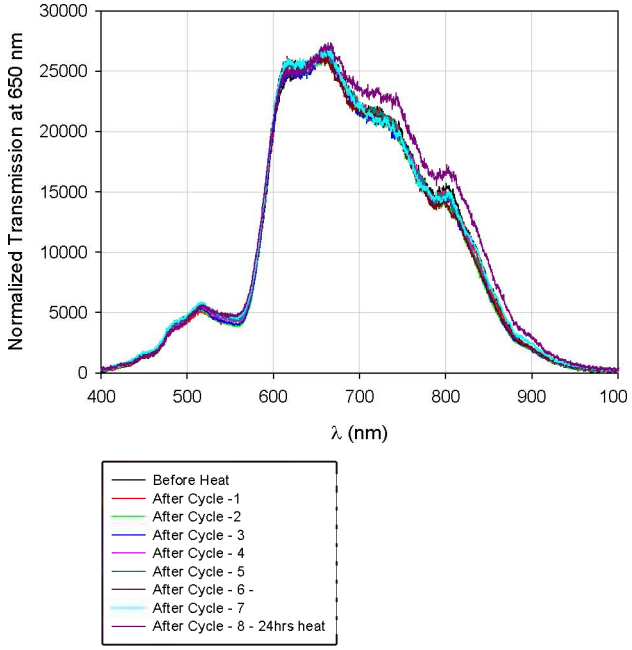

Figure 21 Transmission spectra for selected fiber optic sensors in ADT study.

In addition to their transmission properties, the responses of the sensors to varying levels of CO_2 under standard conditions were recorded and used to evaluate sensor stability. Figure 22 shows the sensitivity (Normalized Sensor Signal = Transmission at 575 nm/Transmission at 575 nm in nitrogen) for the two types of fiber sensors under evaluation in these tests.

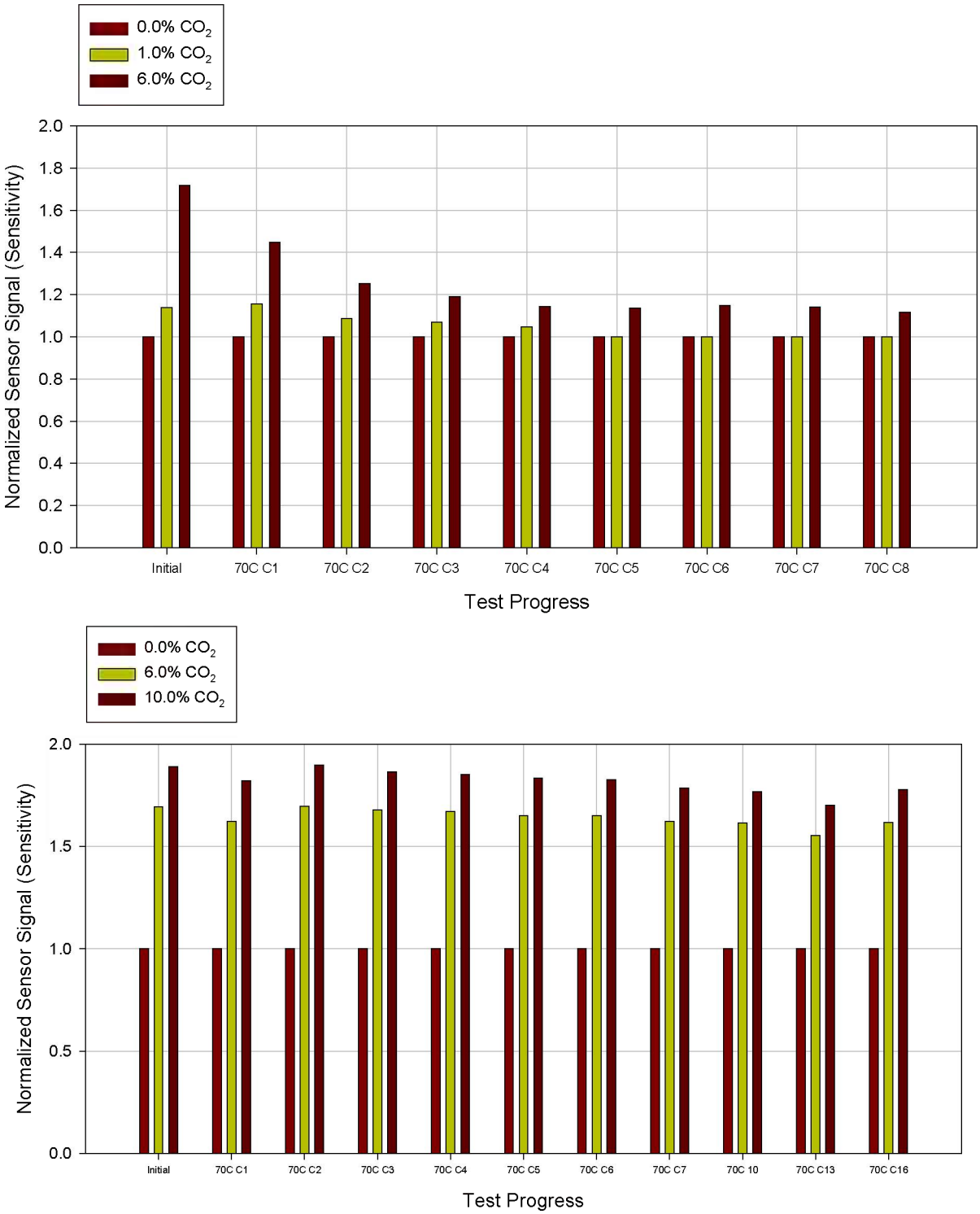

Figure 22 Sensor response to varying levels of CO_2 for fiber optic prototype fabricated with formulation hydroxide base (top) and nanoblock base (bottom) during ADT test. Normalized Sensor Signal = Transmission at 575 nm / Transmission at 575 nm in nitrogen.

The response of the sensors prepared with nanoblock base to varying levels of dissolved carbon dioxide was stable throughout the ADT study. Further analysis has confirmed their potential for

subsurface monitoring at elevated temperature and for long term monitoring. Figure 23 shows 16 or 17 cycles of ADT stress for this fiber, in contrast with the standard 8 cycles applied to all our sensors, which include hydroxide bases. Continuous operation for more than two months at elevated temperature has been also conducted.

Figure 23 (left) compares the sensor degradation when exposed to the stress conditions of the ADT (cycle of elevated T and low T), and when operated continuously at elevated temperature. The faster decrease in sensitivity during the ADT cycles in comparison with normal operating conditions validates the strategy of this study. Only eight cycles of our ADT protocol degrade the sensor significantly more than two months of continuous operation. By comparing sensor degradation under the two conditions we can calculate that eight ADT cycles actually corresponds with three years (1095 days) of sensor operation at constant temperature, as shown on the right graph of Figure 23. This calculation could be refined by adding more data.

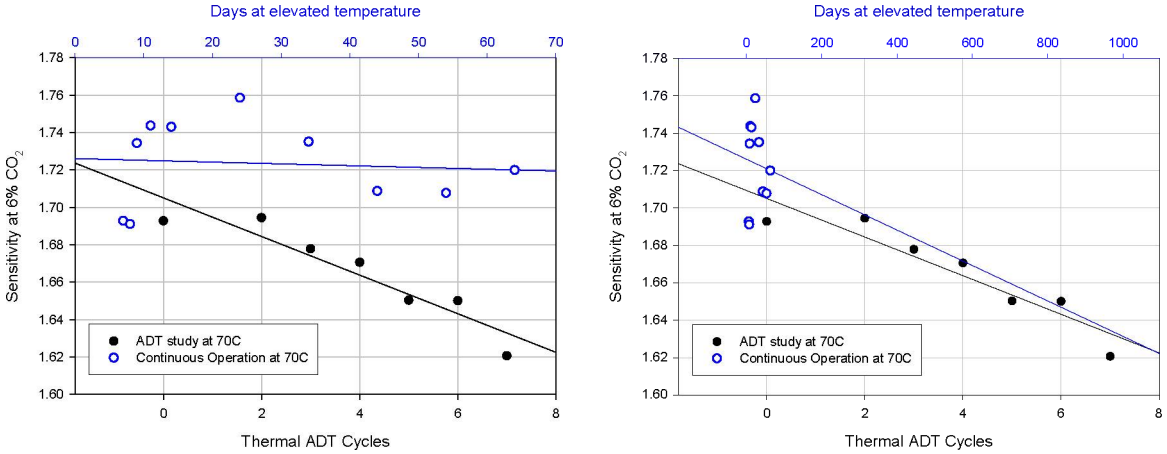

Figure 23 Comparison of the change in sensor sensitivity (and therefore calibration parameters) through ADT studies and during continuous sensor operation at elevated temperature. Sensitivity = Transmission at 575 nm / Transmission at 575 nm in nitrogen. Note the difference in time scale at the top of the two plots.

From the data collected both in the ADT tests and during continuous operation at elevated temperature, we can estimate the potential of the sensor for long-term monitoring. Our target was to demonstrate sensor performance for at least five years, after which the sensors should be either replaced or recalibrated. Figure 24 shows calculations made for continuous sensor operation over five years at the established conditions of the ADT studies, which correspond to sensor deployment at a depth of 1,000 m. Two sets of the experimental data are considered for the calculation and function adjustment: one adjustment uses the full set of data collected, and a second adjustment has been made removing the extremes of the data set. Based on these calculations, at the end of five years of operation the deviation of the system reading from the actual value would be 35%-40%. A linear correction of the calibration function with time, which is typically applied in our sensor system, would significantly reduce this deviation. More importantly, after five years the sensor would maintain full capability of detecting CO_2 leaks and monitoring plume migration. Depending on the injection project requirements, the sensor could be kept in operation without further calibration, or could be recalibrated so that replacement would not be necessary. From this data and using the most conservative data adjustment, we can predict a sensor lifetime of over 10 years, defining the sensor as not being operative when its sensitivity reaches a value of 1.05 (Transmission at 575 nm in 6% CO_2/Transmission at 575 nm in nitrogen).

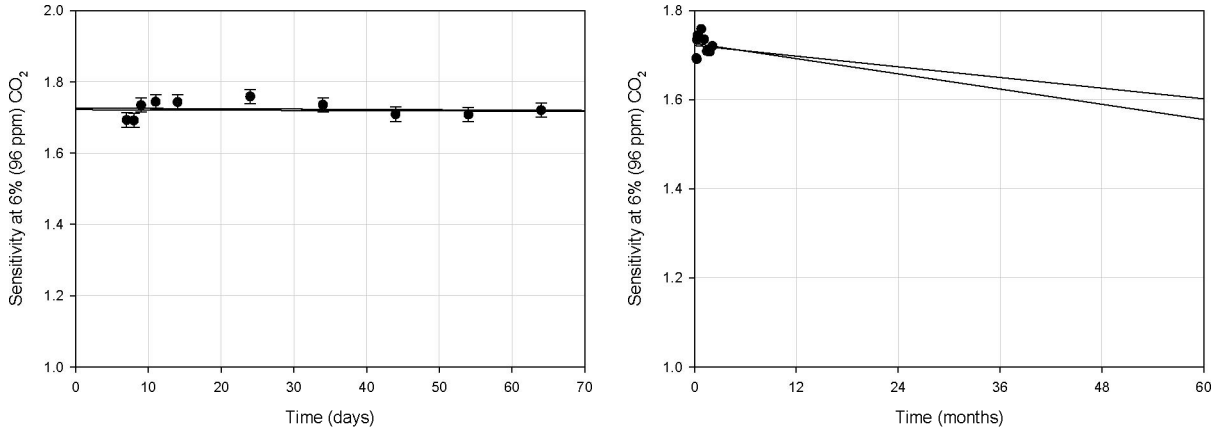

Figure 24 Calculation of sensor sensitivity through a five year operating period, based on stability studies.

At this point, a fiber sensor formulation was selected based on the ADT tests conducted at elevated temperature.

ADT in Aqueous Matrices - Photodegradation

Indicator photodegradation for a particular sensor will depend on the total number of photons used for sensor interrogation in the course of the life of the sensor. The total number of photons is a function of the light intensity of the sensor interrogation, the time performing a measurement, and the number of measurements performed.

Photodegradation is accelerated by incrementing the number of measurements per hour, and thus the total illumination time and number of photons. Considering that a system operating in the field will perform a measurement every 10 to 60 minutes, and considering 10 seconds of interrogation time per measurement, tests performed with continuous sensor interrogation increase the number of photons (and accelerate the sensor photodegradation) by a factor of 60 to 360 (i.e., one day of continuous illumination simulates two months to one year of real sensor operation).

Sensor prototypes have been exposed to continuous illumination for periods of over 44 hours, with no sensor photodegradation being observed. These results support the potential of the sensor for long term monitoring and for meeting the target operational period of at least five years.

ADT in Aqueous Matrices - Biofouling

Three types of materials were subjected to ADT studies under highly biologically contaminated media: (1) cladding materials coated with a protective layer of silicone DC-3140, which has known antimicrobial properties, (2) cladding materials coated with a protective layer of IOS 21-1 doped with Ag nanoparticles, and (3) cladding materials coated with a protective layer of GE premium waterproof silicone.

To measure the antimicrobial effect, we coated oxygen sensor films with each protective coating under evaluation. This enables us to nondestructively monitor the oxygen consumption of any biofilm growing on the cladding materials. After we expose the films for a set period of time to a highly colonized nutrient medium, the nutrient solution is removed and replaced with a solution of glucose in DI water, free of biological contamination. The glucose solutions is initially saturated with air, but if there is any biological contamination on the coating the permeation of oxygen from the glucose solution towards the oxygen sensitive films is affected, as the biological layer

consumes oxygen by respiration. Oxygen consumption can be correlated with the thickness of the biofilm as long as the nutrient concentration is controlled and kept constant for all the tests. By periodically repeating the oxygen consumption measurements, we gather information about the microbial activity of the three protective coatings.

Three samples of each of these films were exposed to a solution of nutrient broth highly colonized with bacteria, in order to accelerate the biofilm growth. With pure strains of *P. putida*, we were able to reproduce the tests (Figure 25). For each film, three control samples were maintained in DI water.

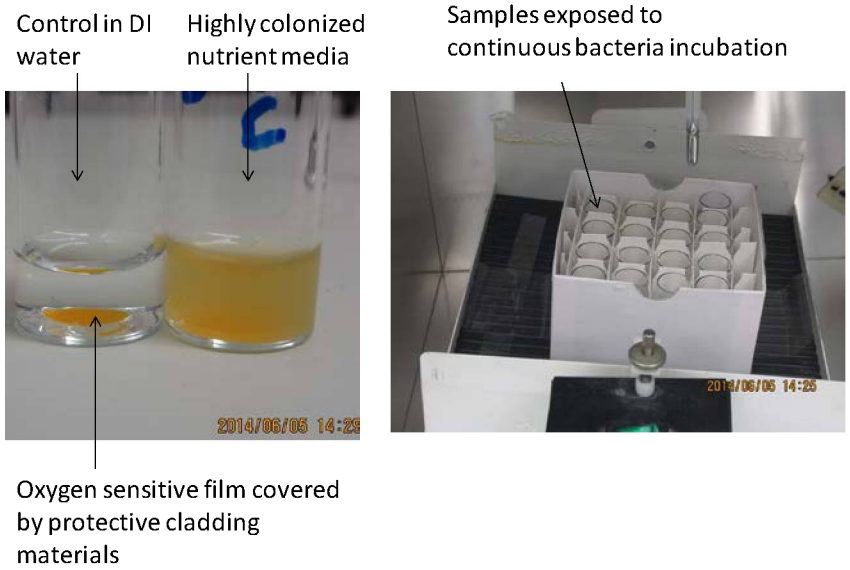

Figure 25 Test conducted to evaluate biofilm protection. Vials were filled with a highly concentrated suspension of *P. putida* in nutrient broth.

Figure 26 shows the oxygen consumption of the three coating materials evaluated over a period of about 55 min. after they had been exposed to nutrient broth highly colonized with bacteria for over a month. Oxygen levels were also recorded using films prepared with the same three coatings but kept in clean DI water for the same length of time.

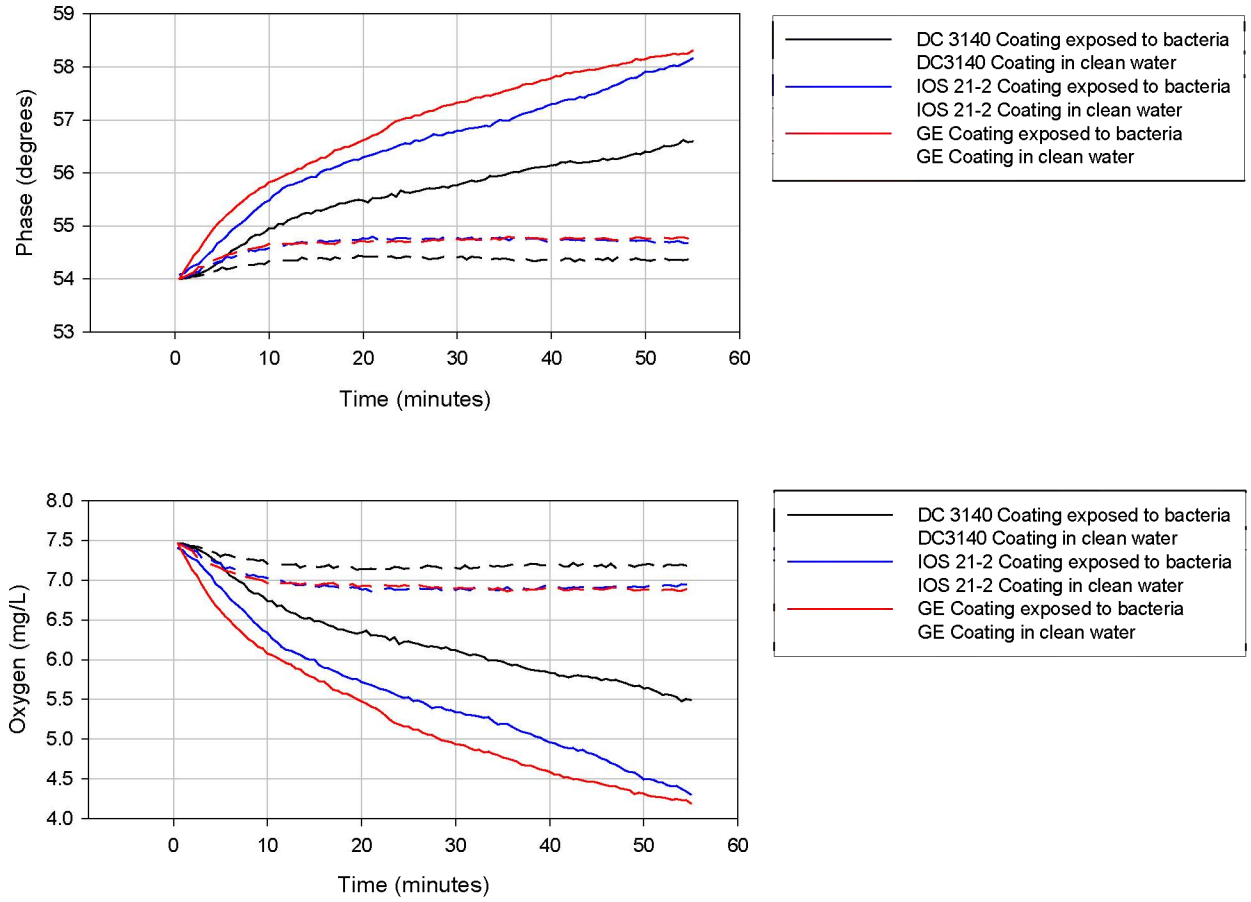

Figure 26 (top) Oxygen sensor signal (phase) profile during the tests performed to determine biofouling of sensor coatings. (bottom) Oxygen consumption profile for the three coatings tested immersed in a solution of glucose after being exposed to bacteria colonies or kept immersed in clean water for one month.

For each coating material, three samples were evaluated. The oxygen consumption was significantly less in the DC 3140 coatings than in the other two materials under evaluation, with ~40% less biofouling. The antimicrobial activity of the DC 3140 was confirmed. This study supported selection of the DC 3140 polymer for protecting the sensor cladding.

ADT in Aqueous Matrices – Elevated Water Flow Rate

Chemistry migration to water can be a cause of sensor degradation. For a particular sensor it will depend largely on the total amount of water flowing around the sensor, and on the pressure profile. The total amount of water is a function of the water flow rate around the sensor, and of time.

Accelerated tests were conducted with a 5 L reservoir connected to a medium flow rate pump that can produce a flow rate of 760 m per day. Fiber optic sensor prototypes prepared with the formulations 042814SM01 (fiber type 1) and 042814SM02 (fiber type 2) were subjected to this ADT study. Seven segments of each sensor type were exposed to an elevated water flow rate, and two additional samples were kept in water with no flow as controls (Figure 27).

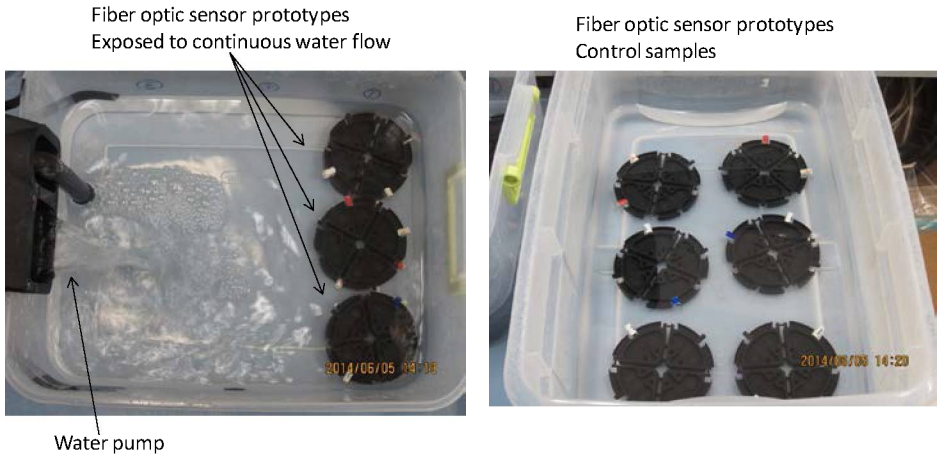

Figure 27 Experimental setup for evaluating chemistry migration at continuous water flow rate: (left) fiber optic sensors exposed to continuous water flow; (right) fiber optic sensors immersed in still water as control.

Reproducibility among sensor segments was determined before starting the study. Sensor segments that showed deviation from the average sensitivity to CO_2 of >10% were discarded. Reproducibility among sensor segments was first evaluated based on the transmission spectra. Figure 28 shows the transmission spectra of several sensor segments with only minimal differences among them.

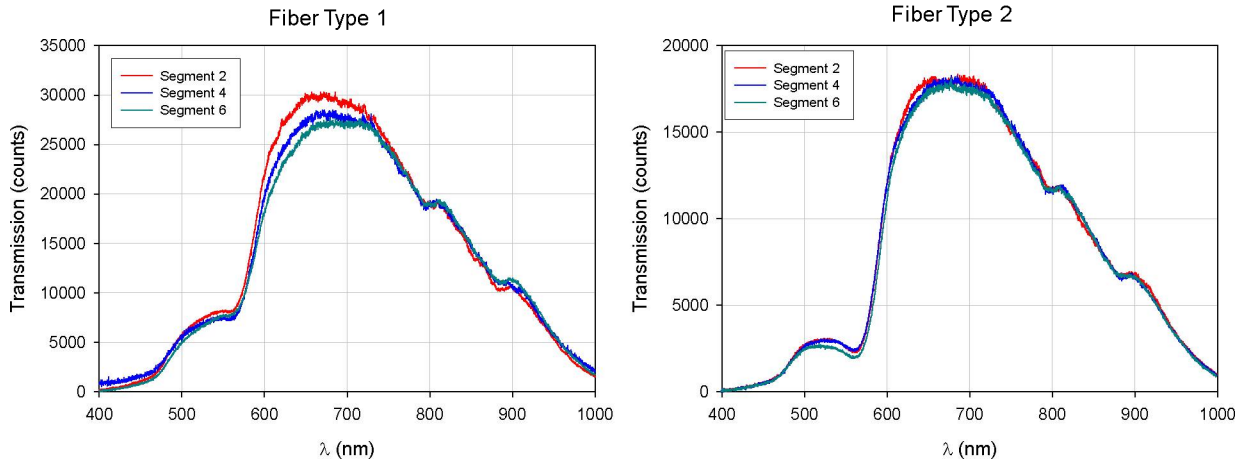

Figure 28 Transmission spectra (normalized at 850 nm) of fiber optic segments in water before starting the ADT study of **(left)** fiber optic sensors type 1 and **(right)** fiber optic sensors type 2.

Response profiles recorded before starting the evaluation under stress for the sensor segments included in the study are recorded in Figure 29. Those segments that exhibited more than 10% deviation from the average sensitivity of all the segments prepared for the study were discarded. The calibration curves of the selected sensor segments (sensor signal vs. CO_2 concentration) are shown in Figure 30.

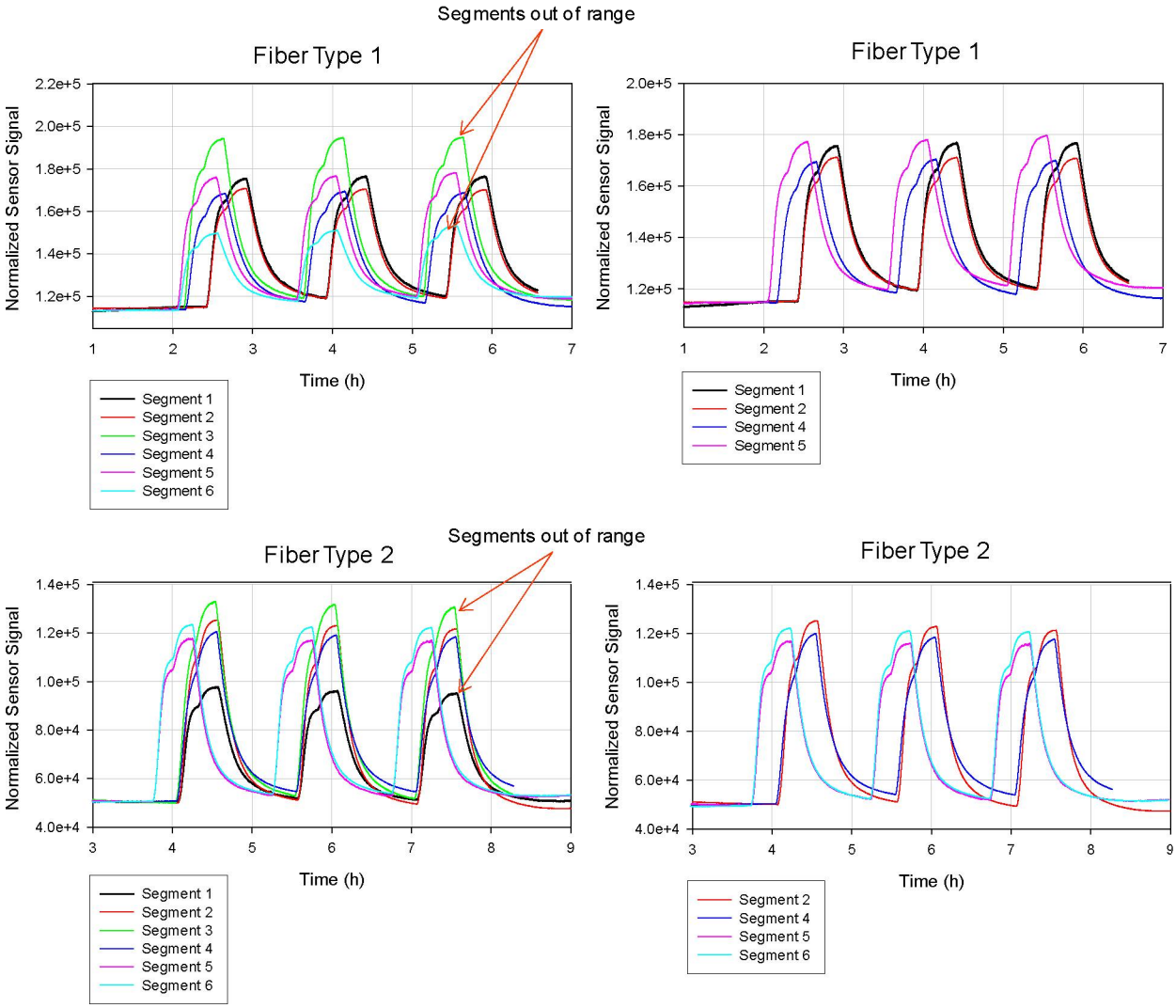

Figure 29 Response profiles (sensor signal = transmission at 575 nm) to 6% and 10% v/v CO_2 of (top) fiber optic sensor segments type 1 and (bottom) fiber optic sensor segments type 2. Sensor segments 1, 2, 4, and 5 were selected to evaluate fiber optic sensors type 1. Sensor segments 2, 4, 5, and 6 were selected to evaluate fiber optic sensors type 2.

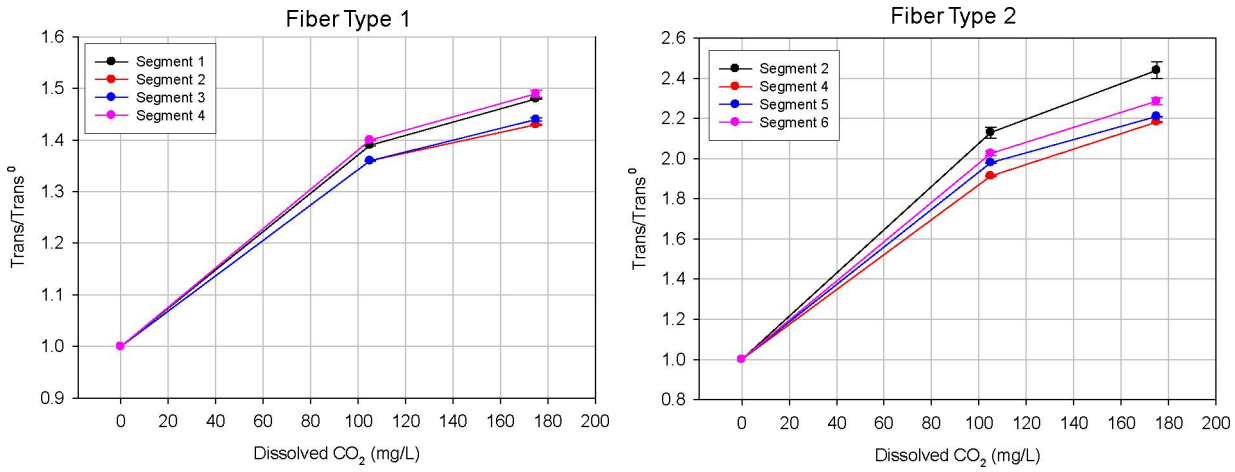

Figure 30 Calibration function (sensor signal vs. dissolved CO_2 concentration) for fiber optic sensor segments type 1 and type 2.

The transmission spectra and sensor response to CO_2 were recorded after 45 days and 90 days. The sensitivity to a set concentration of carbon dioxide decreased through the initial period for both fiber types—by 10% for the 042814SM02 fiber and by 7% for the 042814SM01 fiber. For the 042814SM01, the sensitivity stayed almost constant for the rest of the study. For the 042814SM02, the sensitivity decreased more slowly as the fiber stayed longer in the water (Figure 31). Similar behavior between the fiber segments under stress and stored in still water suggested an aging mechanism other than indicator permeation to the environment. The evolving sensitivity suggests a slow internal stabilization process on the fibers, independent of the environmental conditions, which could be modeled to correct the sensor sensitivity (calibration parameters) over time when sensors are operating in the field. This behavior is very similar to that observed in other ADT studies such as the evaluation performed at elevated temperature. Fiber sensors fabricated with formulation 042814SM01 proved more stable, supporting the selection of this formulation for the fabrication of the sensors.

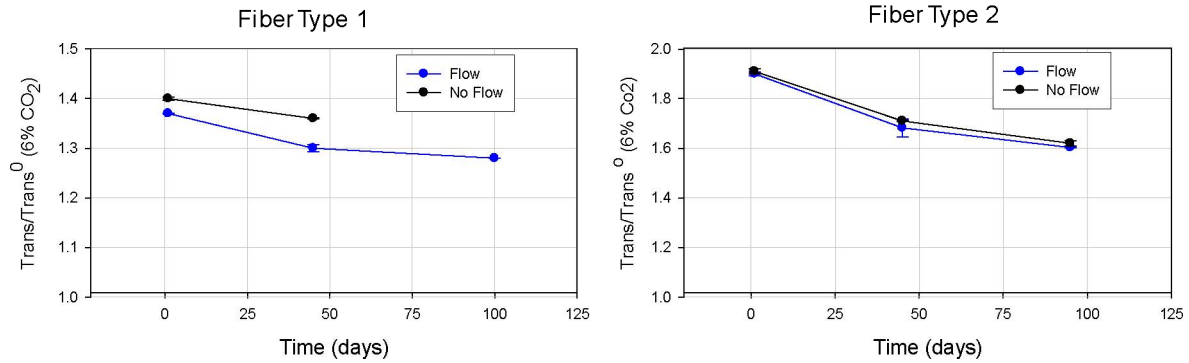

Figure 31 Evolution of the sensitivity (trans/trans^0, where *trans* is the transmission at 575 nm and *trans*^{0} the transmission at 575 nm under nitrogen) with time when the sensors were exposed to elevated flow and kept in still water.

ADT in Aqueous Matrices – Corrosive Water

Following a protocol similar to that described for the ADT study under elevated flow rate, sensors were exposed to stress conditions in corrosive water. Repeatability among sensor segments was determined before starting the study, and sensor segments fabricated with formulations 012414SM01 and 012414SM02 were included. The sensors were stored in a solution at pH = 3.8 and salinity of 250,000 ppm for 1 month. Figure 32 compares the sensor response to carbon dioxide before and after starting the study. Similar responses to CO_2 are observed before and after exposure to the corrosive environment, demonstrating the capability of the sensor to operate at extreme chemical conditions. The variation in sensitivity (trans/trans^0, where *trans* is again the transmission at 575 nm and *trans*^{0} the transmission at 575 nm under nitrogen) for the fiber optic sensor type 2 is similar to that observed during the flow tests, supporting the hypothesis that it is related to an internal process. The fiber optic sensor type 1 was more affected than in the flow tests, but there was no evidence of sensor degradation in the course of the tests.

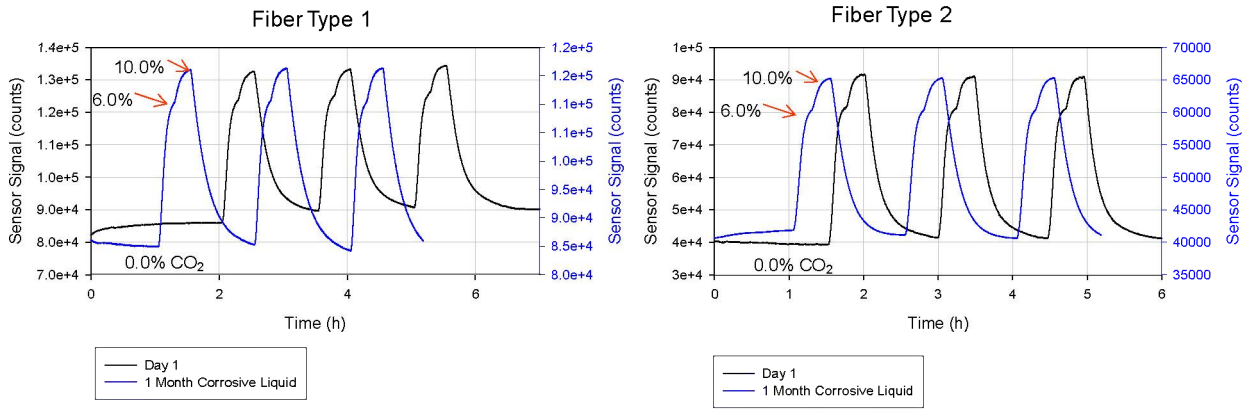

Figure 32 Response profiles (sensor signal = transmission at 575 nm) to 6% and 10% v/v CO_2 of sensor segments fabricated with polymer 042814SM01 (left) and polymer 042814SM02 (right) before and after being exposed to corrosive solutions (pH <4 and 25% w/w salinity).

8.0 *TASK 8.0* SENSOR SYSTEM ANALYTICAL CHARACTERIZATION

In this task, the sensor system was assessed for its precision, limit of detection, dynamic range, calibration function, response time, and reproducibility.

Analytical Characteristics at Ambient Temperature. A typical response profile of a LOH sensor in gas phase is shown in Figure 33.

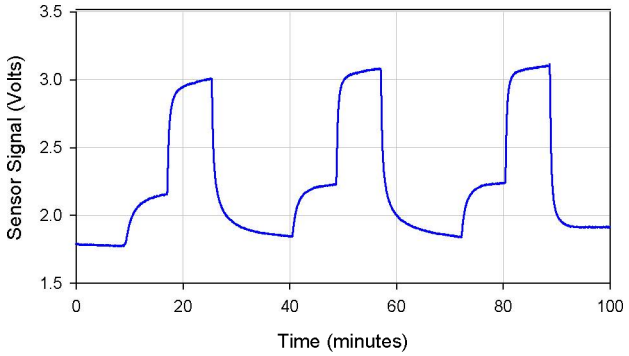

Figure 33 Response profile of fiber optic sensors to varying concentrations of carbon dioxide in gas phase (0.0, 1.0% and 60% v/v CO_2).

The limit of detection (LOD) and limit of quantification (LOQ) were determined according to IUPAC Gold Book recommendations, using 3X and 10X the standard deviation of the signal in the absence of CO_2, respectively. The LOD was determined to be 0.12% v/v CO_2 under standard conditions, and the LOQ was determined to be 0.35% v/v CO_2. The precision of the sensor was determined as the repeatability of the sensor readings at 1.0% v/v CO_2 levels. The average precision at 1.0% CO_2 was determined to be 0.1% v/v CO_2. The measurement range at ambient pressure for optimal sensors was determined to be from 0 to 100% v/v CO_2, although some fiber optic sensors showed narrower measurement range, with signal saturation at 85% v/v. The response time of the sensor was determined to be faster than 240 s, which is fast enough for monitoring CO_2 level changes in CCS applications.

A typical response profile for a HOH-based sensor to dissolved carbon dioxide is shown in Figure 34(a). A typical response profile to dissolved carbon dioxide for a sensor prepared with nanoblock base on the cladding materials is shown in Figure 34(b). The time observed for response of the sensor signal when the percentage of CO_2 is increased includes the time for gas system stabilization, the time for equilibration between the CO_2 in the gas phase and the dissolved CO_2, and the response time of the sensor. The equilibration between the CO_2 in the gas phase and the dissolved CO_2 is a major contribution to this overall time.

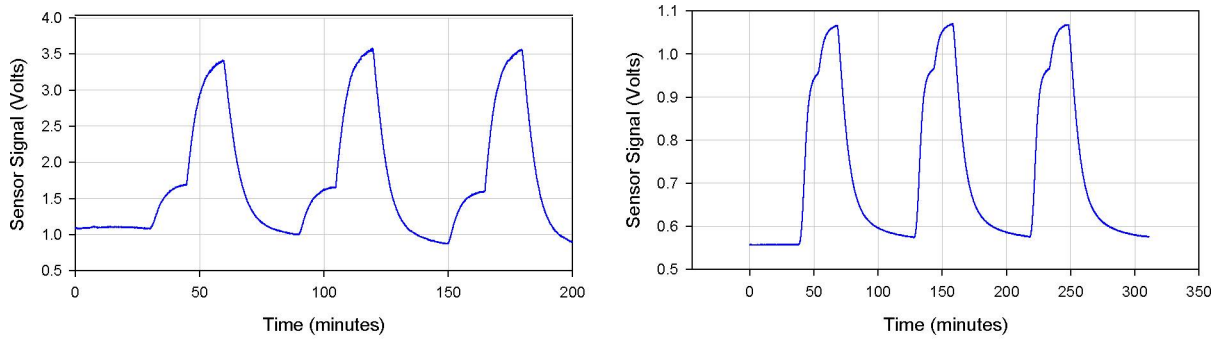

Figure 34 Response profiles of fiber optic sensors to three concentrations of dissolved carbon dioxide in water. (left) HOH-based fiber sensor (0.0, 17, and 102 mg/L CO_2). (right) No hydrophilic base fiber sensor (0.0, 102, and 170 mg/L CO_2).

The LOD for the HOH-based sensors was determined to be 0.8 mg/L CO_2 (which corresponds to 0.05% v/v CO_2 or 0.35 mmHg pCO_2) under standard conditions, and the LOQ was determined to be 2.4 mg/L CO_2 (which corresponds to 0.14% v/v CO_2 or 1.05 mmHg pCO_2. The LOD for the sensors prepared with nanoblock base (no hydrophobic base) on the cladding materials was determined to be 2.0 mg/L CO_2 (which corresponds to 0.1% v/v CO_2 or 0.9 mmHg pCO_2under standard conditions, and the LOQ was determined to be 6.0 mg/L CO_2 (which corresponds to 0.6% v/v CO_2 or 3.6 mmHg pCO_2)

The average precision of the HOH-based sensors at 17 mg/L CO_2 was determined to be 1 mg/L CO_2. The average precision of the sensors prepared with nanoblock base on the cladding materials at 17 mg/L CO_2 was determined to be 3 mg/L CO_2.

The measurement range at ambient pressure was determined to be from 0 to at least 1,500 mg/L for the two sensors under evaluation.

The response time of the sensor was determined to be 360 s, which is fast enough for monitoring CO_2 level changes in CCS applications.

Analytical Characteristics at Elevated Temperature. The sensor response (variation of transmission) for an established level or percentage of CO_2 decreases as the temperature increases. This is due to the lower solubility of the CO_2 gas in the cladding material, as in any polymeric material, as the temperature is increased. At the same time, as the temperature increases in the well the pressure also goes up, and with it the partial pressure of carbon dioxide (for a given percentage of CO_2). The higher the CO_2 partial pressure the greater the sensor signal variation (as demonstrated in studies conducted at IOS).[1] In summary, increasing temperature results in lower sensitivity and increasing pressure results in higher sensitivity; as they both increase together in the well, we expect that the overall effects on the sensor response at deep locations will partially offset one another.

Applying the results of the ADT tests, we were able to produce sensors with enhanced thermal resistance, and we demonstrated sensor operation at 175°C. Figures 35 and 36 show the response profile of a sensor prototype to 25% v/v CO_2 at temperatures from 40°C to 175°C.

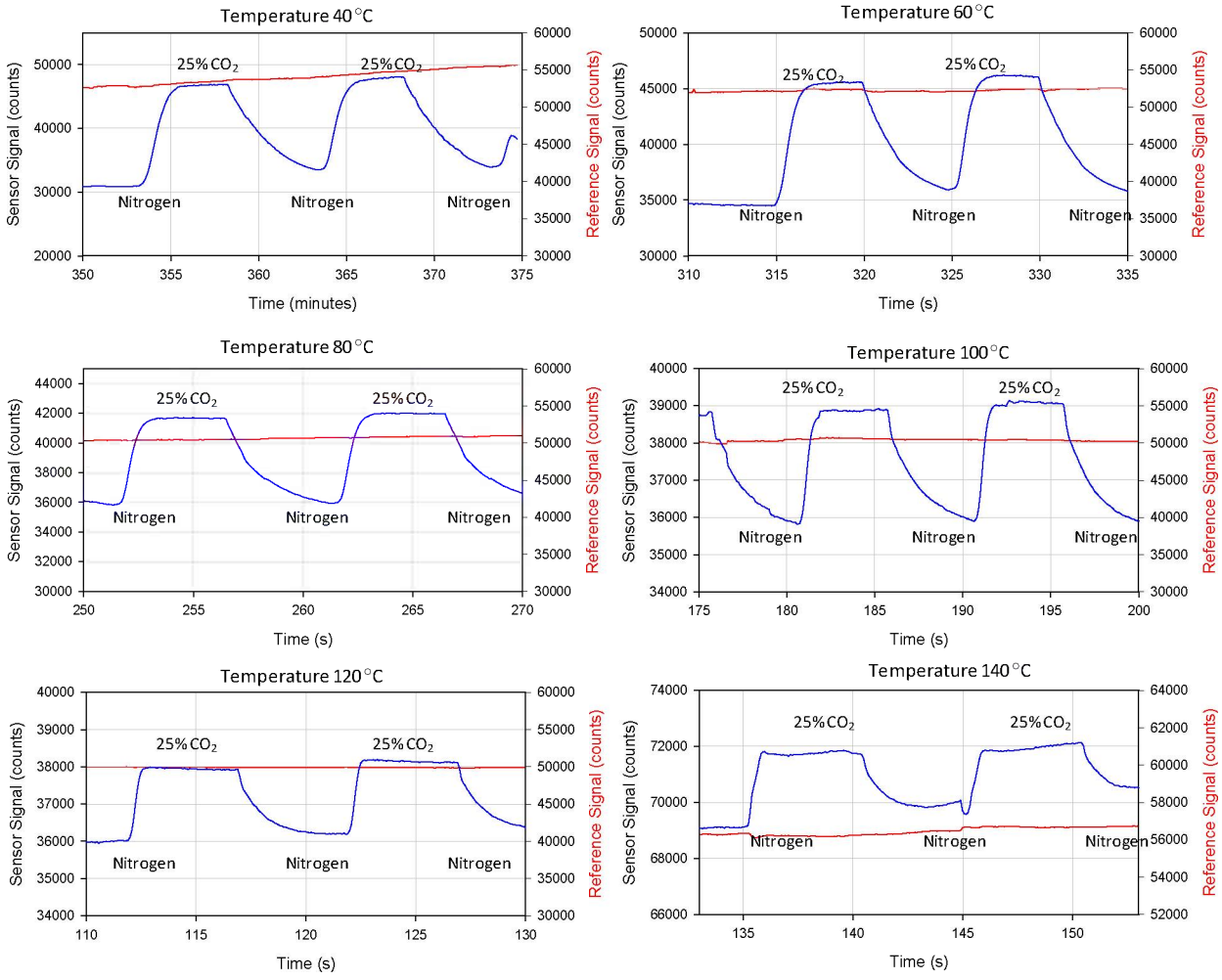

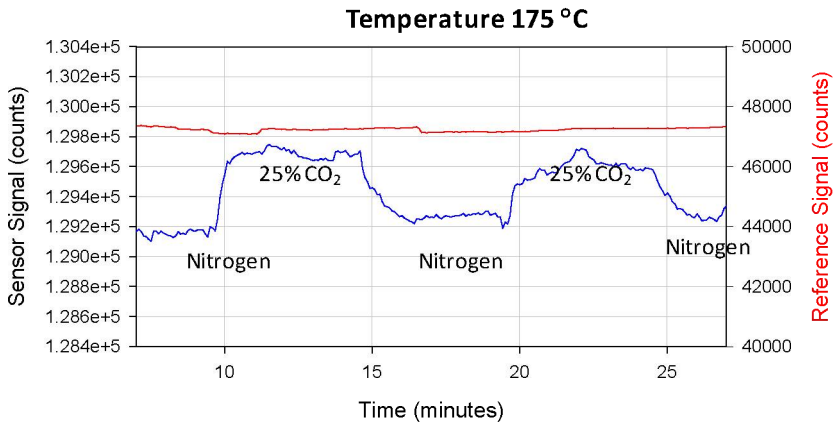

Figure 35 Response profiles (sensor signal = transmission at 575 nm) of a fiber optic sensor to 25% v/v CO_2 at temperatures from 40°C to 175°C. The sensor signal has been corrected according to the reference signal algorithm or by a time-based algorithm.

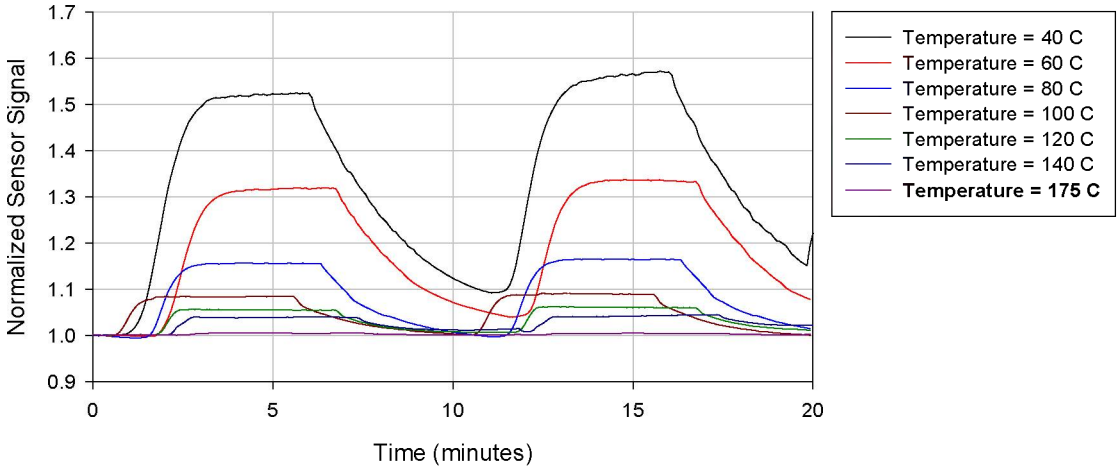

Figure 36 Response profiles (normalized sensor signal = transmission at 575 nm / transmission at 575 nm in nitrogen) of a fiber optic sensor to 25% v/v CO_2 at temperatures from 40°C to 175°C.

As expected, as the temperature increases the sensitivity decreases. Nevertheless, the sensor exhibits excellent sensitivity up to 140°C and is still capable of detecting CO_2 at 175°C. The limit of detection in the range of temperature calculated from the data obtained in the test is recorded in Table 3. These calculations correspond to a 2 m long segment, and longer sensors show higher sensitivity as in prior studies.

Table 3 LOD (% v/v) Determined for a 2 m Long Sensor Segment at Seven Temperatures (°C)

40	60	80	100	120	140	175
0.0716	0.1178	0.2413	0.4475	0.691	0.9708	8.866

From the data in Table 3, the sensitivity in a range of environmental conditions can be calculated, as shown in Table 4 and in Figure 37. The response of the sensor is proportional to the partial pressure of CO_2, and not to the molar fraction or percentage. For a given percentage of CO_2, the partial pressure increases linearly with the total pressure ($pCO_2 = XCO_2 \times P$, where pCO_2 is the partial pressure of CO_2, XCO_2 is the molar fraction, and P is the total pressure). Thus, the lowest

percentage of CO_2 detected by the sensor (LOD) is lower as the pressure increases, as shown in Table 4.

Table 4 LOD for a Fiber Optic Sensor for Seven Values of Temperature (°C) and 22 Values of Pressure (psi)

P/T	40	60	80	100	120	140	175
15	0.072	0.118	0.241	0.447	0.69	0.98	8.87
50	0.021	0.035	0.072	0.13	0.21	0.29	2.66
100	0.011	0.018	0.036	0.07	0.10	0.15	1.33
200	0.005	0.009	0.018	0.03	0.05	0.07	0.66
300	0.004	0.006	0.012	0.02	0.03	0.05	0.44
400	0.003	0.004	0.009	0.02	0.03	0.04	0.33
500	0.002	0.004	0.007	0.01	0.02	0.03	0.27
600	0.002	0.003	0.006	0.01	0.02	0.02	0.22
700	0.002	0.003	0.005	0.01	0.01	0.02	0.19
800	0.001	0.002	0.005	0.01	0.01	0.02	0.17
900	0.001	0.002	0.004	0.01	0.01	0.02	0.15
1000	0.001	0.002	0.004	0.01	0.01	0.01	0.13
1100	0.001	0.002	0.003	0.01	0.01	0.01	0.12
1200	0.001	0.001	0.003	0.01	0.01	0.01	0.11
1300	0.001	0.001	0.003	0.01	0.01	0.01	0.10
1400	0.001	0.001	0.003	0.01	0.01	0.01	0.09
1500	0.001	0.001	0.002	0.01	0.01	0.01	0.09
1600	0.001	0.001	0.002	0.01	0.01	0.01	0.08
1700	0.001	0.001	0.002	0.01	0.01	0.01	0.08
1800	0.001	0.001	0.002	0.01	0.01	0.01	0.07
1900	0.001	0.001	0.002	0.01	0.01	0.01	0.07
2000	0.001	0.001	0.002	0.01	0.01	0.01	0.07

Cells in green indicate the environmental conditions at which the sensor meets the established sensitivity target of 0.1% v/v CO_2. Only under unrealistic conditions of elevated temperature and low pressure is the sensor sensitivity below the established target. In addition, it is likely that such sensitivity (0.1% v/v CO_2) is not required for operation in deep locations, but rather is only a reasonable requirement for leak detection above the reservoir zone, where little or no CO_2 should be expected. Sensitivity of 0.5%, 1.0%, or even 5% could be a more realistic requirement for deep wells close to the CO_2 plume.

Figure 37 graphs the data in Table 4, and shows the LOD for the fiber optic sensors in gas phase as functions of both temperature and pressure. The same plot is reproduced cutting the LOD vs. T vs. P surface at LOD 0.1%, LOD 0.5% v/v and at LOD 1% v/v. The dark green plane at the bottom represents the environmental conditions at which the sensors meet the target LOD (0.1%, 0.5%, or 1.0% v/v).

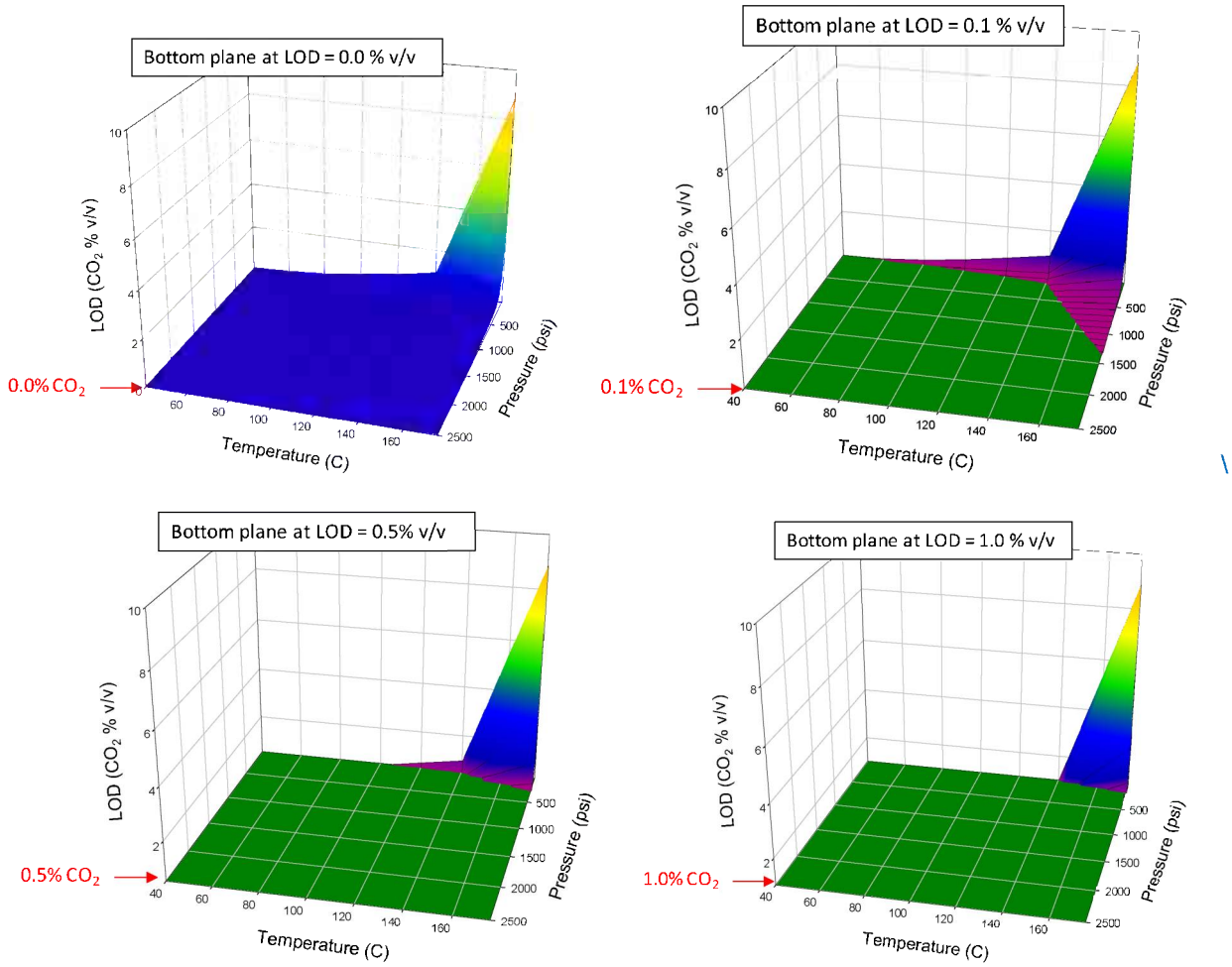

Figure 37 LOD for a fiber optic sensor at a range of temperature and pressure values. The bottom plane of the plot has been established at 0.1%, 0.5%, and 1.0% CO_2 v/v. The green area in each plot represents the environmental conditions (temperature and pressure) at which the sensor exhibits an LOD lower than the level established in the bottom plane.

9.0 *TASK 9.0* EVALUATION OF THE SENSOR SYSTEM IN SIMULATED FIELD CONDITIONS

We assembled a sensor evaluation setup to replicate downhole conditions, which include elevated pressure, high salinity, and varying carbon dioxide concentrations. The system is shown in Figure 38.

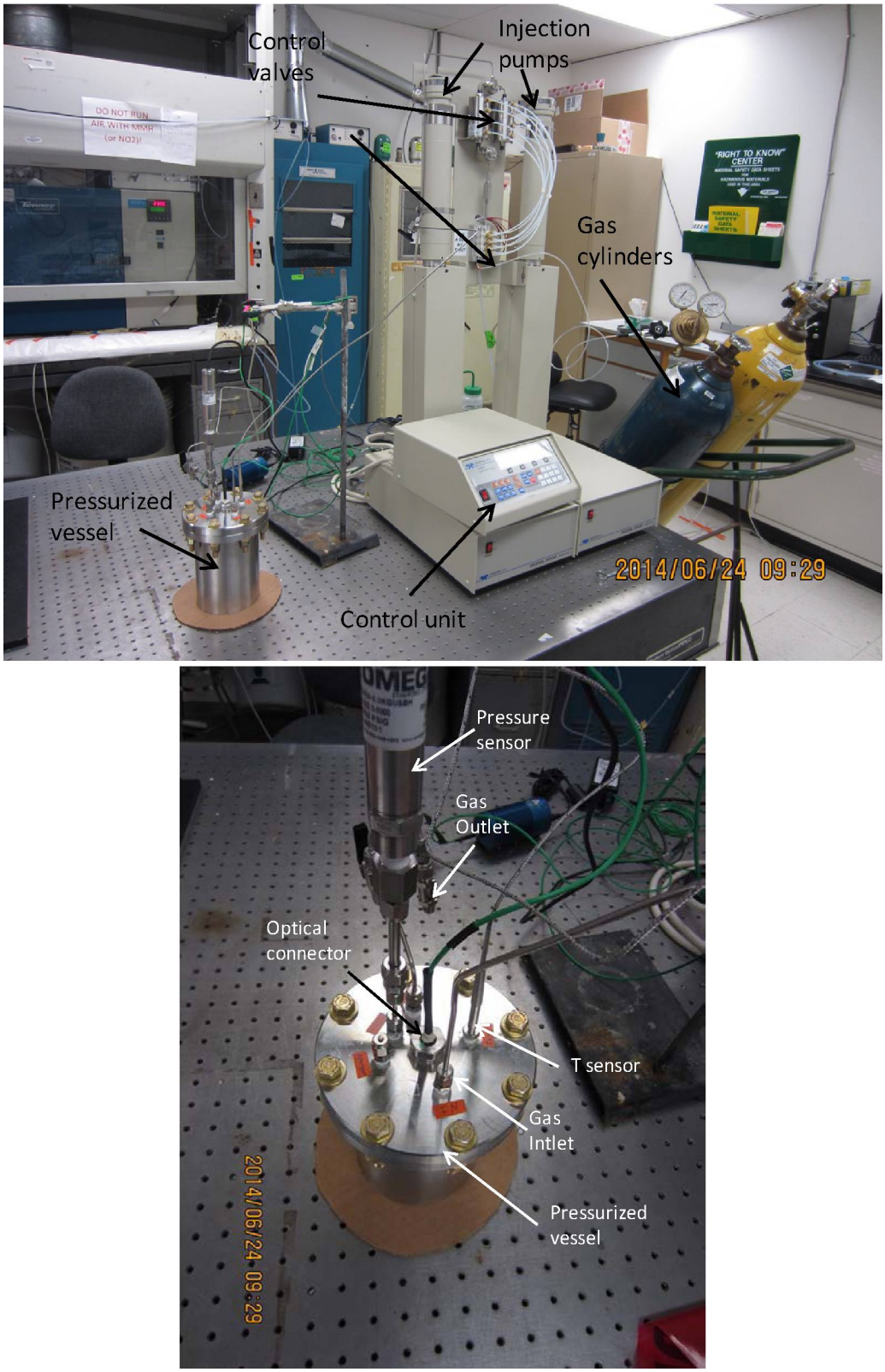

Figure 38 Assembled system for sensor testing at elevated pressure, and detail of the pressurized vessel.

For the initial test we used a fiber optic connector rated at up to 500 psi, and the tests were conducted at up to 300 psi. Those tests were conducted in gas phase.

Figure 39 shows the sensor signal for a fiber optic prototype fabricated according to the formula and procedures optimized during the ADT, at pressures from 20 to 300 psi, when exposed to nitrogen (0.0), 1%, and 6% v/v CO_2. The partial pressure of CO_2 was increased by incrementing system total pressure, and the sensor responded to those increments in the partial pressure of CO_2. The LOD calculated at 300 psi is 0.05% v/v CO_2, and the measurement range is from 0.0 to 100% CO_2. Figure 40 shows the calibration curve (signal vs. pCO_2) calculated with the data collected at elevated pressure in gas phase up to 300 psi.

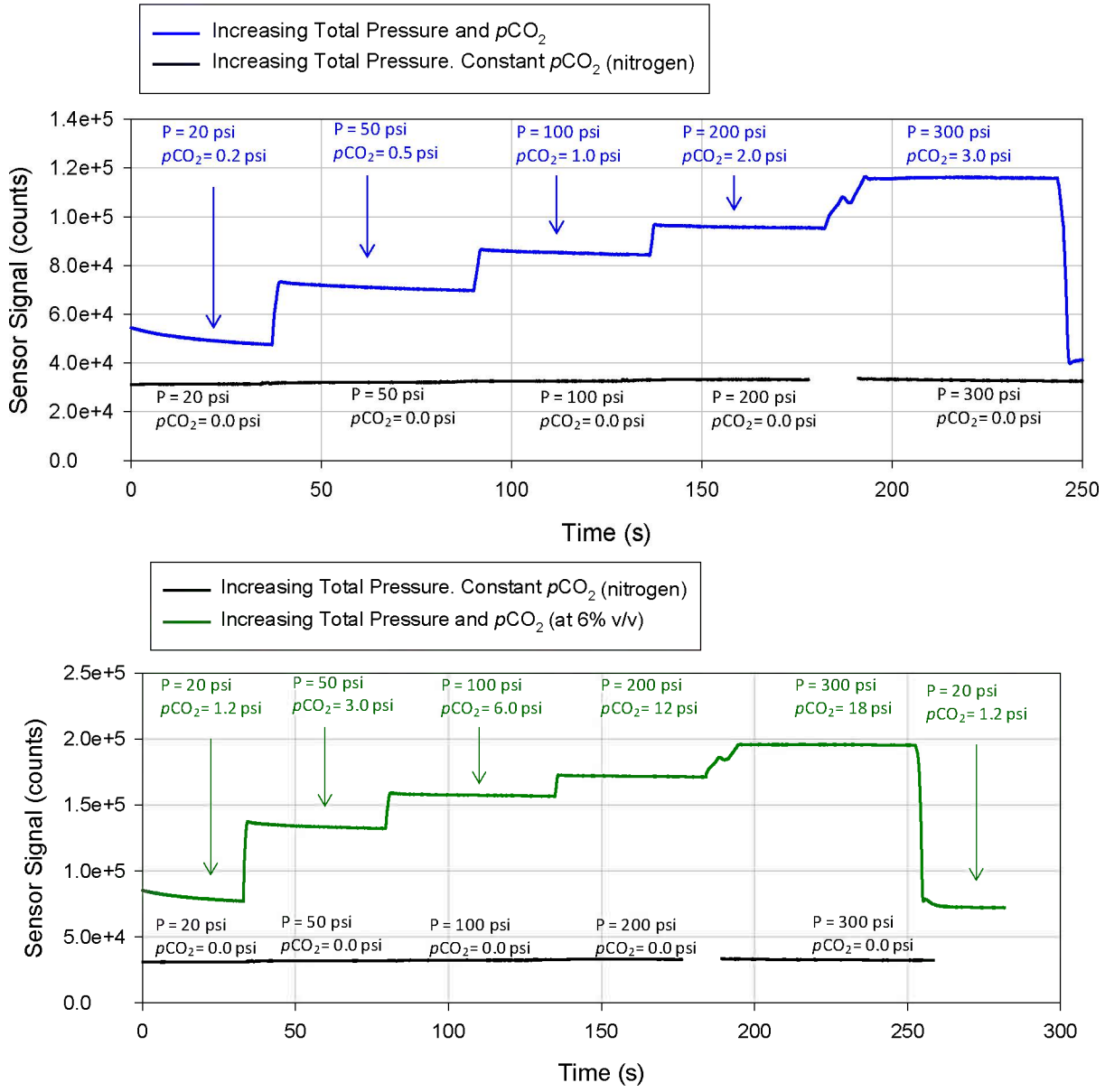

Figure 39 Sensor signal profile when a fiber optic sensor prototype was exposed to increasing total pressure and either increasing or constant partial pressure of CO_2. Top: comparison of the tests performed under nitrogen and at 1% CO_2. Bottom: comparison of the tests performed under nitrogen and at 6% CO_2.

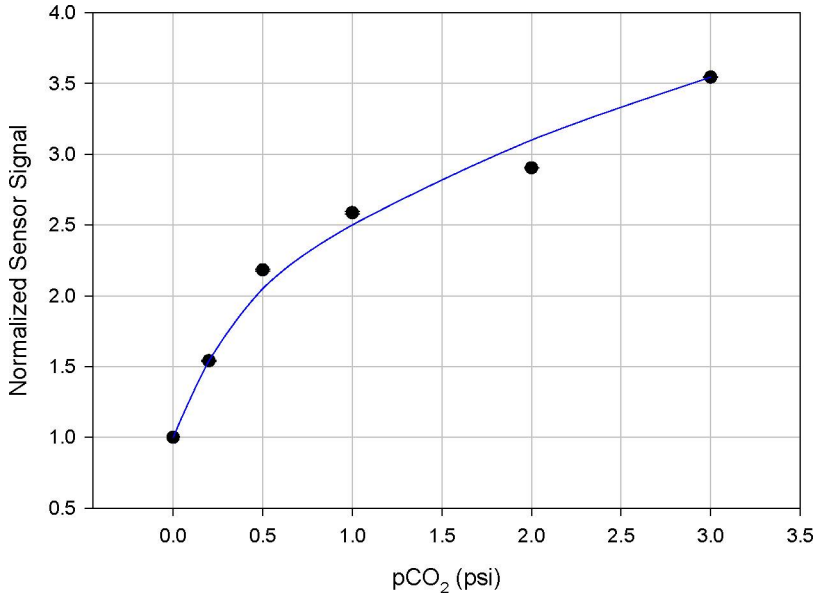

Figure 40 Calibration curve (normalized sensor signal vs partial pressure of CO_2) for a fiber optic sensor prototype.

After the tests conducted in gas phase and up to 300 psi, we acquired an optical connector rated for 3,000 psi, which allows us to conduct tests at higher pressure, and we tested the sensors immersed in water, simulating the conditions found downhole, at up to 2,050 psi.

Significant effort was dedicated to optimizing the setup design and the operation protocols for equilibrating water samples with different gas mixes of nitrogen and carbon dioxide at varying pressure levels. Once the design of the setup was optimized, the sensors were tested following two operational protocols:

(1) **Constant total pressure and increasing molar fraction:** After the system was equilibrated at a constant total pressure, the water was equilibrated with gas at varying molar fractions of CO_2 in nitrogen (using gas cylinders with different mixes of CO_2 in nitrogen) in the course of the test, increasing the partial pressure of gas and the concentration of CO_2 dissolved in the water. The test was then repeated, equilibrating the system at another total pressure.

(2) **Constant molar fraction and increasing total pressure**. The water was equilibrated with gas at constant molar fraction of CO_2 in nitrogen throughout the test (using the same gas cylinder throughout the test), and then the total pressure of the system was increased stepwise, from ambient to 2,050 psi, increasing the partial pressure of gas and the concentration of CO_2 dissolved in the water. The test was then repeated using a gas cylinder containing a different molar fraction of CO_2 in nitrogen.

A typical sensor response in two tests performed following Protocol 1 is shown in Figure 41. The quick pressure changes experienced by the sensor and optical connectors in these tests affected the signal readings and made data interpretation difficult. Nevertheless, the corrected sensor signal (signal at 575 nm corrected against signal at 850 nm) showed the sensor response to varying concentrations of CO_2 dissolved in water, which were proportional to the partial pressure of CO_2 in the gas phase, at a total pressure of 300 psi and at total pressure of 2,050 psi. To the best of our

knowledge, this is first time that the operation of any sensor for carbon dioxide has been demonstrated at this elevated pressure.

Constant total pressure while **increasing molar fraction** results in increasing partial pressure of CO_2.

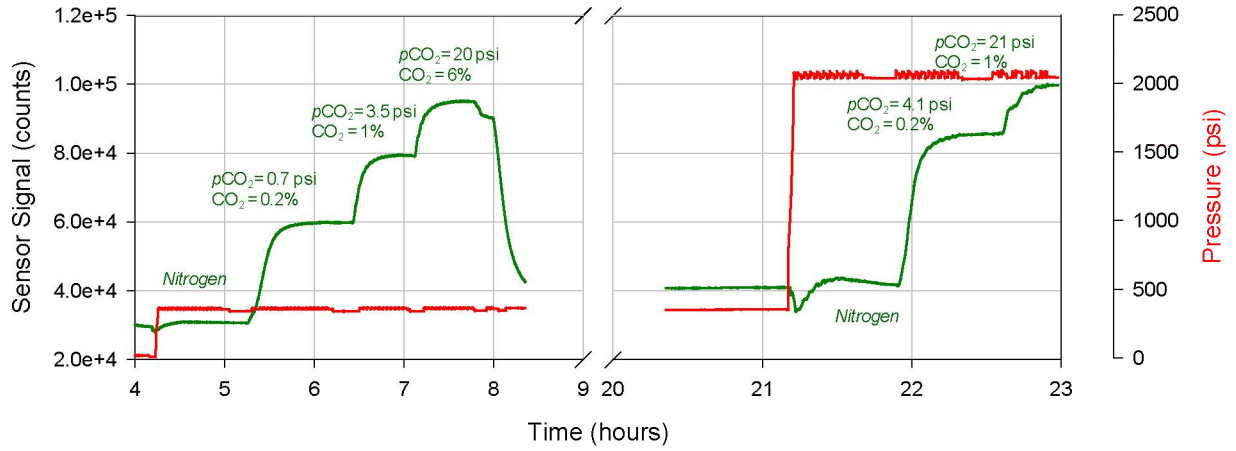

Figure 41 Response profile (sensor signal = transmission at 575 nm) of a fiber optic sensor to 0.0, 0.7, 3.5, and 20 psi partial pressure of CO_2 at total pressure of 300 psi and to 0.0, 4.1 and 21 psi partial pressure of CO_2 at 2,050 psi total pressure. The sensor signal has been corrected according to the reference signal algorithm.

A typical sensor response in two tests performed following protocol 2 is shown in Figure 42. In the first test the water was equilibrated with nitrogen, making the partial pressure of CO_2 zero (and constant) throughout the test. The black line corresponds to this test conducted under nitrogen, and shows little or no sensor response to pressure. In the second test the water was equilibrated with a mix of CO_2 in nitrogen (0.2% v/v), so the partial pressure of CO_2 and the concentration of CO_2 increased throughout the test as the total pressure increased. The green line shows the sensor response to the increasing concentration of dissolved CO_2.

Constant molar fraction with **increasing total pressure** results in increasing partial pressure of CO_2.

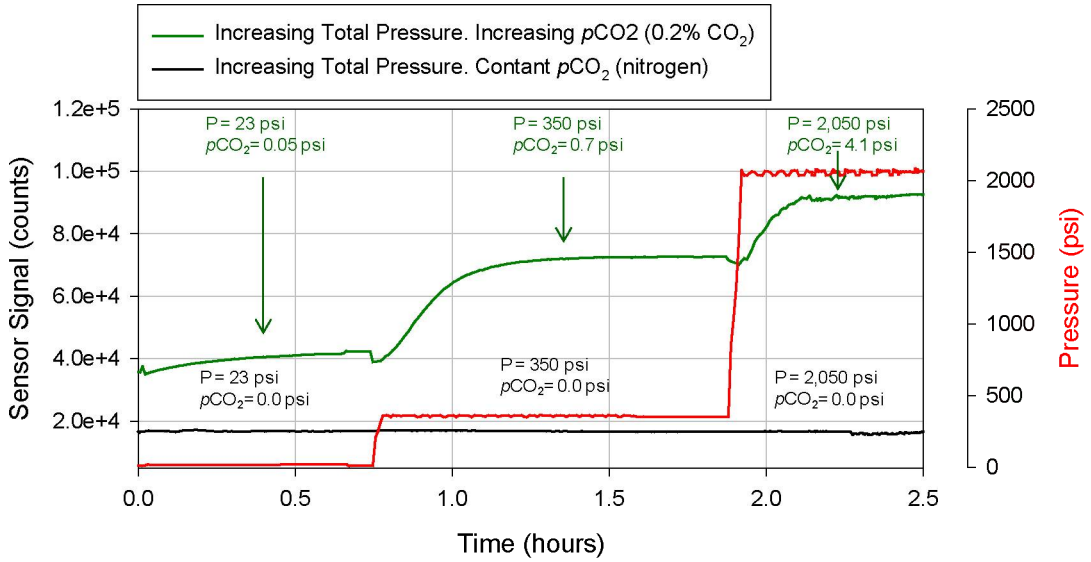

Figure 42 Response profile (sensor signal = transmission at 575 nm) of a fiber optic sensor to 0.0, 0.05, 0.7, and 4.1 psi partial pressure of CO_2 at total pressure of 23, 300, and 2,050 psi. The sensor signal has been corrected according to the reference signal algorithm.

The calibration function in Figure 43 shows that the sensor reached saturation around a partial pressure of CO_2 of 21 psi. Thus, with this sensor design and the formulation selected, concentrations of CO_2 above those levels will not be measured.

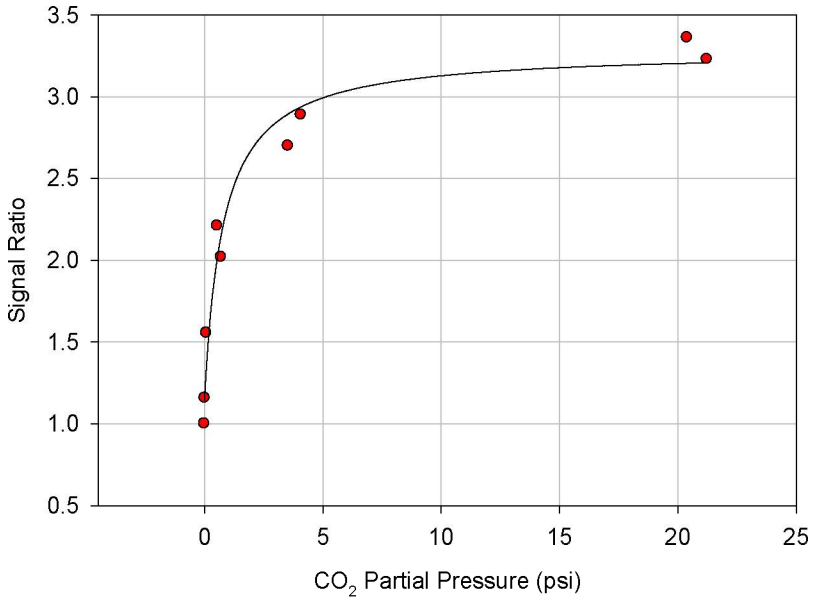

Figure 43 Calibration curve (normalized sensor signal vs partial pressure of CO_2) for a fiber optic sensor prototype immersed in water.

10.0 *TASK 10.0* DESIGN AND TEST SENSOR CABLES

We designed a sensor cable capable of integrating several fiber optic chemical sensors, to be deployed downhole. A modular cable was designed constructed by integrating distribution segments and sensor segments (Figure 44). The cable design included four elements: (1) distribution cable segments, (2) sensor cable segments, (3) connector segments, and (4) a loop segment.

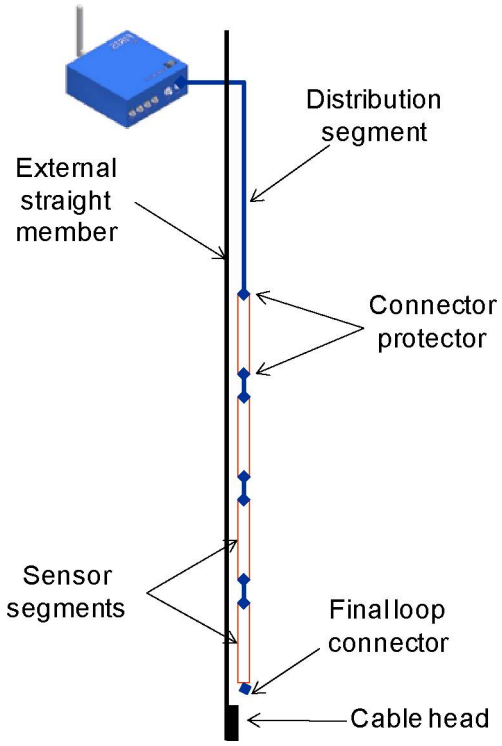

Figure 44 Representation of the sensor cable, including four sensor segments at variable depths.

IOS established communication with several potential vendors for cable elements, and discussed the technical and cost advantages and limitations of the options. Prototypes of some of the parts were assembled and evaluated. After fabricating and testing several prototypes, and through extensive communication with several potential vendors for the cable elements, we selected the elements of the optical cable.

Distribution Cable Segment. Polymicro designed a cable that incorporates the distribution fiber selected by IOS (200 µm diameter low-OH glass fibers). That required custom fabrication of the cable, which is a service that Polymicro offered. For our research project, Polymicro fabricated the optical cable with only a single strength member instead of the exterior metallic armor that will be used in the final product, reducing the cost of the cables. With this distribution cable, an external stainless steel wire is used for sensor deployment; an external metallic support for sensor deployment is routine in downhole monitoring, and in our field tests was used also for gas release. The cable cross-section is sketched in Figure 45, and the characteristics of the distribution cable finally selected are as follows:

- The cable incorporates eight optical fibers and a Kevlar strength member.
- The protection jacket of the cable is PVC.
- The fiber type is JTFLH200230500.
- Ultra low-OH core: 200 µm ± 4 µm
- Hard polymer cladding: 230 µm +0/-10 µm
- Total fiber OD (Tefzel): 500 µm ± 30 µm
- Total cable OD with PVC: 3.048 mm ± 127 µm.

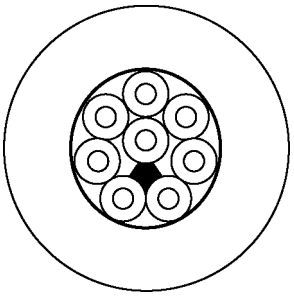

Figure 45 Distribution of fibers and the strength member.

In selecting the distribution segment and other elements of the senor cable, IOS pursued synergies with other projects for subsurface monitoring. Having common elements for multiple products targeting the same market reduces cost and increases competitiveness.

A 1,600 m segment was connectorized and prepared for field testing. This segment includes eight optical fibers and a total of 12,800 m of fiber (Figure 46). Integrity of all the fibers and proper light transmission were initially tested by measuring the absolute light power transmitted through each of the fibers. A fiber optic CO_2 sensor was then connected to the distribution cable, and measurements were taken using the SUS-CO2-DICAST instrument.

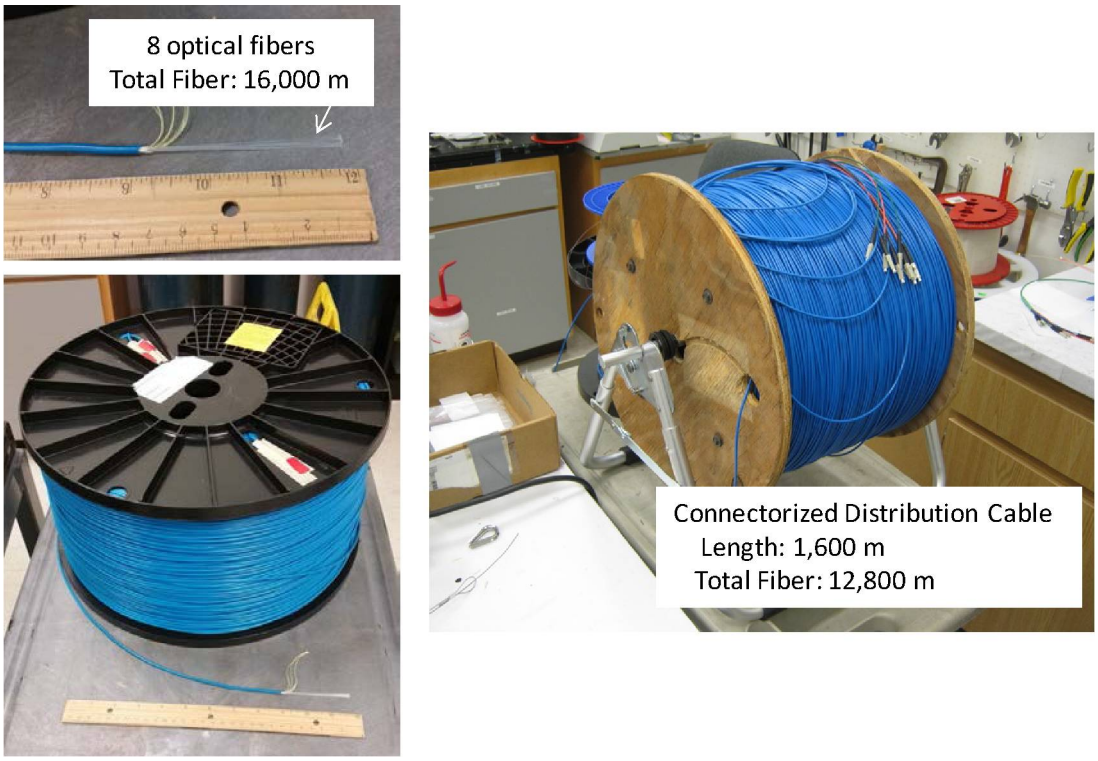

Figure 46 Distribution cable incorporating eight optical fibers.

Sensor Cable Segment. We considered two cabled designs (Figure 47, top) based on previous sensor cables developed for IOS distributed chemical sensing systems.

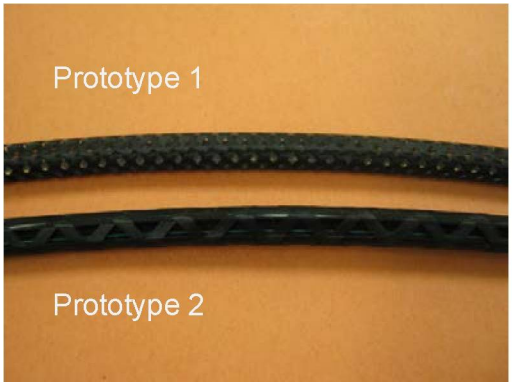

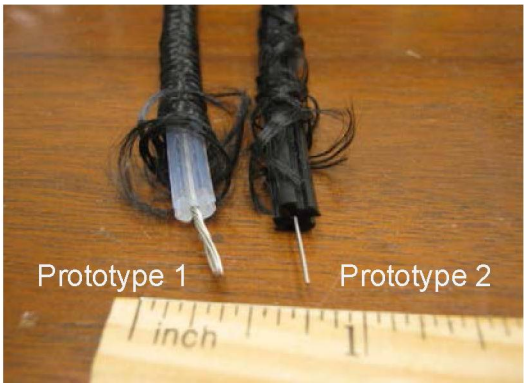

Cable Engineered by Draka

SLOTTED CORE PROFILE

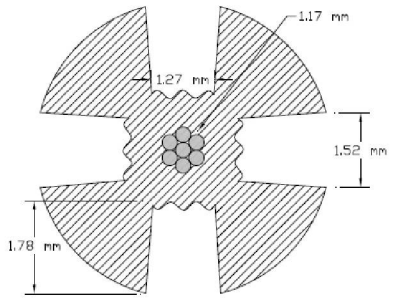

CENTER ID HOLE	#18 AWG 7/0.39 mm Tin Coated Copper; O.D.: 1.16 mm (0.046") Nominal O.D.: 1.17 mm (0.046") nominal
TOP CHANNEL WIDTH	1.52 mm (0.060") Nominal
BOTTOM CHANNEL WIDTH	1.27 mm (0.050") Nominal
CHANNEL DEPTH	1.78 mm (0.070") Nominal
CHANNEL CORRUGATIONS	100 µm
OVERALL DIAMETER	6.0 mm (0.236") Nominal
MATERIAL RATED	UL 910 (NFPA 262)
MIXTURE	FEP (Fluorinated Ethylene Propylene, Teflon-FEP, or FEP is a copolymer of hexafluoropropylene and tetrafluoroethylene
TEMPERATURE RATING	150°C
BRAID	A black Dacron braid will be applied over the core. Coverage: 60% Nominal

Rev	DATE	CHANGE DETAIL
0	07/21/14	New Issue
1	12/02/14	Remove Ripcords

PRYSMIAN Draka

Draka Engineered Specialties
22 Joseph E. Warner Blvd
North Dighton MA 02764
Phone: 508-822-5444 Fax: 508-822-1944

Figure 47 (top) Sensor cable prototypes evaluated at IOS. (bottom) Sensor cable design by Draka, approved by IOS engineers.

After evaluating the relative merits of the two approaches based on the prototype segments, Draka, a leading producer of wire and cable for multiple applications, designed a sensor cable based on prototype 1. The characteristics are shown in Figure 47, bottom. As with the distribution cable, one of the criteria considered for the selection of the sensor cable was compatibility with parallel IOS products for underground monitoring. The fiber optic sensors (from one to four) are located in any of the four external groves of the cable, and therefore are exposed to the water in the well.

Connector Segment. The connector segment may be the most challenging segment of the modular cable because of the diameter restrictions, and because the distribution cable must be opened up

and then resealed at its interface with the connector segment. Figure 48 shows a prototype connector segment, integrated with a sample of the AFL Fiber Optic Component initially selected for the distribution segment. The AFL cable was cut open, and the distribution fibers were terminated with LC fiber optic connectors. To preserve the pressure protection inside the distribution segment, a resin resistant to high pressure was used to seal the AFL cable once the distribution fibers was connected with the fiber in the connector segment. **The LC connector and the resin were tested in the elevated pressure setup at pressures up to 2,050 psi, and resistance to those conditions was demonstrated.**

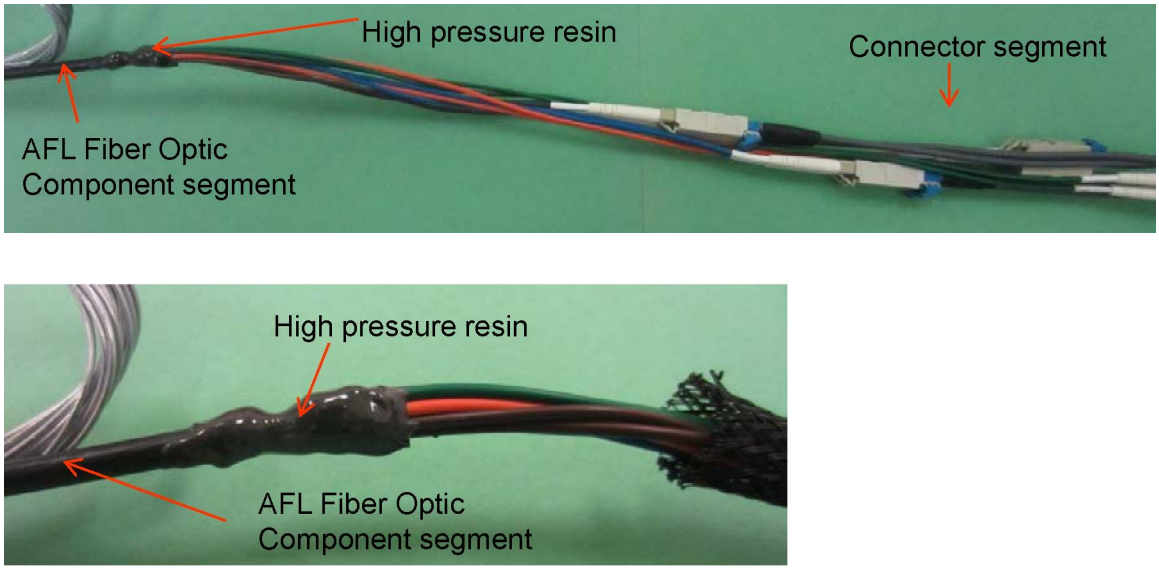

Figure 48 Connector segment prototype with details of the LC fiber optic connectors and junction between the connector segment and the distribution segment.

The connector segment can be protected by an extendible plastic jacket that facilitates the deployment of these segments (Figure 49).

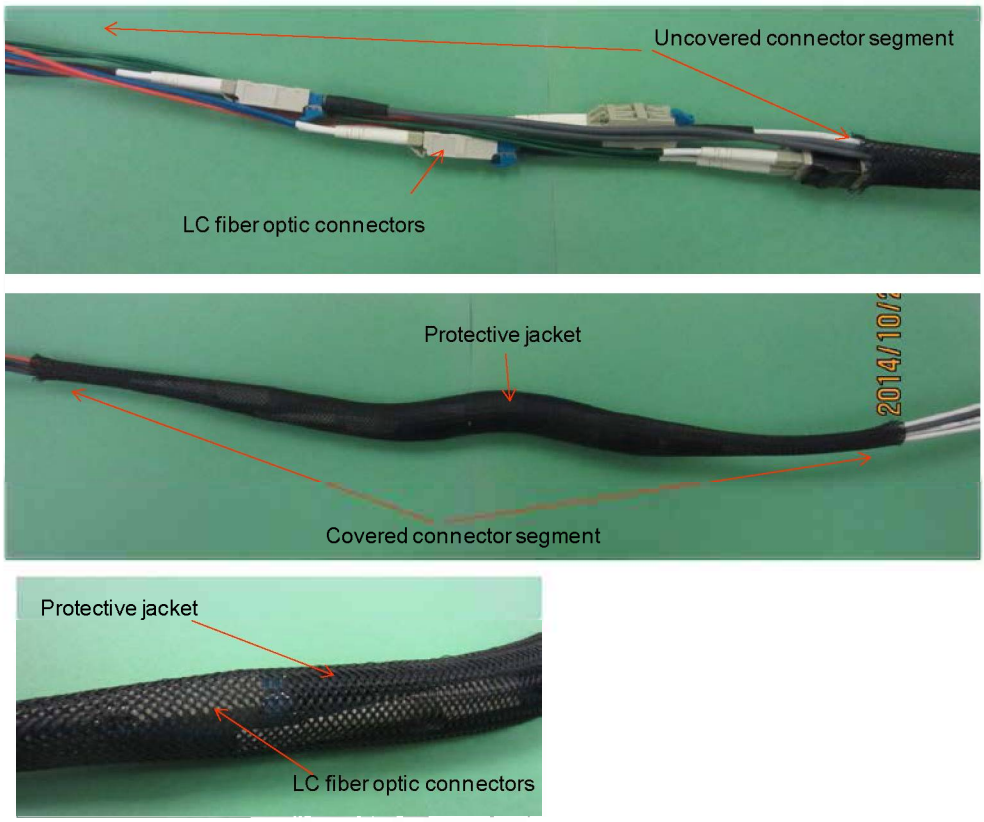

Figure 49 Connector segment prototype.

Loop Segment. Commercially available parts were evaluated, and the fabrication of a customized loop segment was based on the design of those parts (Figure 50).

Figure 50 Optical parts selected for the loop segment.

11.0 *TASK 11.0* DESIGN AND ASSEMBLE SENSOR DEPLOYMENT SYSTEM

Geomechanics designed the mechanical system for deploying fiber optic sensors in an existing 5,200 ft. monitoring well at the Terminal Island Renewable Energy Project in combination with an adjustable depth CO_2 injection system.

Concept Design and Requirements. The first step consisted of generating the concept design, including a description of the requirements, means, tools, and procedures for deploying the sensor. In the first concept design, the following components were selected for the sensor deployment system:

- Two spooling systems capable of managing ~5,100 ft. of cable and tubing weighing ~1,000 lb.
- Two trailer mast systems or cranes to lift the cable and tubing and position it over the wellhead for deployment
- A support system to hold the sensor cable segments during connection and deployment
- A weighted support cable or tubing system to guide the cable down the well
- A tubing system to inject CO_2 at specific downhole locations, with support mast and winch system for deployment
- Centralizer to help guide the combined assembly downhole and reduce wall contact
- A special wellhead to accommodate the sensor cable and CO_2 injection tubing.

To reduce system costs and make deployment easier, we decided to install a bridgeplug in the monitoring well above the existing perforations to isolate the wellbore system from formation of pressure and risk of flow. This enabled us to deploy the sensor more safely at lower pressure.

The deployment system characteristics and capabilities were defined as follows:

- The system will be capable of deploying the sensor cable to depths up to ~5,100 ft. within the well.
- The CO_2 injection tubing will be ¼ in. stainless steel, and will also act as the carrier to guide the sensor cable down the well.
- The CO_2 sensor cable will be connected to the injection tubing with periodically spaced metal clips.
- Centralizers and connection protectors will be placed at each of the connections between the distribution segments and the sensor segments.
- Downhole pressure in the well can be controlled to any specified level, within the range of about 2,500 to 4,000 psi.
- An outlet port on the CO_2 injection tubing can be placed at any specified depth.
- CO_2 can be injected at controlled rates to the subsurface outlet port, from a gas cylinder and pressure regulators at the surface.

Testing a Deployment System Demonstrator. Based on the system concept design and requirements, the detailed design of the elements was generated, and prototypes were fabricated, including a sensor head, centralizers, and connector protectors.

A cable was deployed in a shallow water well at the Terminal Island site to test the deployment protocols and check the integrity of all the elements during sensor deployment. The short sensor cable prototype included a 300 m distribution cable and a 2 m sensor cable. The cable incorporated the cable head and two connector protectors. A stainless steel tubing spooling trailer was used. The sensor cable was deployed manually, since the total depth of the well is only about 30 ft. That test enabled us to identify improvements and potential limitations of the deployment protocols. At the same time, the test enabled us to closely monitor the integrity of all the optical cables and connectors during deployment.

Figure 51 Installation of one of the connector protectors, and sensor cable deployment in a shallow water well.

Assemble Sensor Deployment System. The final sensor deployment system consisted of the following elements:

Spooling and Control Elements. The two spooling systems were capable of managing ~5,100 ft. of cable and tubing weighing ~1,000 lb., one for the stainless steel tubing and one for the sensor cable, with two trailer mast systems to lift the cable and tubing and position them over the wellhead for deployment.

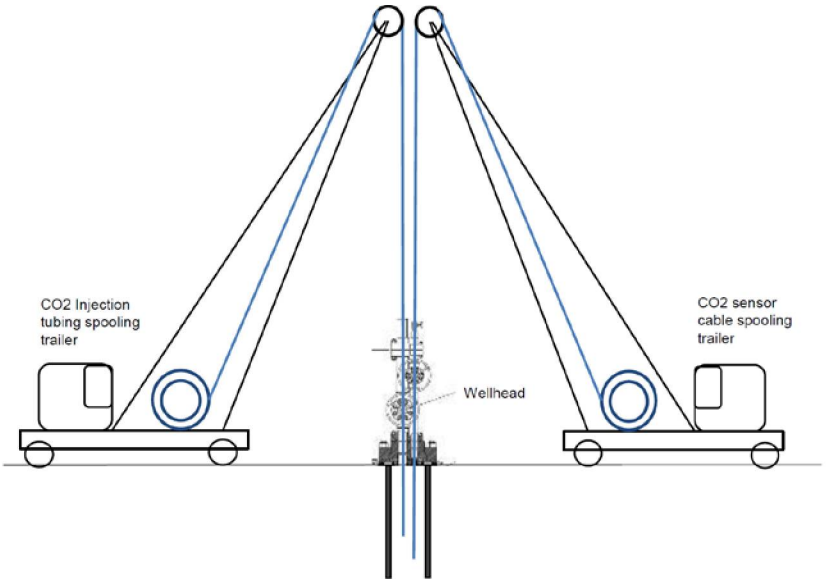

Figure 52 Sensor cable and CO_2 injection tubing deployment system.

Sensor Cable Head. The sensor cable head, at the end of the cable, is the first element that goes downhole, protecting the rest of the cable from impact. At the same time, it applies the weight needed on the cable to keep it vertical.

Connector Protector. The connector protector protects the union between the distribution segment and the sensor segment. The connector segment includes four double LC connectors that couple the eight optical fibers. The connector segment is the part of the optical cable with the largest diameter. The protector assures that the connector segment and the optical cables can be deployed and removed without any mechanical problem. The connector protector was designed to allow water to enter, and does not include any sealed space, avoiding stress at elevated pressure. All the components to be included in the connector segment were tested immersed in water up to 2,000 psi in the laboratory, assuring that they stand direct contact with water at depths over 2,000 m.

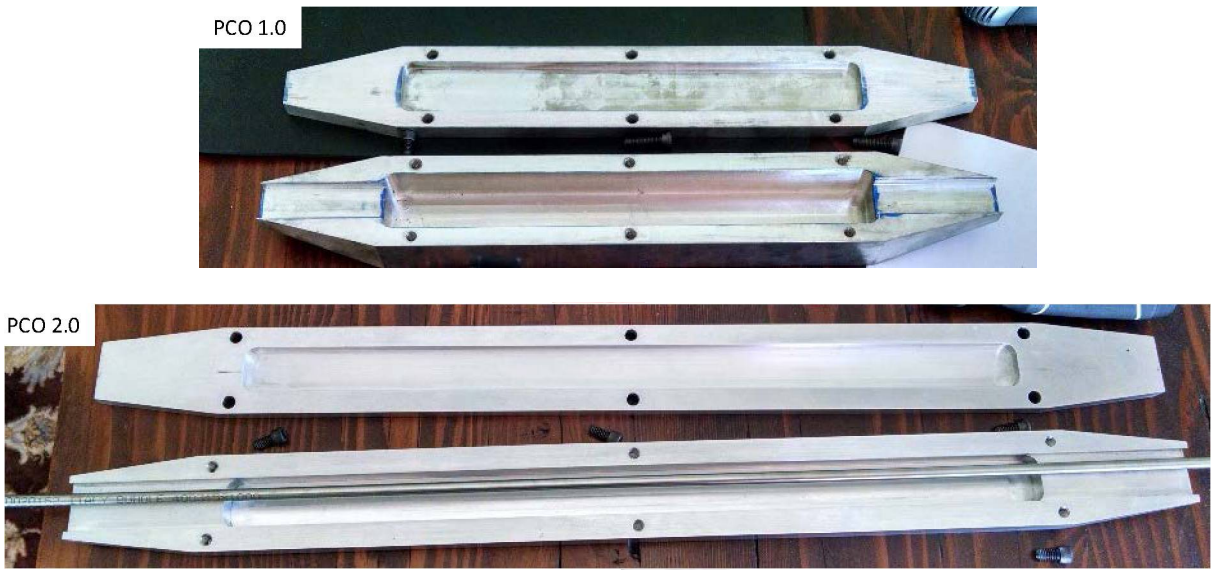

Figure 53 First version (PCO 1.0) and revised version (PCO-2.0) of the connector protector.

We assembled the monitoring system and fabricated all elements for the field deployment and validation. All the elements fabricated were integrated with the SUS-CO2-DICAST unit. The proper operation of each element was verified prior to integration. As each element was added to the system, the resulting partial system was tested to verify that system performance was not degraded by unexpected interactions among elements. At the conclusion of system assembly, the proper operation of the entire system was verified before starting the field validation.

Sensor segments and distribution segments were fabricated to conduct three cable deployments without reusing any of those elements, and backup units were also assembled in case of any unexpected event during deployment.

Initially, a cable incorporating four sensor segments was designed, with the plan of using two of them to detect carbon dioxide and having the other two below the point of CO_2 release. The deployment through the well head of the connector protector, which connects the sensor segments with the distribution segment, is the most critical step of system deployment. We finally decided to demonstrate the functionality of the system with a reduced number of sensor segments, which significantly simplified the system deployment, using only those segments that were going to detect the CO_2 release.

12.0 *TASK 12.0* SENSOR DEPLOYMENT AND VALIDATION IN THE FIELD

Three sensor cable deployments were performed, and sensor cable recovery was conducted after each of the validation tests. In the first sensor test, only one sensor segment was deployed. For the second and third sensor deployments, two sensor segments were incorporated into the sensor cable.

The data collected during the first two sensor tests was used to review the testing protocol, which enabled us to perform the most complete sensor validation in the thirst sensor deployment. In the following subsections we describe the sensor deployment, the results collected in the first two tests, and finally, the results collected in the last sensor test with a detailed discussion.

Sensor System Deployment. The steps of system deployment are explained below, with a sequence of photographs from the first and second tests.

Step 1. Cable head deployment. The sensor cable head, connected at the end of the external strength member, is the first element that goes downhole. The sensor head gives the cable the weight needed for vertical deployment. It also protects the other elements of the cable from impact.

Figure 54 (left) 5,200 ft. well head. (right) First step of the deployment, introducing the cable head into the well.

Step 2. The cable head and external member, the tube for gas release, are dropped 50 m before the first sensor segment is connected. The tube has a gas output at that exact point.

Step 3. Sensor segment integration. A connector protector is installed, and all the connectors of the first sensor segment and the parallel distribution segment are connected. The sensor segment, the parallel distribution segment, and the external cable, all held together by the connector protector, are slowly pulled down the well.

Figure 55 (left) Integration of the first connector protector and first sensor segment. (right) Optical connections inside the protector connector.

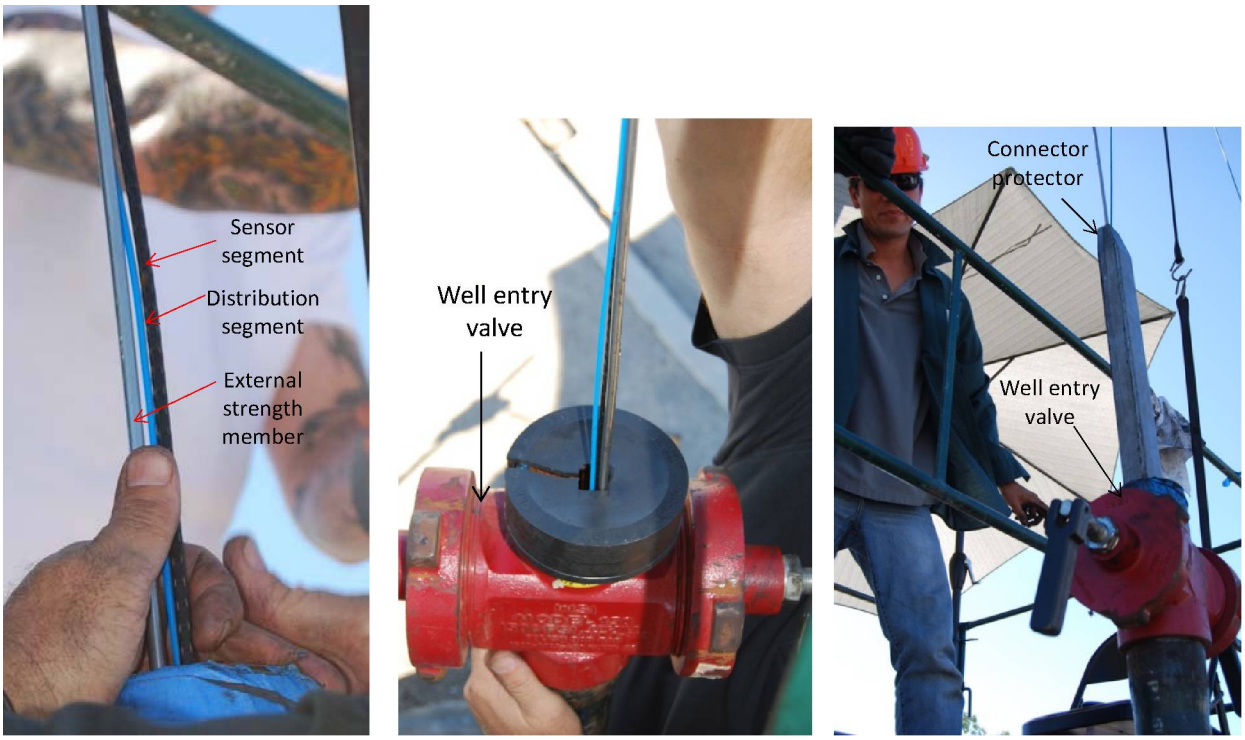

Figure 56 (left and center) Details of the three members that were pulled down together. (right) Introduction of the connector protector through the well head.

Step 4. Intermediate distribution segment integration. A second connector protector was installed, and all connections between the sensor segment and the distribution segment were locked. Light transmission was inspected to assure proper connection before moving to the subsequent steps. Steps 3 and 4 were repeated for each sensor segment.

Step 5. Final distribution segment integration and deployment. After the installation of all sensor segments, the 1,500 ft. distribution segment that was to be directly connected to the electronic unit was connected. Light transmission was inspected, and the sensor cable was pulled down to the desired depth.

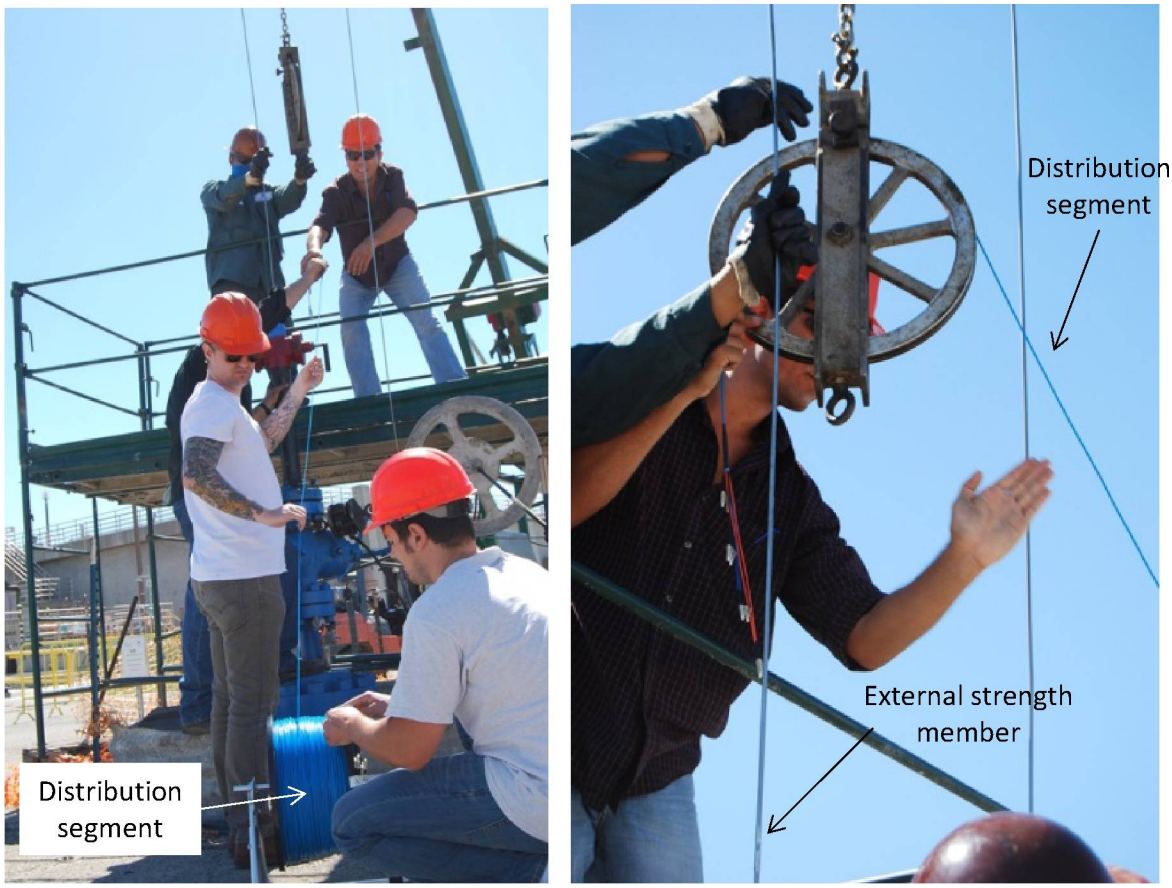

Figure 57 Integration of the final distribution segment before starting the final cable descent.

Step 6. Connection with the electronics unit. Once the cable was at the desired depth, the last distribution segment was connected to the electronics unit and sensor signal monitoring began.

System Validation and Carbon Dioxide Detection

First System Test. The deployment was successful at the first attempt, and light transmission through all the connected optical cables was detected, demonstrating that the deployment operation was safe and no connector or optical cable was damaged.

After sensor final deployment and immersion below the water table, we observed a significant increase in the attenuation of both the sensor signal and the reference signal, which led to the detection of very weak light power. That higher than expected attenuation became more significant as the deployment depth increased, preventing us from detecting CO_2 with the full length of the sensor cable in this first study.

In order to operate at proper signal-to-noise levels, we conducted the first test for CO_2 detection at 1,000 ft. However, in the second test we observed that the light power recovered after a day of cable deployment. This effect seems to be related to the effects of pressure and water on the distribution cable. Thus we were able to conduct tests at greater depths, by waiting for signal stabilization and recovery after 24 hr.

Figure 58 shows the electronic unit during the first validation test, and the sensor signal during the first release of CO_2 in the field, with a quick and sensitive signal change immediately after we

started the CO_2 release. In order for gas to be released through the tube, the pressure of the tube had to be above the hydrostatic pressure in the well.

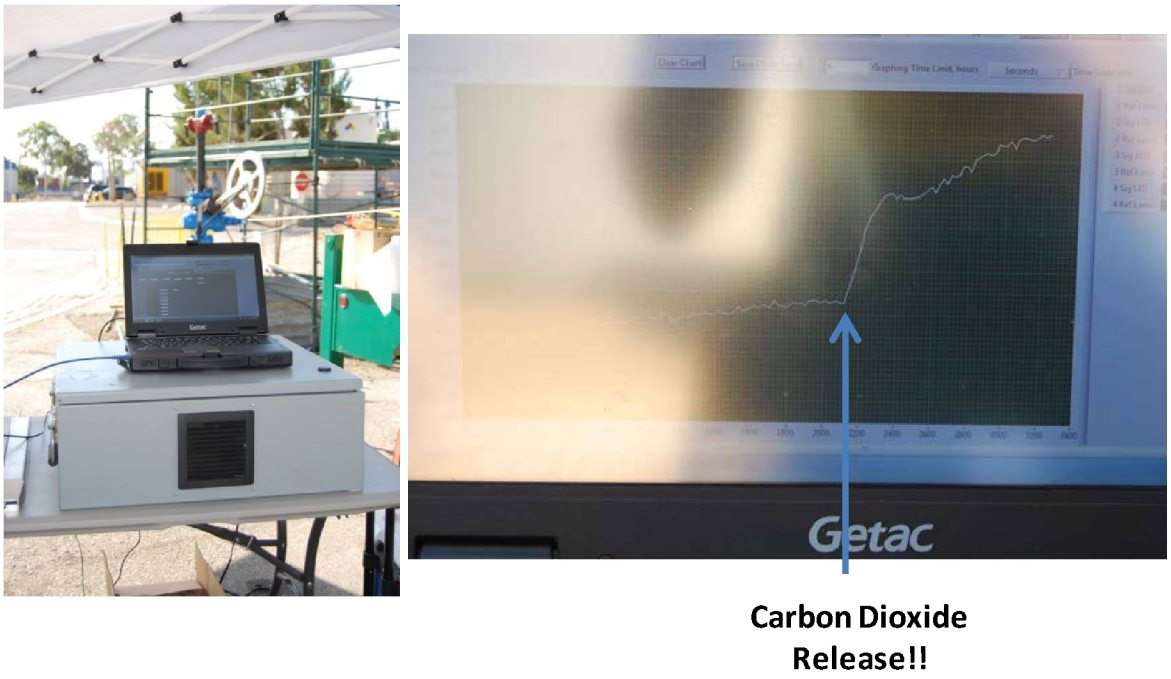

Figure 58 SUS-CO2-DICAST system during field validation, and sensor signal during first detection of CO_2 in the field at 1,000 ft. and 251 psi.

Figure 59 shows the sensor signal (595 nm) and reference signal (850 nm) during the first validation test, including the release of CO_2 and data collection overnight. A gas cylinder containing 10% v/v CO_2 in nitrogen was used for the test. The plot clearly shows how the light transmission increased significantly for both the sensor signal and reference signal through the hours following the sensor cable deployment. A proportional correction of the sensor signal based on the transmission at 850 nm resulted in the corrected signal (blue line), which was stable throughout the data collection period.

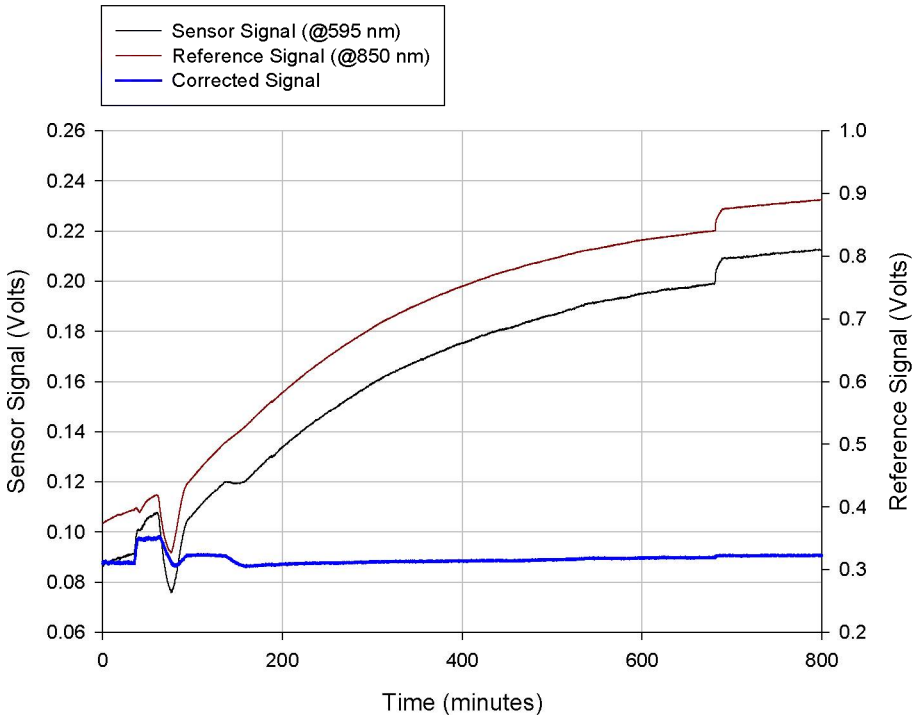

Figure 59 Sensor signal and reference signal profile during the first validation test. Corrected signal shows the detection of CO_2, and sensor stability throughout the test. Movement of the optical fiber around 690 minutes after the start of data recording was also detected by the sensor and reference signals, but was not noticed in the corrected signal.

Figure 60 shows the corrected signal profile during the release of CO_2. The gas delivery system installed in the field enabled us to control the pressure in the release tubing. The gas flow rate was proportional to that pressure, so the higher the pressure in the system the faster the dissolved CO_2 level should increase in the well. The sensor detected the CO_2 release within less than a minute. The signal stabilized when the CO_2 flow was stopped. The sensor returned to its baseline signal after we purged the system with nitrogen. A second release of CO_2 was performed at lower pressure, and therefore lower gas flow rate. The increase of CO_2 in the well was detected by the sensor system at a lower rate than the first gas release, as expected. A final purge with nitrogen resulted in signal baseline recovery. We stopped the N_2 release after a few minutes, so it can be assumed that any initial content of CO_2 was not completely purged. In this first test we did not apply the calibration functions to calculate the actual levels of carbon dioxide, due to the uncertainties induced by the effect of pressure in the distribution cable. In the final tests, after we had learned about this effect, we were able to determine CO_2 concentrations.

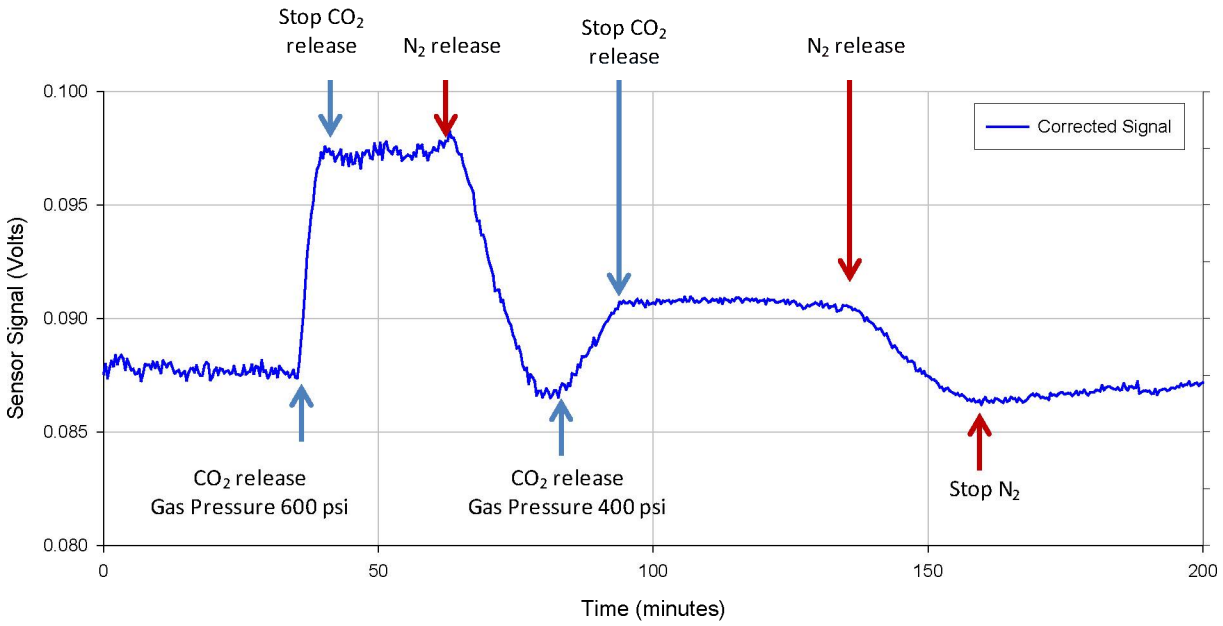

Figure 60 Corrected signal showing the detection of CO_2 and recovery to baseline with nitrogen, during field validation tests.

Second System Test. A sensor cable incorporating two sensor segments was used for the second CO_2 detection test. The sensor was deployed in the steps recorded above. As described above, the signal transmission after immersion was initially weak.

A first release of CO_2 was performed at 1,380 ft. and 407 psi. As in the first test, the gas flow rate was controlled by controlling the pressure in the release tube. The first sensor detected the CO_2 less than a minute after CO_2 release started, and the second sensor, situated above it, detected the CO_2 5 min. later. Both sensors recovered their baseline signal levels after the system was purged with nitrogen. A second release of CO_2 was performed at lower pressure, and therefore lower gas flow rate, but was maintained for a longer time. The increase of CO_2 in the well was detected immediately by the first sensor, and later by the second. A final purge with nitrogen was not performed, and the well was left for natural stabilization, with progressive dilution of the gas in the aqueous mix.

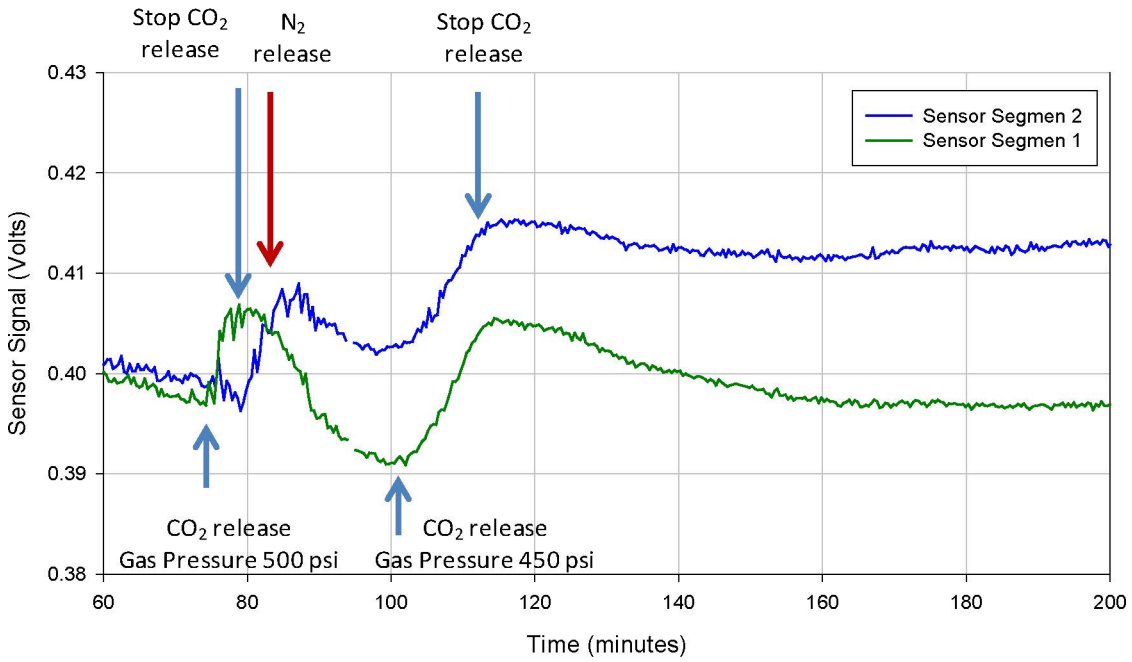

Figure 61 Corrected signal showing the detection of CO_2 and recovery to baseline with nitrogen, during field validation tests. The response of the sensor located above the gas release point (Sensor 2) is delayed in comparison to the response of the sensor located next to the gas release point (Sensor 1).

After the test at 1,300 ft., the sensor cable was placed at 2,180 ft. and 736 psi and we released CO_2 (10% CO_2 v/v in nitrogen) slowly, keeping the pressure of the gas in the tube at 750 psi, just above the hydrostatic pressure in the well at the point of gas release (736 psi). The CO_2 release was detected by both sensors, but reversibility could not be tested this time because we had run out of nitrogen. As for the first test, in this second sensor test we did not apply the calibration functions to calculate the actual levels of carbon dioxide.

Lessons learned from this series of tests enabled us to perform a more complete sensor validation in the third test.

Third System Test. This third test was designed based on the data collected in the first two tests, accommodating the testing protocol to the observations made in the field, and also introducing some modifications to the sensor cable assembly. That enabled us to record the most complete set of data, and perform a valuable validation of the system. The data collected in this test was more thoroughly processed, and is discussed here in detail.

For the third test the sensor cable incorporated two sensor segments, which we refer to as the lower and upper sensors. The distance between the bottom end of the lower sensor and the bottom end of the upper sensor was 30 ft. The sensor cable was deployed in the steps recorded above. Four gas releases were performed, all four at 2,350 ft. and 750 psi. The gas output was located at the bottom end of the lower sensor. As in the previous tests, the gas flow rate was controlled by controlling the pressure in the release tube. Before starting the tests, the sensor cable was left for signal stabilization over 24 hours, so we could apply the calibration functions and determine the carbon dioxide concentrations during the tests.

We released CO_2 three times, which we refer to here as Tests 3-A, 3-B, and 3-C, in the same six steps: (1) recording baseline, (2) releasing CO_2, (3) stopping the gas release and waiting for signal

stabilization in the lower sensor, (4) continuing with release of carbon dioxide, (5) purging with nitrogen without stopping the gas flow, and (6) finally stopping any gas release. Cylinders of 20% v/v of CO_2 in N_2 and pure N_2 were used for these tests.

Signal Processing and Environmental Effect Compensation. Figure 62 shows the raw data recorded for Test 3-A, including the sensor signal and the reference signals. As in previous tests, the sensor signal responded in about one minute to the release of CO_2. We had observed in the previous tests and confirmed in this test that the reference signal is also affected by the gas release (both CO_2 and nitrogen). In fact, it showed significant variations immediately after we stopped the gas release, which were not observed in the baseline recording. This signal variation is not due to the variations in the CO_2 concentration but rather to a side effect that also affected the sensor signal. We had never observed this effect in the laboratory, and we do not have enough data to find a good explanation for this observation, though it is apparently related to a physical effect on the fibers. This effect is proportional in the sensor and reference signal, and can easily be subtracted, which enables us to perform gas detection and quantification. Figure 62 shows the corrected signal (blue trace), together with the sensor and reference signals. The effect of the gas in the sensor and reference signals and the effective signal compensation is best observed in Figure 62 in the data collected from 140 to 170 minutes. While the black and red traces are drifting up, the corrected signal, blue line, is stable when the gas release is stopped.

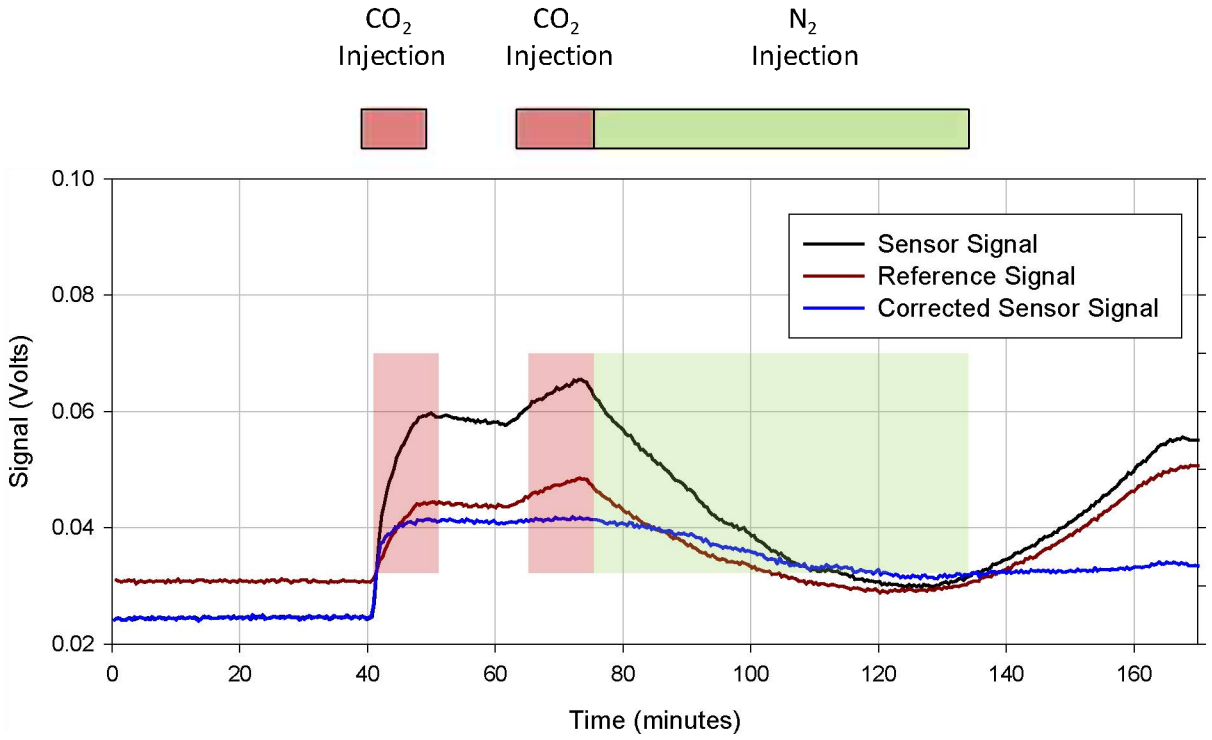

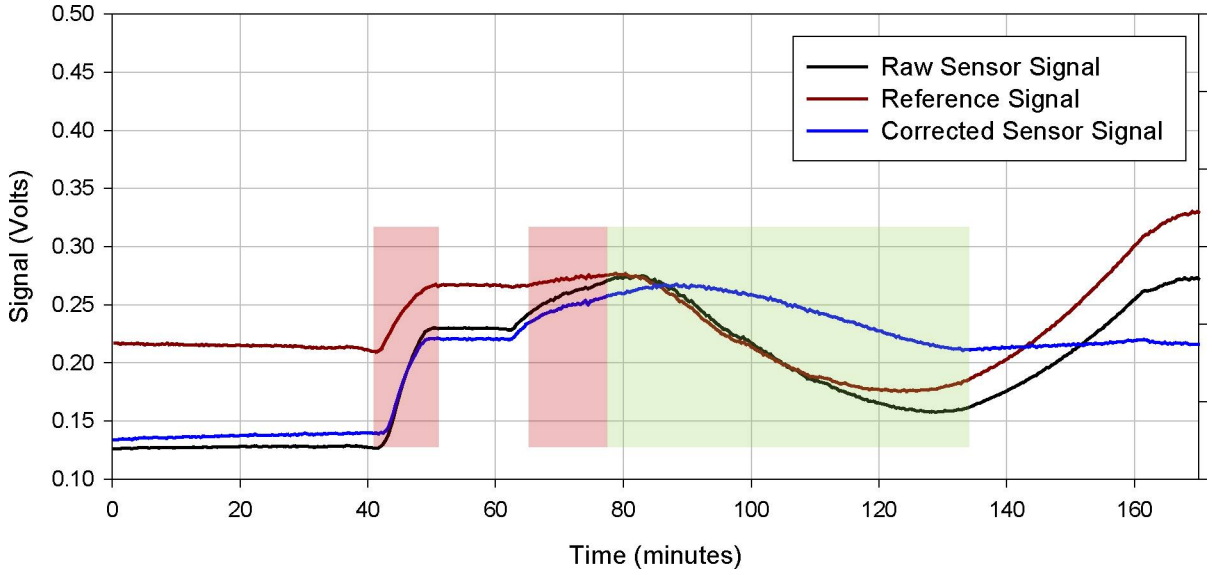

Figure 62 Raw sensor and reference signal and corrected signal, during the first carbon dioxide release conducted in the third field validation test. (top) Upper sensor signals. (bottom) Lower sensor signals.

In this final test, we were able to apply the calibration functions (signal vs CO_2 concentration) previously determined in the laboratory. Based on the tests performed in the laboratory, the sensor saturation is reached at 25 ± 2 psi partial pressure of CO_2, which corresponds to a concentration of dissolved CO_2 at 70°C of 1.05 ± 0.08 g/kg. Any concentration above that level does not further affect the sensor signal. In all three gas releases (Tests 3-A, 3-B, and 3-C) both sensors reached their saturation levels, and after that the sensor reading remained at the saturation level, though the actual concentration of CO_2 was above 1.05 ± 0.08 g/kg. Note that the equilibration of water with 20% CO_2 at 70°C and at 750 psi would result in a concentration of dissolved CO_2 as high as 6.31 g/kg.

A sensor with lower sensitivity but a wider measurement range can be prepared based on the optimized formulation, but we prioritized early leak detection, and therefore high sensitivity. Sensor cables incorporating two types of sensor segments, one with high sensitivity for quick leak detection and one with a wide measurement range, are envisioned for the next-generation system.

CO_2 Leak Detection. Figure 63 shows the dissolved carbon dioxide profile recorded for the three gas releases.

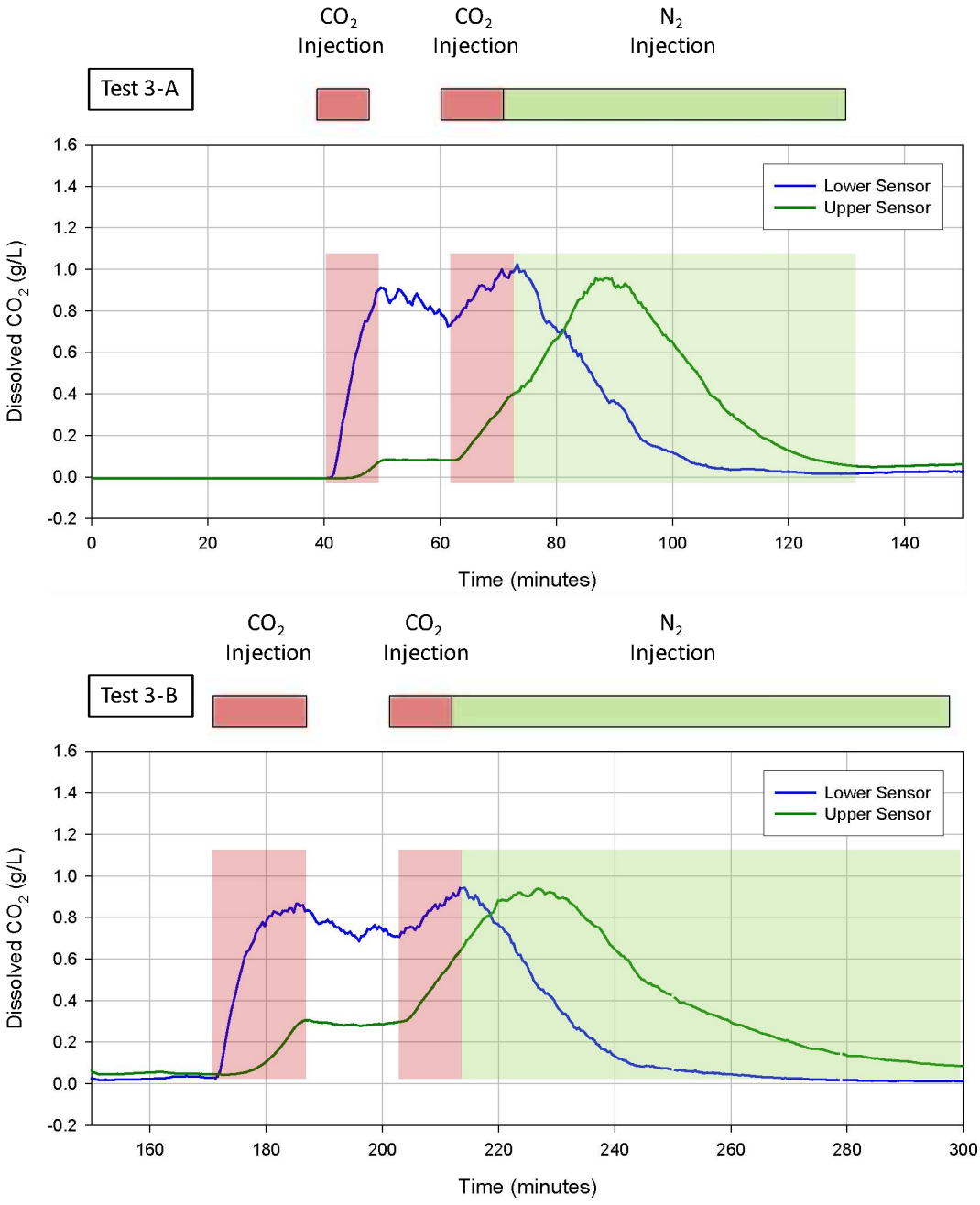
CO2 Injection
CO2 Injection
N2 Injection
Test 3-A
Lower Sensor
Upper Sensor
Dissolved CO2 (g/L)
Time (minutes)
CO2 Injection
CO2 Injection
N2 Injection
Test 3-B
Lower Sensor
Upper Sensor
Dissolved CO2 (g/L)
Time (minutes)

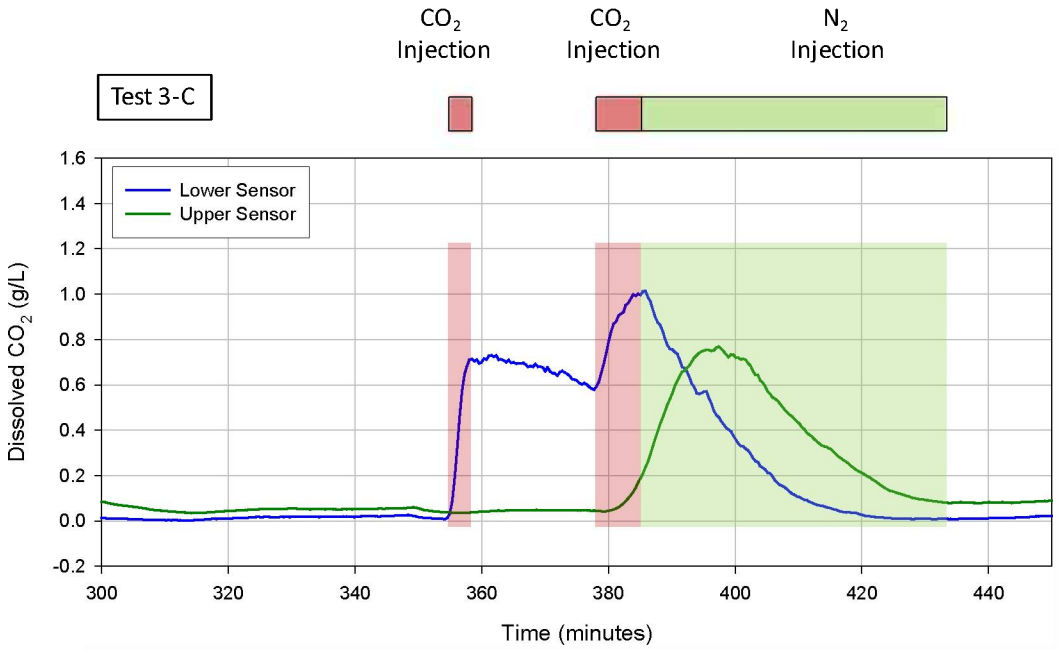

Figure 63 Dissolved carbon dioxide profile for Test 3-A, Test 3-B, and Test 3-C for the lower and upper sensor. Injection of CO_2:N_2 at 20% v/v is highlighted with red shadows, and injection of N_2 is highlighted with green shadows. No gas was flowed in the unhighlighted periods.

In Test 3-A, the pressure applied to the gas tube was 800 psi, 50 psi above the pressure in the well at the point of gas release. The initial CO_2 release lasted ten minutes, after which the gas flow was stopped. The lower sensor detected the CO_2 release approximately two minutes after we open the CO_2/N_2 gas cylinder, which we believe was the time it took for the gas to fill the injection tube. The upper sensor detected the CO_2 release three minutes after the lower one. After the gas release was stopped, both sensors recorded almost stable CO_2 levels, with a smooth decrease in the concentration at the lower sensor. The water in the well is not subject to any dynamic process. The CO_2 saturated the signal capacity of the lower sensor, while only a low concentration of CO_2, 0.13 g/kg, reached the upper location.

When the gas cylinders were opened again, additional CO_2 was released first, followed by pure nitrogen. Both sensors detected the increase on the CO_2 levels, which saturated the lower sensor first and later the upper sensor. The purge with nitrogen was detected by both sensors with the expected delay between them, and carbon dioxide concentration had returned almost to the baseline levels by the time we stopped the nitrogen purge.

The same sequence was followed for Tests 3-B and 3-C, varying the time and flow rate for the initial release of CO_2. The graphs for these three gas releases show a similar profile, with differences in the time delay between the lower and upper sensor readings (Figure 63).These tests demonstrated the capability of the multi-sensor system to rapidly detect a gas leak reaching one of multiple monitoring or observation wells, the capability of locating the leak, with the potential to evaluate the importance of that leak. The tests were conducted with two sensors in the same monitoring well, but the conclusion can be extrapolated to sensors in different monitoring wells.

Leak Location and Quantification. The location of a leak can be estimated from two parameters: (1) the slope of the CO_2 increase at the sensors, and (2) the delay between detections.

For a similar leaking flow rate, the leak will be detected first by sensors closer to the leakage spot. In addition, comparing the slope of the CO_2 increase at the sensors reveals the relative distance between those sensors and the release point. Figure 64 compares the slope of CO_2 increase between the lower and upper sensors. In the test, the gas flow rate was the same for both sensors, but the sensor closer to the leak reports a much faster CO_2 increase. Thus, there is not only a delay between the CO_2 detection in the lower and upper sensors, but the kinetics are different.

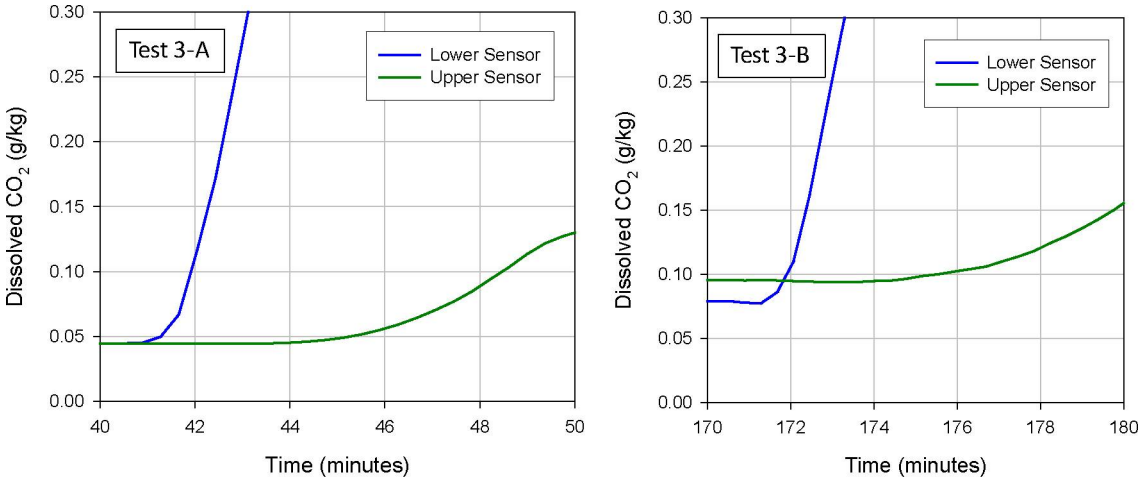

Figure 64 CO_2 release detection in Test 3-A and Test 3-B by the lower and upper sensors. The slope in the upper sensor is significantly faster than that of the upper sensor in both tests.

Quantification of the leak can also be estimated from two parameters: (1) the slope of the CO_2 increase for a particular sensor, and (2) the difference in the concentration at two depths.

In Tests 3-A and 3-B the pressure in the gas tube was set 50 psi above the hydrostatic pressure at the gas release point, and in Test 3-C at 100 psi above that pressure. As a result, the flow rate of the leak in Test 3-C was twice the flow rate of the leak in Tests 3-A and 3-B. The flow rate of CO_2 injection was above the measurement range of our flow meters, and we were unable to measure the flow rate during the tests. Instead, based on the consumption of gas, we calculated that the CO_2 was released at 80 SLPM in Test 3-A and Test 3-B, and at 160 SLPM in Test 3-C.The slope in the CO_2 detection clearly shows that difference (Figure 65), providing information from which to estimate the leak flow rate for a particular well of known dimensions.

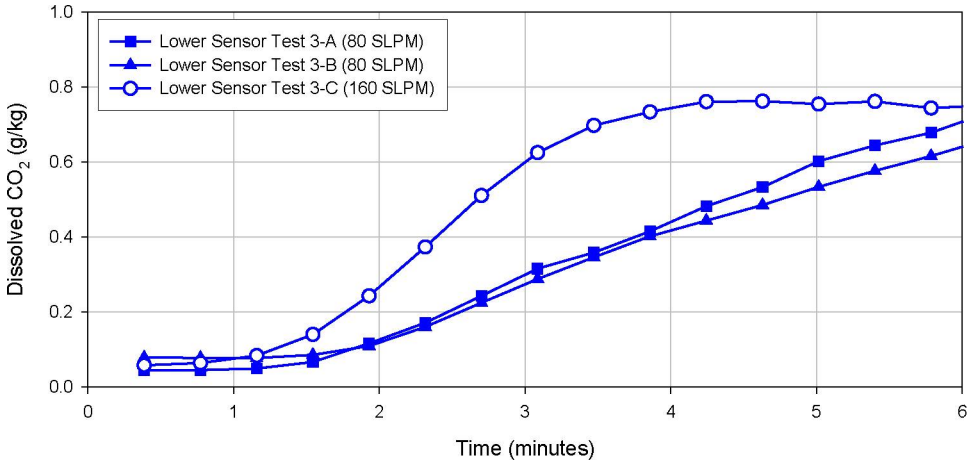

Figure 65 Comparison of the slope in the increase of CO_2 detected by the lower sensor in Test 3-A and Test 3-B conducted at 80 SLPM flow rate, and Test 3-C conducted at 160 SLPM flow rate.

The total amount of CO_2 injected, which is a function of the flow rate and injection time, was varied in each of the tests by controlling the injection pressure and time, and the calculated amount of CO_2 injected and ratios among the amounts in the three tests were as follows:

- CO_2 injected in Test 3-A = A-CO_2 kg = 0.350 kg
- CO_2 injected in Test 3-B = 1.5 × A-CO_2 kg = 0.500 kg
- CO_2 injected in Test 3-B = 0.5 × A-CO_2 kg = 0.175 kg

Figures 66 and 67 show the CO_2 concentration increase detected by the upper sensor 15 minutes after the leak detection by the lower sensor, as a function of the CO_2 leaked.

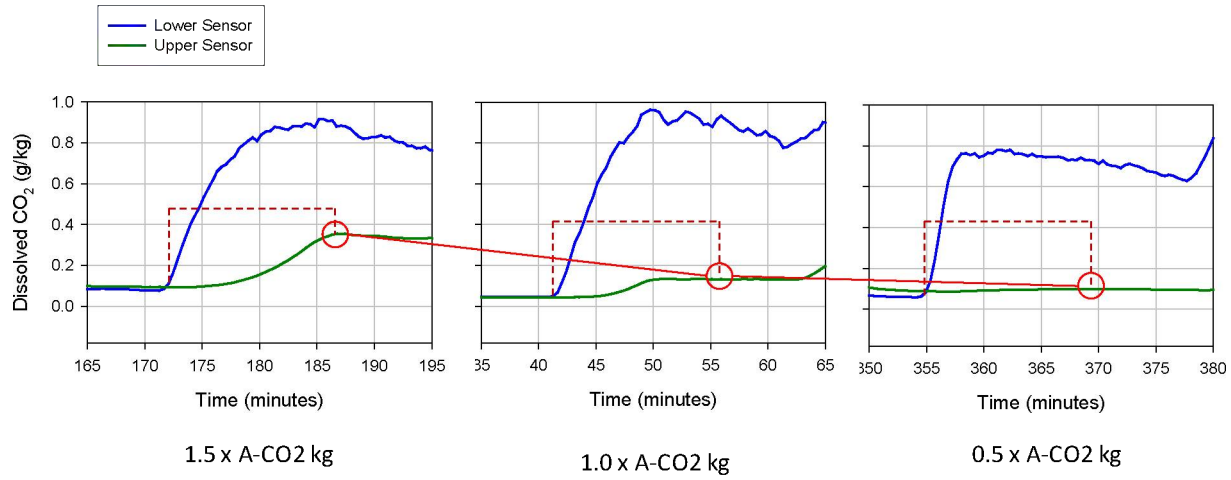

Figure 66 Dissolved CO_2 profile during Tests 3-A, 3-B, and 3-C. Red lines mark the concentration of CO_2 detected by the upper sensor 15 minutes after the first detection of the CO_2. Below the graphs the relative amount of injected CO_2, from left to right 1.5:1.0:0.5.

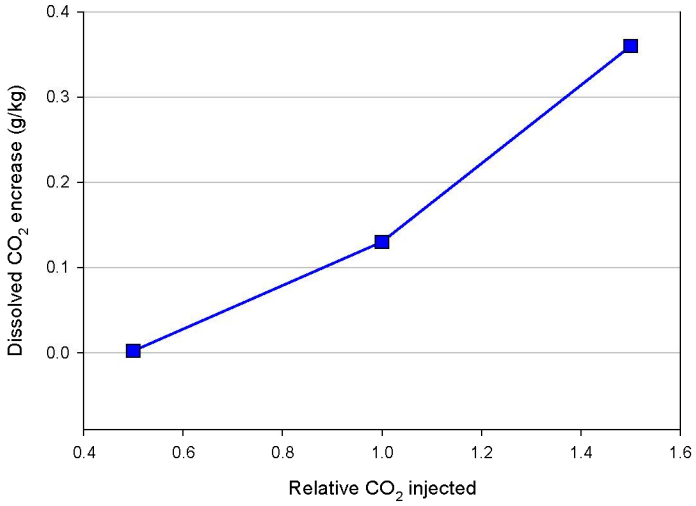

Figure 67 Increase in the concentration of CO_2 at the upper sensor 15 minutes after the detection of the leak as a function of the relative amount of CO_2 injected during Tests 3-A, 3-B, and 3-C.

As expected, there is a clear relation between the amount of CO_2 injected or leaked and the concentration of CO_2 above the leakage point, at a set time after the leak is detected. This correlation would support quantification of the leak by a multi-sensor system such as the one we have validated, even if those sensors saturated after some time. Obviously, after the sensors are saturated further leak quantification would not be possible. To prevent that effect, at least one sensor should be placed way above the lower sensor in the well, so only low levels of CO_2 would reach the sensor in the early stages of the leak, and that would enable the system to perform continuous leak quantification.

Sensor Robustness. The sensor cables were removed from the well after each of the tests. Inspection of the sensor cable did not reveal any damage. The water in the well was highly contaminated, and all cables were completely covered with a thick layer of grease and black particles (Figure 68). Nevertheless, sensor functionality was not significantly affected, demonstrating that the technology can operate under those conditions.

Figure 68 Optical connector covered with particles, and an optical cable covered with grease after being removed from the well, showing the contamination to which the sensors were exposed.

The availability of the well at Terminal Island was not sufficient for us to extend the tests to validate sensor stability. Sensor stability was tested by recording data overnight after the CO_2 releases. Figure 69 plots the CO_2 profile recorded after Test 3-C. Both sensors recorded stable CO_2 concentrations and sensor drift. A final CO_2 release yielded similar results.

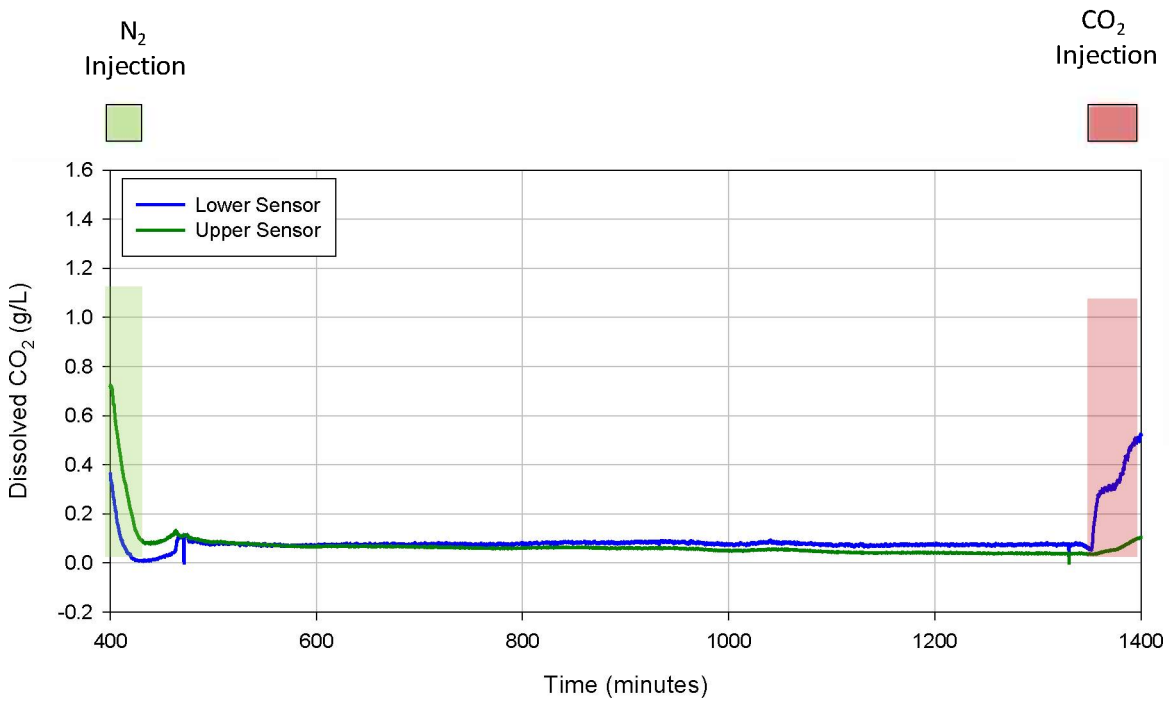

Figure 69 Dissolved CO_2 profile after Test 3-C. Stable CO_2 levels were recorded until a final CO_2 injection.

13.0 *TASK 13.0* CRITICAL DESIGN REVIEW

The design of the system, including the readout unit and the sensor cable, and the fabrication protocols, were reviewed several times in the course of the project, and in particular during the validation studies in the field.

Many of the modifications identified at the Design Review had already been implemented before the final system validation, and are described in this report under the respective tasks.

A final review of the design of the SUS-CO2-DICAST unit was performed in order to have a more compact instrument at a lower cost, without losing the excellent performance of the instrumentation developed in the project, in particular the high sensitivity and excellent signal-to-noise ratio. Thus, the first task of the review focused on the control module, which does not impact the system performance. The second review affected the user interface. Finally, the Tx-Rx module was reviewed following the basic approach of the SUS-CO2-DICAST unit, but targeting a more compact module.

The objective of this task was not implementing the proposed system modifications but guiding the development of the next system generation. The design reviews conducted throughout the project formed the basis for the development of the next system generation in a new project.

CONCLUSIONS

- Developed novel polymeric sensor materials for dissolved carbon dioxide monitoring in aqueous matrix, and for carbon dioxide monitoring in gas phase.
- Performed studies to make the sensor materials resistant to adverse environmental conditions, and identified and implemented effective strategies. Resistance to corrosive environments, including high salinity, low pH, elevated water flow rate, high pressure, and presence of hydrocarbons demonstrated. The effectiveness of strategies to protect the sensor material from biofouling contamination was also studied, and selected approaches were implemented.
- Optimized the capability of the sensor materials to survive and operate at the elevated temperatures found in deep wells, and demonstrated operation at up to 175°C. The sensor materials showed that they could operate continuously at up to 140°C. Life studies were performed, and based on the data collected an operating life at 70°C for a period of over five years, without sensor replacement, can be projected.
- Established at IOS a fiber optic recoating apparatus and fabrication protocols for manufacturing fiber optic sensors at a rate of hundreds of meters per day using either UV-curing or heat-curing polymers.
- Fabricated fiber optic sensors using the novel sensor materials, and determined their analytical characteristics in the laboratory over a range of temperature and pressure conditions. Determined sensitivity down to 0.8 mg/L CO_2 (corresponding to 0.05% v/v CO_2 or 0.35 mmHg pCO_2) under standard conditions.
- Demonstrated direct determination of dissolved CO_2 at elevated pressure up to 2,050 psi for the first time using fiber optic sensors, and demonstrated the capability of detecting a leak of 0.1% CO_2 v/v under realistic conditions of pressure and temperature in the range of 15 to 2,000 psi and 25°C to 175°C.
- Designed, fabricated, and validated a multi-sensor optoelectronic unit to monitor carbon dioxide with large depth coverage. The system is designed to operate sensor cables, integrating multiple sensor segments at various depths along the cable. Demonstrated the capability of the system to operate sensor cables as long as 3000 m with excellent signal-to-noise readings (noise 0.03% of signal).
- Demonstrated the system in the field, deployed in a deep well. Conducted multiple CO_2 releases simulating gas leaks reaching an observation well, locating sensor segments at variable depths (and pressure). Demonstrated early leak detection with high sensitivity in the field tests. Demonstrated the capability of multiple sensor segments distributed at various depth throughout a sensor cable to profile the CO_2 concentration (CO_2 vs. depth). Field data demonstrate that using multiple sensor segments not only can detect the leak but can quantify it, based on the dissolution and distribution rate of CO_2 from sensor segment to sensor segment.
- Field tests demonstrated the capability of the sensor cables to survive and operate properly immersed in highly contaminated aqueous matrixes.
- Developed a new generation of fiber optic sensors for direct subsurface detection and monitoring of carbon dioxide under this project, and demonstrated them in the field, exhibiting capabilities not yet achieved by any other monitoring technology. For the first time, low levels of dissolved carbon dioxide were monitored, in-situ and in real time, at multiple depths, in a deep monitoring well, at elevated pressure and temperature. This project represents a breakthrough in our CCS monitoring capabilities.

REFERENCES

1. J. Delgado Alonso, "Distributed sensors for dissolved carbon dioxide," DOE SBIR Phase II Grant No. DE-SC0004444, 08/15/11 to 12/14/13; J. Delgado Alonso, S. Phillips, C. Chullen, E. Mendoza, "Compact multi-gas monitor for life support systems control in space: Evaluation under realistic environmental conditions," 44th International Conference on Environmental Systems, 13-17 July 2014, Tucson, Arizona.